A RELIABILITY ASSESSMENT OF GRANDSTAND ELEMENTS

Master of Science thesis

H.J.J. Weijs

Delft University of Technology

TU Delft

TNO innovation for life

A RELIABILITY ASSESSMENT OF GRANDSTAND ELEMENTS

How can the structural reliability of a concrete grandstand element subjected to dynamical crowd loads be determined?

A case study: Football stadium the Goffert in the Netherlands

by

H.J.J. Weijs

to obtain the degree of Master of Science
at the Delft University of Technology,
to be defended publicly on Thursday March 2nd, 2023 at 16:00.

Student number:	4350936	
Project duration:	Monday 9th May, 2022 – Thursday March 2nd, 2023	
Thesis committee:	Prof. dr. ir. M.A.N. Hendriks,	Delft University of Technology, chair
	Dr. ir. K.N. van Dalen,	Delft University of Technology
	Prof. dr. ir. R.D.J.M. Steenbergen,	TNO, Ghent University, daily supervisor

Cover: Het Goffertstadion Nijmegen by Karsten Russ (modified)

An electronic version of this thesis is available at http://repository.tudelft.nl/.

TU Delft

TNO innovation for life

Preface

Failing. It was May 5th 2015 when, for the first time in my life, I faced failure. Up until that point, my study progress had always gone steadily. Although the grades were minimal, too, it took me minimal effort to pass all my classes. However, as I were to find out the hard way, this lazy mindset would not be sufficient to make it in Delft. Within no time, I was lagging behind in all my courses. I did not understand what I was doing and why I was doing these things. I felt completely lost. It was on this day that I quit my study civil engineering at the Delft University of Technology.

I then enrolled for the same study at the Hogeschool van Arnhem en Nijmegen. Here, all the puzzle pieces started to fit together again. Unlike the theoretical mindset in Delft, the practically-minded courses here made sense to me, and very quickly, I excelled in all my courses. It was here that I regained my interest in the world of civil engineering again. As my progress in Arnhem continued smoothly, I became more interested in the why questions. This was the point where I let go of my lazy mindset and became a fanatic student. In my final year, I knew I wanted to return to Delft: it felt like unfinished business.

This has turned out to be a great decision: not even a global pandemic could stop me. I have felt very motivated to complete this study. Despite having to study at home most of the time, I have made some great friends along the way. I also started to develop an interest in probabilistic design. When I was given the opportunity to write my thesis about the topic that I eventually did, I could not be happier: as someone from Nijmegen who likes football, it looked like the perfect match for me.

Now I can say that it indeed was the perfect match for me. In the last nine months, I have always managed to stay motivated in bringing my thesis to a good result. When I started last May, I would never have expected the progress to go as smoothly as it has. For this, I would like to thank my committee, who always allowed me to continue developing my thesis on my chosen path and especially my supervisor Raphaël Steenbergen for his excellent supervision, guidance, and, most of all, enthusiasm. Secondly, I would like to thank my parents, who, despite not always understanding what I was doing precisely, kept on supporting me throughout this journey. Finally, I would like to thank my girlfriend, family, and friends for all our joyous moments throughout this process, allowing me to also forget about this thesis from time to time.

Looking back at how I have changed since May 5th 2015, I see someone who has matured massively and finally found a drive, which made me let go of the lazy version of myself that I had always been and become a person determined to succeed by working hard. I do not know if I would have accomplished all this if I had not taken the path that I did. On that day I learned that failing presents the basis of something great: Growing.

H.J.J. Weijs
Delft, February 2023

Abstract

On the 17th of October 2021, a concrete grandstand element collapsed at the Goffert stadium in the Netherlands after a crowd jumped on it for 8 seconds. An investigation by an engineering consultancy firm concluded that the design loads in the building code are too low, raising questions about the safety of grandstand elements. Currently, no method to assess the reliability of grandstand elements exists.

This thesis presents a state-of-the-art method to determine the reliability of concrete grandstand elements. The reliability is assessed by performing a non-linear dynamical analysis. The element is modelled as a non-linear single-degree-of-freedom system. Excitation signals are synthetically generated by consulting the literature and by analyzing a data set of jumping crowds. A bi-linear force-displacement relationship based on technical drawings of the collapsed grandstand element is adopted and extended by a model uncertainty parameter which accounts for both the non-linearity of the analysis and the uncertainty related to the dynamical basis of the analysis. The reliability is determined through a Monte Carlo simulation: almost 100,000 simulations can be performed per assessment.

Out of the 100,000 simulations, 0 failed. This result is not in line with what happened; one failed out of only a few elements. This gives rise to two different investigations. On the one hand, the failure of the Goffert stadium grandstand elements has to be explained. On the other hand, the lifetime reliability of a grandstand element has to be determined.

The first assessment indicated that if the element's resistance conforms to the technical drawings, there is no cause for concern regarding its reliability. Measurements on 23 other grandstand elements in the same stadium showed a high variation in the concrete cover. The collapsed element was, therefore, also likely subjected to a high variation in the concrete cover. To understand the influence of an increased concrete cover on the reliability, two additional analyses were performed, where the post-yielding resistance of the structure was slightly reduced. This resulted in an increase in the probability of failure, which indicates that this parameter plays a crucial role in determining the reliability of grandstand elements. These points combined make it more plausible that the element failed because the concrete cover was larger than intended rather than the design loads being too low, as concluded by the engineering firm.

When investigating the lifetime reliability of grandstand elements in general, no collapse is expected after 8 seconds but rather after 30 seconds or even longer durations. Therefore, two additional analyses were performed where signals of longer durations (120 seconds and 300 seconds) excited the system. In these analyses, it is assumed that the resistance of the grandstand element conforms to the technical drawings. Signs of a converged reliability were perceived as 120- and 300-second excitation signals led to a probability of failure of the same order of magnitude, indicating that a steady-state solution is obtained after 120 seconds of jumping. In that case, the lifetime reliability of a grandstand element would be equal to the 120-second reliability. The corresponding reliability passes the lifetime reliability requirements for existing structures in consequence class 2 (for a reference period of 15 years).

While the results presented are estimations, and a larger sample size is needed for a converged probability of failure, the proposed method provides a valuable framework for assessing the reliability of grandstand elements. This method can easily be extended to any grandstand element by changing the model parameters, and the true reliability of grandstand elements can be assessed by performing more (1-10 million) simulations.

Contents

List of Figures

List of Tables

Nomenclature

Abbreviations

Abbreviation	Definition
CoV	Coefficient of variation
DOF	Degree of freedom
EOM	Equation of motion
FEM	Finite element method
LSF	Limit state function
MCT	Motion capture technique
SDOF	Single-degree-of-freedom
sts	series to series
ws	within series

Symbols

Symbol	Definition	Unit
EI	Bending stiffness	[N/m^2]
F	Force	[N]
$\tilde{F}$	Jump factor	[-]
$\tilde{F}_{sts}$	Series to series jump factor	[-]
$\tilde{F}_{ws}$	Within series jump factor	[-]
F^*	Portion of applied force shared by the hysteretic spring	[N]
F_y^*	Yield force of the hysteretic spring	[N]
F_y	Yield force	[N]
F_u	Ultimate force	[N]
G	Weight	[N]
N	Parameter controlling the smoothness of the transition from elastic to inelastic	[-]
P_f	Probability of failure	[-]
R	Resistance	[m]
S	Solicitation	[m]
T_p	Jump period	[s]
V	Coefficient of variation	[-]
Z	Limit state function	[m]
c	Viscous damping	[kg/s]
f	Factor between a force signal and an acceleration signal	[-]
g	Gravitational constant	[m/s^2]
k	Stiffness	[N/m]
k_0	Elastic stiffness	[N/m]
k_{eq}	Equivalent stiffness	[N/m]
k_{hys}	Hysteretic spring stiffness	[N/m]
k_{nl}	Non-linear stiffness	[N/m]

Symbol	Definition	Unit
m	mass	[kg]
n	Number of simulations	[-]
n_f	Number of failed simulations	[-]
r_k	Ratio between pre-yield and post-yield stiffness	[-]
t_p	Contact duration	[s]
u	Displacement	[m]
u_y	Yield displacement	[m]
u_u	Ultimate displacement	[m]
uc	Unity check	[-]
α	Contact ratio	[-]
α	Stiffness-proportional damping coefficient	[-]
β	Reliability	[-]
β	Mass-proportional damping coefficient	[-]
β	Newmark-β parameter	[-]
γ	Newmark-β parameter	[-]
ϵ_{tol}	Energy tolerance	[Nm]
ζ	Damping ratio coefficient	[-]
η_1	Parameter controlling the shape of the unloading curve	[-]
η_2	Parameter controlling the shape of the unloading curve	[-]
θ	Model uncertainty parameter	[-]
μ	Mean value	n.a.
ρ	Correlation coefficient	[-]
σ	Standard deviation	n.a.
ϕ	Phase lag	[s]
ω_n	Natural angular frequency	[rad/s]

1

Introduction

On the 17th of October 2021, a concrete grandstand element of the Goffert stadium partially collapsed in Nijmegen, the Netherlands. It happened just after the football match NEC Nijmegen - Vitesse Arnhem. The victorious away team celebrated their triumph with the accompanying supporters by jumping at a certain rhythm conducted by the football players. After about 8 seconds of this rhythmic jumping, the grandstand collapsed. Fortunately, no one got injured. However, the consequences could have been catastrophic. Luckily there was a steel container below the grandstand element, which prevented it from falling.

Figure 1.1 shows the grandstand a few moments after the collapse. It can be appreciated that the structure broke in two, with the break line in the middle of the element. This indicates that exceedance of the bending moment capacity is the most probable failure mechanism. At the moment of collapse, 93 people were present at the grandstand. They were either jumping, bobbing, or standing still. The frequency at which they were jumping or bobbing was around 2 Hz.

Figure 1.1: The collapsed grandstand element, with people still on top of it. Below the element, the steel container can be seen. Image is taken from NU.nl [1].

1.1. Problem formulation

A structure should withstand the most severe conditions expected during its design lifetime with sufficient reliability. The collapse of the Goffert stadium means that its ultimate capacity was exceeded. This collapse has led to many discussions in the Dutch media, as the Goffert stadium comprises several of these elements. Another Dutch football stadium, the Erve Asito in Almelo, was built similarly, using the same components. Its structural integrity also became under investigation.

The municipality of Nijmegen, the stadium's owner, asked an engineering consultancy firm to investigate this partial collapse. One of the conclusions of this analysis [7] was that the loads generated by a jumping crowd are much higher than what the European Standard, EN 1991-1-1 [8], prescribes. The European Standard imposes loads of 4 kN/m^2 for seated and 5 kN/m^2 for standing places, whereas the consultancy firm claims that a jumping crowd can generate a load effect up to 9 kN/m^2. They concluded that the European Standard significantly underestimates the load. Therefore they recommend that the loads should be increased. If this is true, no grandstand element in the Netherlands probably complies with the obligatory reliability level.

Since its collapse, several reinforcements have been applied to the grandstand elements, meaning spectators can again, safely, enter the football stadium: one issue is hereby solved. The other, much more complex problem, has yet to be resolved: what is the reliability of such elements? Based on the conclusions of the previously mentioned report, the solicitation that a jumping crowd generates on a grandstand element is severely underestimated, which makes the structure less reliable than required. Does this mean no (concrete) grandstand element built in the Netherlands is safe? What about other countries in the European Union that design their constructions using the same Standards?

The Dutch government wants to know if the European Standards can guarantee obligatory safety levels. If not, the consequences would be far-reaching. Currently, no state-of-the-art method for determining a grandstand element's reliability is available.

1.2. Research objective and questions

This thesis aims to perform a reliability assessment of a concrete grandstand element. This thesis uses the Goffert stadium as a case study. Background documents of European Standards are examined. The physics behind jump-type loads is investigated. Safety levels are quantified to perform an unbiased reliability assessment of a crowd jumping on these elements. Non-linear material behaviour[1] is included. This approach results in a probability of failure. The reliability β and the probability of failure P_f of a structure are related through equation (1.1). This thesis describes the general steps required to create a probabilistic model, which can be used as a reference for future studies. The Goffert stadium is used as a case study and demonstrates the suitability of this approach.

$$P_f = \Phi(-\beta) \tag{1.1}$$

where:

P_f is the probability of failure;
$\Phi(\square)$ is the probability density function of the standard normal distribution;
β is the reliability level.

This study addresses three different topics: (1) dynamic loads generated by a jumping crowd; (2) modelling a concrete grandstand element suitable for non-linear analyses and subjected to dynamical loads; and (3) determining the reliability of a grandstand element using full probabilistic analysis. Together, they should lead to an answer to the main question, which is formulated as follows:

[1] Every structural element has an elastic and a plastic region regarding its capacity. The elastic region describes the point up to where a structure can be loaded and unloaded without permanent deformation. If a structure were to be loaded beyond this region, some deformation would be permanent. This results in a non-linear relation between external forces and the corresponding deformation. The plastic region allows for a higher external load than the elastic region, thus increasing the structure's capacity.

How can the structural reliability of a concrete grandstand element subjected to dynamical crowd loads be determined?

This question is decomposed into the following sub-questions, which provide a structured way to answer the main question:

- What load does a jumping individual generate?
- What load does a jumping crowd generate?
- Which shape is appropriate for modelling a jumping impulse?
- How can a concrete grandstand be modelled for dynamical analyses?
- How can the reliability of a grandstand element be determined?
- What is the probability of failure of a concrete grandstand element, such as found in the Goffert stadium?

1.3. Scope of this research

It is only feasible to include some possible scenarios in this thesis that contribute to the probability of failure of a concrete grandstand element. This report focuses on addressing the uncertainties related to solicitation. Therefore, some constraints are applied. The following constraints apply to this report:

- The focus is on two types of (vertical) loads: (1) the construction's self-weight; and (2) loads induced u a jumping crowd;
- Bending moment is considered to be the governing failure mechanism;
- The resistance model is based on the numerical resistance modelled of the engineering firm.

A construction's self-weight is always present and can not be omitted. Besides, loads induced by a jumping crowd are assumed to be the most severe. In reality, other loads, such as wind or snow, may simultaneously excite the structure, but these are not considered in this thesis. Including these would decrease the reliability. Additionally, crowds can also induce horizontal loads. These are also outside the scope of this study.

A concrete structure can fail in many ways besides bending moment failure. In order to completely map the reliability level of a structure, all possible failure mechanisms should be considered, but more information is needed for the complete study. The motivation behind this thesis is the collapse of the grandstand element in the Goffert stadium, which most likely exceeded its bending moment capacity, as depicted in figure 1.1. Therefore, this thesis considers bending moment as the failure mechanism.

Uncertainties are also found on the resistance side. As this thesis focuses on solicitation, the resistance model is partially mapped. It is assumed that the numerical resistance model of the engineering consultant is correctly determined. Two different type of sensitivity studies are incorporated, to evaluate their influence on the reliability of the structure. The probability of failure, as determined in this thesis, indicates what to expect. Future research should be devoted to these topics to map the complete probability of failure to a greater extent.

1.4. Structure of the thesis

Chapter 2 presents the literature study performed for this analysis. The literature presented in this chapter acts as the theoretical background. The physics behind jumping on rigid and flexible bodies are examined. Chapter 3 mentions the method used to perform the reliability analysis. This chapter first introduces the underlying equations. This is followed by sections about the generation of excitation signals. Next, a reliability method is proposed. The final paragraph introduces a case study. Chapter 4 presents the results of the reliability analysis, including those of the case study. A discussion of the results is provided in chapter 5. Chapter 6 concludes this thesis. Finally, recommendations for future research are found in chapter 7.

2

Literature review

A proper load model is an essential part of the reliability analysis. The loads are introduced on the grandstand element because people jump on it. This chapter summarizes the most relevant findings related to the physics behind a jumping crowd. This chapter has two aims. Firstly, where possible, quantify each parameter that is relevant for jumping loads as a random variable. Secondly, be able to generate synthetic excitation signals. These signals are required for the reliability analysis. First, an introduction to loads exerted by jumping is given. This is followed by a section that discusses the load an individual generates when jumping on a rigid body. In the third section this phenomenon is extrapolated to loads generated by a crowd. the fourth section mentions how jumping on a rigid body differs from jumping on a flexible body. Finally, conclusions of the literature review are presented.

2.1. An introduction to loads generated by jumping

When a person jumps on a body, they generate a force on it. In figure 2.1, this is visualized. The person can be schematized as a point mass (denoted as m) and spring (with spring stiffness k). In the left figure, the person is in the air: they exert no force on the floor. The central figure represents the initiation of contact. The person is no longer in the air, but their knees have not yet bent. This is the initiation point. In the right figure, the person has bent their knees. Their point mass has lowered, compressing the spring and resulting in a force exchange with the ground through equation (2.1).

$$F(t) = k\, u(t) \tag{2.1}$$

where:

$F(t)$ is the dynamic force of a jump at time t;
k is the equivalent spring stiffness of the person's legs;
$u(t)$ is the displacement at time t.

Multiple people can jump on a body at the same time. The total force exerted is equal to the summation of each individual's contribution. However, even when people try to time their jumping motion together perfectly, the total force will not be equal to the force that an individual exerts multiplied by the number of people: tiny phase differences result in a reduced total load. There is also a difference between jumping on a rigid body and jumping on a flexible body. Take, for example, jumping on a concrete floor and jumping on a mattress. A concrete floor does barely deform when someone jumps on it, meaning the forces exchange rapidly. However, when jumping on a mattress, the mattress also deforms and slows down the exchange of forces. This results in a reduced peak of the force exerted on the structure. The following three sections handle one of the above-introduced phenomena in the presented order.

2.2. Loads generated by an individual jumping on a rigid body

This section describes the load an individual exerts on a rigid body, which is best described by introducing the jump factor $\tilde{F}(t)$. The jump factor is the ratio of the force an individual generates by jumping divided by that person's static weight. The motivation behind this is that it allows for the comparison of jumping forces of different people with different weights: the exerted dynamic force means little without knowing that person's weight. In practice, only the maximum value of the jump factor is of interest. Therefore, $\tilde{F}(t)$ is often abbreviated to $\tilde{F}$.

$$\tilde{F}(t) = \frac{F(t)}{G} \tag{2.2}$$

where:

$\tilde{F}(t)$ is the jump factor at time t;
G is the static weight of the person.

Bachmann and Ammann [9] were one of the first to describe a model for human-induced loads, including, but not limited to, jumping activities. They concluded that for periodic loads, not only the actual excitation frequency is important: higher harmonics also contribute to the force. They used a Fourier series to describe the load. Similar research from the same period led to the same findings (e.g., Rainier et al. [10]). Later, Ellis and Ji [11] improved the model proposed by Bachmann and Ammann. Their suggestion is shown in equation (2.3). Figure 2.2a shows the result of this equation for three different contact durations. Many Standards (e.g., ISO, British Standards, Canadese Building Code, SBR [12–15]) prescribe this equation for dynamical jumping loads.

$$F(t) = G\left(1.0 + \sum_{n=1}^{\infty} r_n \cdot \sin\left(\frac{2n\pi}{T_p}t + \phi_n\right)\right) \tag{2.3}$$

where:

r_n is the Fourier coefficient of the *n*-th harmonic;
n is the number of the *n*-th harmonic;
T_p is the period of the activity (hereafter: jump period);
ϕ_n is the phase lag of the *n*-th harmonic relative to the first harmonic.

Two questions arise from this equation, which will be discussed in the following two subsections:

1. What is the amplitude of the total load?
2. Is a sine function appropriate to describe the load?

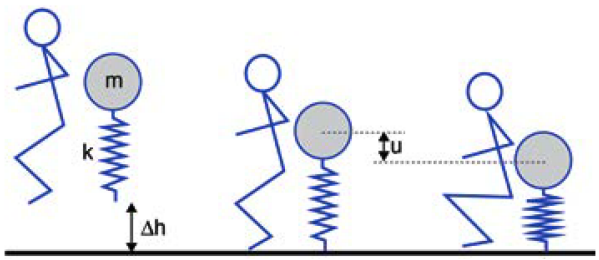

Figure 2.1: A schematization of a person jumping on a rigid body. Image is taken from Spanenburg [2].

2.2.1. The amplitude of a single jump

The load amplitude is related to the coefficients r_n, and phase lags ϕ_n of equation (2.3), which was proposed by Ellis and Ji. They linked the jump factor to the contact ratio α and determined the Fourier coefficients of the first six terms. The contact ratio is defined as follows:

$$\alpha = \frac{t_p}{T_p} \leq 1.0 \tag{2.4}$$

where:

α is the contact ratio;
t_p is the contact duration between the person and the ground.

A lower contact ratio means that the air-time is higher, from which analogously follows that the jump factor will be higher. Bachmann and Ammann [16] stated that, based on physiology, the contact duration is at least 0.15 s.

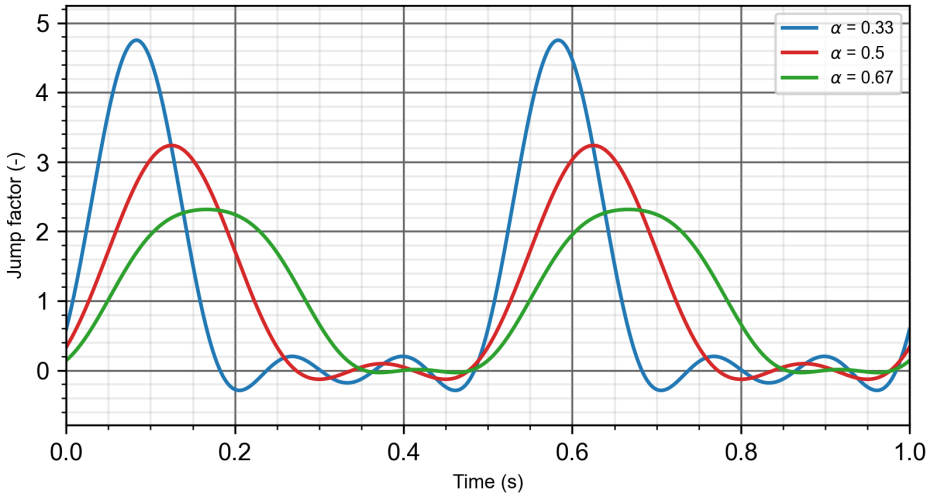

(a) The force signal model of an individual jumping at 2 Hz, as proposed by Ellis and Ji [11].

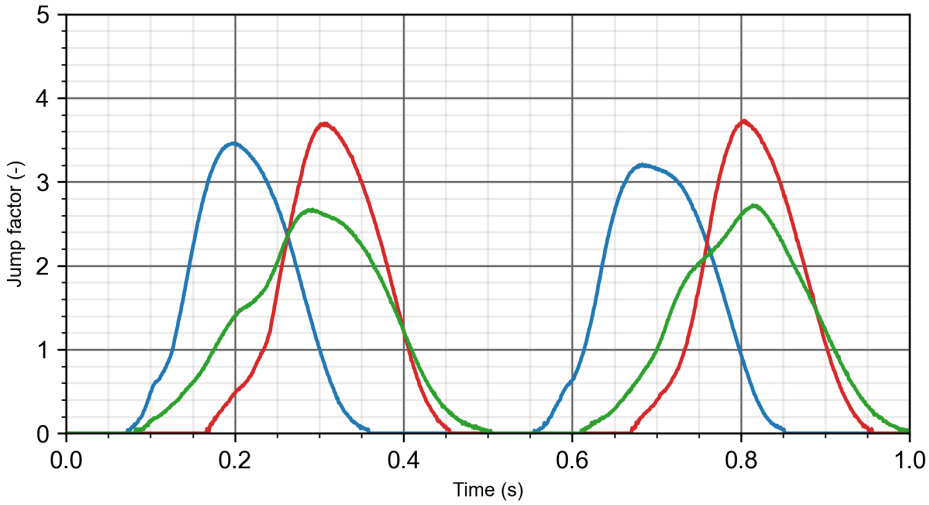

(b) An actual force signal of an individual jumping at 2 Hz. Data is taken from Xiong and Chen [17].

Figure 2.2: A comparison between the force model and the actual force of a jump.

Figure 2.2a presents the force signal for jumping at a frequency of 2 Hz for three different contact ratios. Ellis and Ji determined that the jump factor varies between 2.3 and 4.8, depending on how an individual jumps [11]. The author was not able to establish the statistics behind this value. Spanenburg [2] suggests that these are maximum values but did not mention a source that supports this claim. Almost all future research is built upon this study, but the statistics behind the jump factor's distribution have - to the authors knowledge - yet to be examined.

Xiong and Chen recently published a paper [17] in which they shared data of jumping people. This data set contains the answers to the questions mentioned earlier. Evaluation yields the expected value of the desired quantities, along with their statistical uncertainties. Therefore this contributes significantly to generating a signal that is as close as possible in line with the physics. This data set acts as the basis for finding random variables' distributions. The results will be compared to previous literature.

2.2.2. The shape of the load

Another topic that arises is the use of a sine shape itself. Figure 2.2b presents one second of data for three individuals jumping at 2 Hz from the data set. Comparing these two figures shows that the impulse cannot perfectly be described using a sine function. Sim et al. [6] have shown that this becomes more evident for lower frequencies. Here, the impulse is likely double-peaked. It is not clear what the double peak represents. In 2008, Sim et al. [6] stated that the first peak corresponds to landing and that the second peak represents the new launch, while two years prior to this study, Sim [18] related the first peak to the landing of the toes, and the second peak to the landing of the heels.

Although broadly used, it has only been verified how good of a fit this shape is once Sim et al. [6] fitted a normal distribution, a cosine, and a cosine-squared function over the impulse. Note that taking a cosine function to describe the shape is the same as taking a phase-shifted sine function. They concluded that the cosine-squared function is the best fit to describe the impulse (apart from the lowest frequency), as can be read from table 2.1.

Table 2.1 Mean of All μ_{RMSE} for curve-fitting measured impulses with normal distribution, cosine, and cosine-squared functions. Table is taken from Sim et al. [6].

Beat frequency (Hz)	1.5	2.0	2.67	3.5	Total
normal distribution	0.2551	0.1261	0.0878	0.0984	0.5673
cos(t)	0.1670	0.1298	0.1435	0.1108	0.5511
$\cos^2$(t)	0.1976	0.0894	0.0808	0.0649	0.4327

One of the significant drawbacks of using perfect periodic functions is that harmonics of the Fourier series could result in a resonant response. A perfect periodic signal will only have non-zero values at the base frequency and higher harmonics. This response is purely artificial since the actual frequency spectrum will show some energy leakage to adjacent frequencies around its base frequency, which becomes more profound for increasing harmonics [19]. To the authors' knowledge, no efforts have been made to establish a parameter that prescribes a suitable distribution for each jump period.

Pavic and Racic [20] improved the construction of a signal by reconstructing the shape using two normal distributions, accounting for asymmetries in the jumping impulse, which is impossible to achieve when using a sine-based function. Later they improved their model even further by extending this concept to any number of normal distributions [21]. This model can generate any arbitrary shape, resulting in a narrow-banded spectrum. However, this method can only recreate existing jumping impulses if every normal distribution can be determined randomly. Additionally, computational cost becomes increasingly more important if each jumping impulse is created using multiple normal distributions.

Since creating a synthetic excitation signal is the goal, using normal distributions is not the way forward. To be able to create a narrow-banded spectrum, this thesis investigates the feasibility of randomizing the period of each jump. A 30-second time signal of a person jumping generates a number of sine

functions equal to 30 times its jumping frequency, e.g., a person that jumps at 2 Hz generates 60 sine functions with a different period. Concatenated sine functions with a slight period difference could lead to a narrow-banded spectrum around the jumping frequency and its harmonics.

This section investigated the load induced by a jumping individual. An important parameter is the jump factor $\tilde{F}$, whose values lie between 2.3 and 4.7, depending on the type of activity. No distribution is known for this parameter. Evaluation of the data set should provide a suitable distribution.

The shape of the impulse is most often modelled using a sine. However, a sine-squared function is more suitable for 2 Hz and higher frequencies. Therefore, a sin-squared function is used. In order to overcome artificial resonant effects, a narrow-banded spectrum should be constructed. Parameters to include this in a model have yet to be discovered.

2.3. Loads generated by a crowd jumping on a rigid body

There is a significant difference between the loads generated by an individual and the loads generated by a crowd. The load factor coming from a crowd is more complex than simply multiplying the one from an individual by the number of people in the crowd: the load is attenuated. There are two ways to incorporate this phenomenon in a signal. The first is implementing a coordination factor, which is a scalar multiple (< 1). The second option is multiplying the period of each jump with a random variable and combining it with a phase lag between individuals. The following two subsections each discuss one of the two possibilities.

2.3.1. The coordination factor

The coordination factor is the ratio between the average jump factor a crowd generates and the jump factor an individual generates. This factor can also be written as the ratio between the loads generated by a crowd and their static weight: then it is called the jump- and coordination factor.

Ebrahimpour and Sack [22] concluded that, for increasing group sizes, the jump- and coordination factor tends to go to a constant value. Their study found a factor of 1.55 for a group. Unfortunately, there is no information about one's individual jumping data, so this number cannot be translated into a coordination factor. However, based on Ellis and Ji's findings of the jump factor of an individual (between 2.3 and 4.7), this would result in a coordination factor between 0.32 and 0.67.

Ellis and Ji [23] also concluded that the coordination factor tends towards a constant value for larger crowds. Their research was a lot more extensive than Ebrahimpour and Sack's. Ellis and Ji conducted experiments with up to 64 people, whereas Ebrahimpour and Sack had a limited group size of up to 4 people. Furthermore, unlike Ebrahimpour and Sack, Ellis and Ji's research related the crowd size to the Fourier coefficients of equation (2.3). They could determine the first three coefficients as a function of the number of people. Spanenburg [2] translated the influence of these coefficients to a general reduction in the jump factor while also including a study done by Faísca [24]. Both coordination factors tend to go to a constant, as is shown in figure 2.3. The coordination factor, as determined by Ellis and Ji, leads to a reduction of about 40%, while Faísca claims that the total load halves.

Chen et al. [25] also concluded that the coordination factor tends to go to a constant value. They found that the jump factor quickly decreases for a group of up to 10 people. After this, the gradient becomes more stable, up to 20 people, after which it turns more or less into a constant. They found that the jump factor reduces by only 20%.

ISO [12] makes recommendations on the Fourier coefficients for large group sizes ($n > 50$). Depending on the coordination level of the group, the values for the first three harmonics change. Reduction factors between 0.55 and 0.89 are found, depending on the type of activity and level of coordination.

The major drawback of using a reduction factor is that it does not have any physical meaning: the reduction has to come from some phenomenon. In addition, the literature is divided into what value to

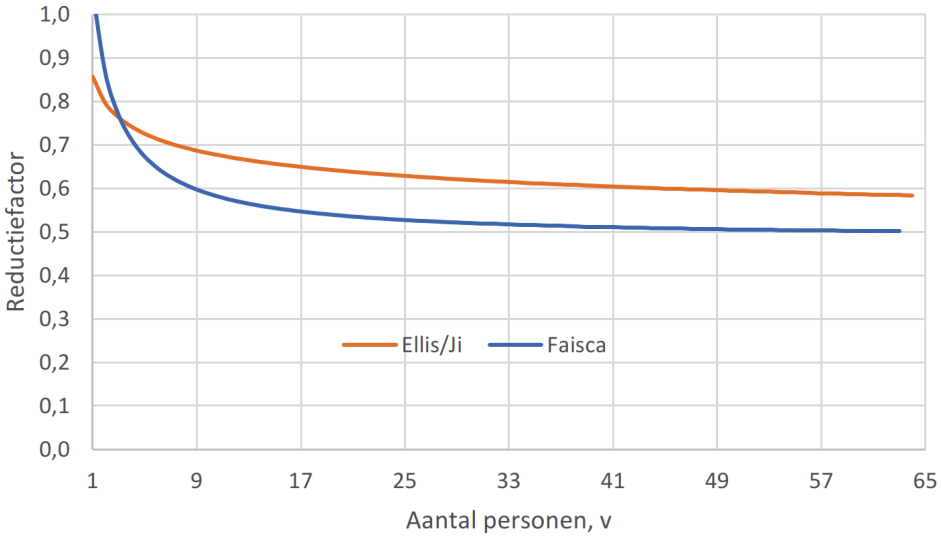

Figure 2.3: Reduction coefficient as a function of the group size, according to Ellis and Ji and Faísca. The reduction coefficient is given on the vertical axis, and on the horizontal axis, the number of persons is shown. Image is taken from Spanenburg [2].

assign to the jump factor, ranging from 0.50 to 0.89. Due to the high spread and the lack of a physical phenomenon, this thesis will not use a coordination factor.

2.3.2. The period of each jump and the phase lag between individuals

To extrapolate the load induced by a jumping individual to that of a jumping crowd, two phenomena can be incorporated. The first one is to multiply the period of each jump T_p with a random variable. This results in an aperiodic signal for each individual. The second one is by incorporating a phase lag ϕ between individuals, which represents the preference of how persons time their jumps.

The period of each jump

Ellis and Ji [23] studied the influence of the variations in jumping period, contact ratio, and phase lag on the Fourier coefficients. While the first two do not influence the result significantly, the latter does play a significant role in the coefficients. Slight differences in timing between individuals in a group can thus lead to significant differences in the response.

Chen et al. [25] showed that the jumping period could be modelled using a normal distribution with a mean of $\mu = T_p$ and a standard deviation of σ = 0.05. This phase lag is more or less frequency-independent. However, Racic and Pavic [26] showed that, for 2 Hz, the jumping period has a standard deviation of $\sigma = 0.011$ s, indicating that the literature is divided over what value to use. To the author's knowledge, these are the only two findings regarding the distribution of the period of each jump.

The phase lag between individuals

Ellis and Ji [23] are, to the author's knowledge, the only ones to mention a standard deviation for the phase lag. They found a value of $\phi = 0.18\pi$. In many cases (e.g., Ebrahimpour and Sack [22]), a uniform distribution is chosen with angles between -180° and 180°, although there are studies that doubt this method (e.g., Pavic and Racic [21]).

The importance of the phase lag can easily be visualized. Figure 2.4 shows a simple illustration where the sum of two sine functions is taken, each having a period of 0.25 s, while one has a phase lag of 0.05 s: the sum of these two is, at its highest point, equal to 1.62. Since the maximum value of a single sine function is 1, the summation of only two sine functions has already led to a reduction of 20%.

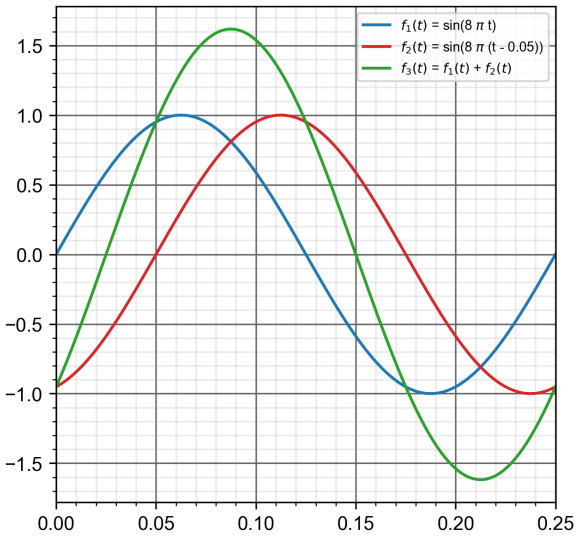

Figure 2.4: Taking the sum of two phase-shifted sine functions clearly shows that small phase shifts can lead to a large reduction in the total outcome.

Estimating the standard deviation of the random variables by using the data set

Xiong and Chens' data set also comprises 92 files of jumping crowds of up to 48 people. Each individual's signal is shared. The summation and normalization of all the data yields a normalized jump - and coordination factor. This reduction is assumed to be solely the combination of the randomized periods and phase lags. In addition to sharing the signal in its time domain, they have also shared the signal in its frequency domain. There is some unity to be found in the literature regarding the distribution of the period T_p: a normal distribution is proposed. This information is lacking for the phase lag ϕ. Here, a normal distribution is also assumed. By trying different combinations of standard deviations for the period and the phase lag, estimations for the standard deviation are found.

In this thesis, the dynamic load belonging to a jumping crowd is modelled by summing up multiple individual excitation signals, each having a random phase lag. In addition, each jump period in each signal is also randomized. Since there is no agreement in the literature on how the jumping period and the phase lag should be modelled, several possible standard deviations are tested in generating the excitation signal. The synthetic signal is compared with the data set to check the suitability of this method.

2.4. The load effect of a crowd jumping on a flexible body

The previous two sections discussed the load that a jumping individual and a crowd induce, respectively. The amplitude of these loads was determined on a rigid body. Rigid bodies do not deform when subjected to external forces: they are infinitely stiff. Flexible bodies, such as a concrete grandstand element, respond when a force is exerted on them, e.g., by vibrating when subjected to dynamic loads. This reaction, in turn, influences the load effect. This section investigates the effect of interaction between humans and structures and how this can be incorporated into creating the excitation signal.

How a structure responds to a load depends, among other things, on the loading frequency. The frequency range of jumping is therefore first investigated. Secondly, the relation between jumping frequencies and structural response in the European Standards is discussed. Thirdly, the influence of human-structure interaction is considered. Human structure interaction could influence the load effect a crowd induces and alter the jumping behaviour.

2.4.1. The frequency range of jumping for crowds

Ginty et al. [27] have done an extensive research on the frequency range of jumping for individuals and crowds. They found the following frequency ranges:

- 1.2 - 2.8 Hz for individual jumping;
- 1.5 - 2.5 Hz for a small group jumping with some degree of coordination;
- 1.8 - 2.3 Hz for a large group jumping with some degree of coordination.

Other studies find higher limits for large groups. Bachmann and Ammann [16] state an upper bound of 3.4 Hz. According to Littler [28], 3.5 Hz is possible; the latter is in compliance with ISO 10137 [12].

Based on this information, the frequency at which people were jumping in the Goffert stadium - 2 Hz - is comfortable for both individuals and large groups.

2.4.2. Requirements to perform a dynamical analysis according to the European Standards

EN 1991-1-1 Dutch National Annex Article 2.2 (3) [8] states that no dynamical analyses are required for small structures with an elastic eigenfrequency[1] ω_n of at least 8 Hz. The reason behind this is that human-induced loads - such as jumping - happen at low frequencies and thus will not lead to a resonant response[2]. Replacing the dynamic force with a higher static one usually is sufficient for designing structures.

Jumping at 2 Hz could lead to a resonant response in, at least, the fourth harmonic, i.e., 8 Hz. However, the amplitude of harmonics decreases for increasing harmonics [29], resulting in a small contribution to the force for that specific frequency. Herefore, it makes sense to refrain from performing a dynamical analysis. However, the assessment that this thesis performs includes non-linearities. Plastic deformation can therefore occur, which reduces the stiffness and, thus, the system's eigenfrequency. The relation between the stiffness and the eigenfrequency is given in equation (2.5).

$$\omega_n^2 = \sqrt{\frac{k}{m}} \tag{2.5}$$

where:

ω_n^2 is a structure's natural frequency or eigenfrequency.

The goal of this thesis is to determine the reliability of a concrete grandstand. That is why a dynamical analysis is performed contrary to the European Standards recommendations. Including dynamics results in a more accurate reconstruction of the actual situation.

2.4.3. Human-structure interaction

Human-structure interaction (HSI) influences the response of a structure to a load. Unlike rigid bodies, (underdamped) flexible structures respond to dynamical loads by oscillating themselves. This oscillation changes the force exchange between the human and the structure.

Ellis and Ji [30] have conducted tests on an empty cantilevered grandstand and a fully occupied grandstand. They noticed a significant damping contribution when humans stood still or sat on the structure. Furthermore, they found a reduced eigenfrequency. This is easily explained by looking at equation (2.5).

[1] The eigenfrequency, or natural frequency, of a structure, is the frequency at which an undamped structure oscillates in the absence of a driving force, given non-zero initial conditions.

[2] Resonance is a phenomenon where the amplitude of an oscillation increases significantly, as a result of the period of the force (or a higher harmonic of it) approaching the eigenfrequency of the system.

A stationary crowd acts as an additional mass to the system, thus reducing the eigenfrequency. No changes in the measured system characteristics were found when people jumped or walked on the structure. This indicates that an active crowd acts solely as a load.

Shahabpoor and Pavic [31] have shown that including HSI can lead up to a 35% reduced force experienced by the human, compared to a model where the structure is assumed to be rigid. They mention three different mechanisms that affect the force.

First, they looked at the momentum exchange between the masses of the two bodies. Under the assumption that energy does not dissipate from the system, the principle of conservation of momentum states that part of the momentum of the human is transferred to the momentum of the structure during the impact. This decreases the momentum of the human. A change in momentum is equal to a change in impulse, hence resulting in a lower force:

$$F\Delta t = m\Delta v \tag{2.6}$$

where:

$F\Delta t$ is the change in impulse;
$m\Delta v$ is the change in momentum.

Secondly, flexible structures do not instantly take up all force: they require time. The result is that there is more time for a person to decelerate, which means that the force, in turn, also decreases. Assuming that the change in momentum stays the same, according to equation (2.6), an increase in the time required to transfer the impulse results in a lower force compared to a rigid body.

The third mechanism is related to the damping of the structure. As mentioned earlier, damping accounts for the dissipation of mechanical energy. A rigid body oscillates, which means it also dissipates energy.

Yao et al. [32] performed tests where an individual jumps with a frequency of 2 Hz on a flexible structure, with an eigenfrequency of either 4 or 6 Hz. An eigenfrequency of 4 Hz results in resonance in the second harmonic, and an eigenfrequency of 6 Hz in the third harmonic.

For the structure with an eigenfrequency of 4 Hz, a maximum jump factor of about 2.5 was found, which is on the lower side, compared to jumping on a rigid body. For jumping at 6 Hz, a maximum jump factor of 3.3 was found, which is more in line with what to expect on a rigid body (see figure 2.2. This suggests that the third harmonic of a signal does not lead to a resonant response.

Another interesting finding from this study is that when an individual jumps at a structure with an eigenfrequency of 6 Hz, no peak is found at 6 Hz when the force signal is shown in the frequency domain. This is shown in figure 2.5a. It seems to be difficult to excite a flexible structure in a frequency equal to its eigenfrequency.

Gaspar et al. [33] came to the same conclusion. They found a substantial reduction in the load factors for the first three harmonics when a resonant motion is induced. Overestimations of up to 192% were found. This is shown in figure 2.5b. For non-resonant excitation frequencies, there is little profit to gain from including HSI.

Appelman [34] conducted numerical experiments on a lightweight steel structure. He concluded that including HSI could result in up to a 17% reduction of the peak force when an individual jumps onto the structure. Additionally, he performed experiments where crowds of 16 people jumped on the structure with small time lags. This test concludes that, on average, there is no reduction of the peak force when taking the flexibility of the structure into account. It should be mentioned that eigenfrequencies of 20 Hz and higher are meant with lightweight structures. Resonance is, therefore, out of the question.

The above-mentioned study has shown that in non-resonant cases, the flexibility of the structure does not necessarily lead to a reduced force. Although including HSI results in a decreased response in the

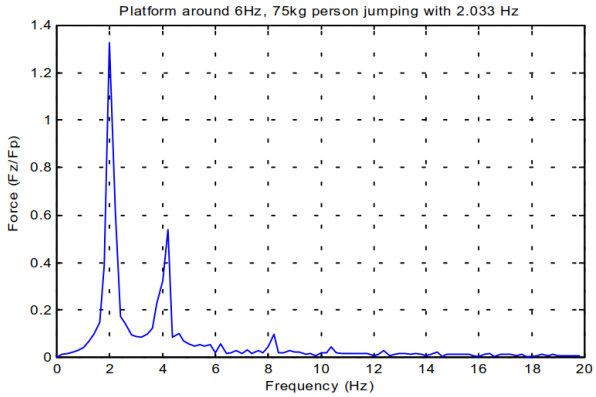

(a) The third harmonic of the forcing frequency, which corresponds with the eigenfrequency of the system, is almost completely attenuated. Image is taken from Yao et al. [32].

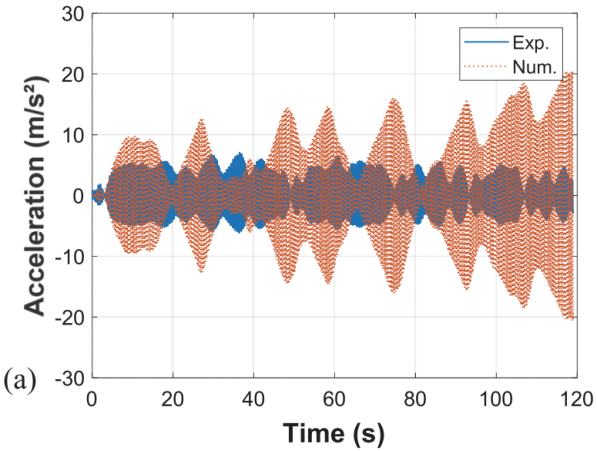

(b) A high difference between experimental and numerical values can occur when a simple model is used. Image is taken from Gaspar et al. [33].

Figure 2.5: Two indications that forces are attenuated when they lead to a resonant motion. This is shown in the frequency domain (left) and the time domain (right).

case of resonance when an individual jumps on it, there is not enough information to extrapolate this to the effect it has on a group. HSI is, therefore, not included in this thesis, which is a conservative approach.

2.5. Conclusions

This chapter investigated the load effect a jumping crowd generates and what can be used to construct a synthetic acceleration signal. This signal is required to perform a reliability analysis.

Currently used load models in building codes are all based on sine-shaped functions, although a sine-squared function is a better fit for higher frequencies. The jump impulses are, therefore, sine-squared shaped. The jump factor is between 2.3 and 4.8 and depends on the contact ratio. The data set serves as a basis for the distribution type and parameters for the two variables.

The amplitude of the total load does not increase linearly with the number of people. As a result of slight differences in timing between individuals, the total load reduces compared to multiplying a load of an individual by the number of people. Although literature and building codes are mainly focused on a coordination factor, in this thesis, the reduction is applied by randomizing the period of each jump and including a phase lag. Suitable standard deviations are estimated using the database.

According to the European Standard, a dynamical analysis is not required for structures with an elastic eigenfrequency of at least 8 Hz. Nevertheless, this thesis will perform a dynamical analysis, as this better represents the actual situation.

Although adding HSI in the system would lead to a more accurate result, there is not enough information on how to incorporate this in a model. Not including HSI is a conservative approach; therefore, it is not included.

3 Method

Chapter 3 describes the method used to determine the reliability of the concrete grandstand element in this study. First, the dynamics of a single-degree-of-freedom (SDOF) system are presented. An SDOF system allows for the schematization of the dynamic response of a concrete grandstand element. The second subsection presents the method of how the system is solved. The system has to be excited by a signal. The data set is analyzed in section 3.3, which is used to create an excitation signal: this is presented in section 3.4. Section 3.5 demonstrates how the reliability of a grandstand element can be determined using full probabilistic analysis. Finally, in section 3.6, the Goffert stadium case study is introduced.

3.1. The mechanical system

This section describes the construction of the mechanical system. The first subsection briefly outlines how structural dynamics of a linear SDOF system work. In the second subsection, the dynamics of a non-linear system are discussed.

3.1.1. Dynamics of a linear single degree-of-freedom system

This subsection describes the dynamics of a linear SDOF system. The dynamics of a linear SDOF system are described in a concise manner, which acts as a stepping stone to the more complex, non-linear SDOF system.

Using Cartesian coordinates, each mass in a dynamical system has six degrees of freedom: three translations and three rotations. However, in most cases, not all degrees of freedom are of interest: this depends entirely on the type of analysis performed. E.g., for a high-rise building subjected to an earthquake, the horizontal displacement at the top is the most interesting unknown parameter. Similarly, the vertical displacement at midspan is the most critical parameter for a grandstand element subjected to a jumping crowd.

For this type of study, a grandstand element can be modelled as a single mass that can only translate vertically. Section 2.4 concluded that the crowd acts solely as a load, leaving this system with one mass. The entire system can therefore be modelled as an SDOF system. SDOF systems are solved quicker than systems of higher order or finite element method (FEM) programs since this system contains fewer variables. Figure 3.1 shows the mechanical system of the grandstand element that can be used for linear analyses.

For each dynamical system, an equation of motion (EOM) should be derived to describe its behaviour. The EOM is an extension of Newton's second law, which equates the balance of forces acting on a mass and describes the displacement of an object as a function of time. It is a second-order, linear

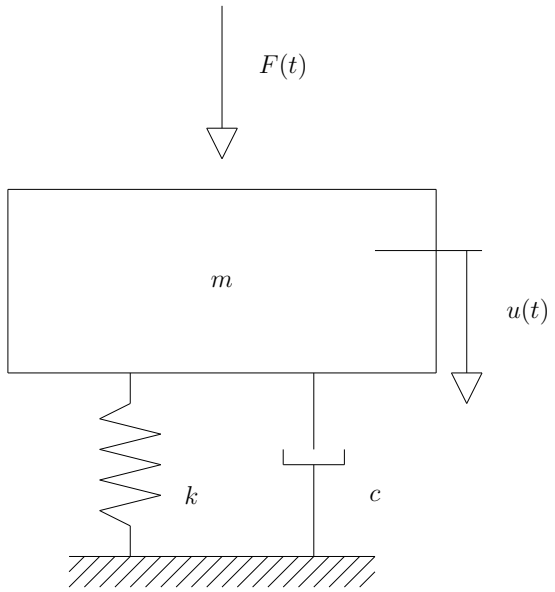

Figure 3.1: An equivalent mass-damper-spring system of the concrete structure, to be used for linear analyses only.

differential equation. Equation (3.1) shows the EOM of a grandstand element. Dividing equation (3.1) by m shows the EOM in its canonical form (see equation (3.2)), which gives a more convenient notation for mathematical operations. All parameters from equation (3.1) and equation (3.2) can be used interchangeably, and in practice, this is done often.

$$m\ddot{u} + c\dot{u} + ku = F(t) \tag{3.1}$$

where:

m is the mass of the grandstand element;
c is the viscous damping of the grandstand element;
k is the stiffness of the grandstand element;
u is the midspan displacement of the grandstand element;
$\dot{\square}$ means a derivative with respect to time;
$F(t)$ is the force at time t.

$$\ddot{u} + 2\zeta\omega_n\dot{u} + \omega_n^2 u = \frac{F(t)}{m} \tag{3.2}$$

where:

$\zeta = c/2\sqrt{km}$ is the damping ratio coefficient of the grandstand element;
$\omega_n = \sqrt{k/m}$ is the angular eigenfrequency (or the natural angular frequency) of the grandstand element.

This EOM is solved for the unknown displacement $u\,(t)$, given a certain excitation $F(t)$. Even when no external force excites the structure, it can still translate. This happens when the object is subjected to non-zero initial conditions, which can be the initial displacement $u_0 = u\,(t = 0)$, the initial velocity $v_0 = v\,(t = 0)$, or both. If a structure has zero damping, i.e., $\zeta = 0$, no energy in the system is dissipated, and the structure would theoretically oscillate forever. The period of this oscillation would be equal to $2\pi/\omega_n$ s.

Equation (3.1) can be solved analytically for certain types of excitation forces (e.g., harmonic loading) by decomposing the solution into a homogeneous part and a particular part. Since the system is linear,

the total solution has to be the sum of the two solutions: this is known as the superposition principle. Another method to solve the EOM is the use of Duhamel's integral. Duhamel's integral is based on the integration of impulse loads, which allows it to be used for any arbitrary excitation signal. This concept is also based on the superposition principle and thus can only be used for linear systems.

Rayleigh damping

Damping is defined as the dissipation of mechanical vibration energy from the system [35]. In equation (3.1), the damping force is presented as a term that is proportional to the system's velocity. This is called viscous damping. In reality, damping is a complex phenomenon consisting of multiple mechanisms. Viscous damping, therefore, only simplifies the actual behaviour, which highly depends on the material properties of a system and the system as a whole. Nevertheless, it is widely used in structural dynamics since the equation of motion becomes a linear differential equation, which reduces the computational effort required to solve the problem.

Computer programs often use modal analysis to solve elastic problems. To quickly solve large systems (i.e., systems with more than one DOF), the equation of motion is decoupled into a set of independent, linear equations. In order to do this, the damping matrix is defined as a matrix proportional to a combination of the mass and stiffness matrices, respectively. This makes the damping matrix diagonal, which generally is not the case. This proportional damping is also known as Rayleigh damping. For an SDOF system, the matrices become scalar values. Rayleigh damping for an SDOF system is defined as:

$$c = \alpha k + \beta m \tag{3.3}$$

where:

α is the stiffness-proportional damping coefficient;
β is the mass-proportional damping coefficient.

Using equation (3.2), the damping ratio can be related to the Rayleigh coefficients:

$$\zeta = \frac{1}{2}\left(\alpha\omega_n + \frac{\beta}{\omega_n}\right) \tag{3.4}$$

Equation (3.4) shows that the stiffness-proportional damping coefficient is proportional to the system's natural frequency, and the mass-proportional damping coefficient is inversely proportional to the system's natural frequency. Caution is therefore required when choosing the parameters. The most common assumption is the case of stiffness-proportional damping, i.e., $\beta = 0$ [36]. The stiffness-proportional damping term is then equal to the following:

$$\alpha = \frac{2\zeta}{\omega_n} \tag{3.5}$$

3.1.2. Dynamics of a non-linear single degree-of-freedom system

This subsection deals with a non-linear SDOF system. Only systems with a non-linear force-displacement relationship are considered: other non-linearities are outside the scope of this study.

The non-linear region is reached once the yield strength of a material is exceeded. This region acts as an additional capacity of the system. Figure 3.2 shows an example of a bi-linear relationship between the force and the displacement of a system. The subscripts y and u stand for yield and ultimate, respectively, indicating the yield point of the structure and its failure point.

Design codes are usually strength-based, meaning that the design loads should not lead to yielding. When including the non-linear region, the focus changes to a displacement-based criterion. This criterion states that the maximum displacement of the system does not exceed its capacity. This is a

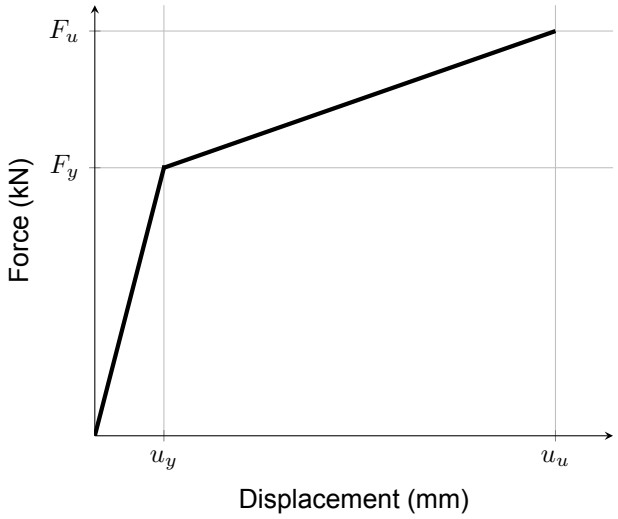

Figure 3.2: An example of a bi-linear force-displacement relationship. A positive slope on the non-linear part indicates strength hardening.

commonly-used design criterion in seismic design [4], but it is also applicable to this analysis.

The EOM of a non-linear SDOF system is presented in equation (3.6). Comparing equation (3.6) to equation (3.1), the restoring force in equation (3.6) is responsible for the non-linearity.

$$m\ddot{u} + c\dot{u} + f_s\left(u, \text{sgn}\left(\dot{u}\right)\right) = F(t) \tag{3.6}$$

where:

$f_s\left(u, \text{sgn}\left(\dot{u}\right)\right)$ is the restoring force of the system;
$\text{sgn}\left(\square\right)$ is the signum function.

There are several phenomena related to the restoring force. This analysis incorporates two phenomena: hysteresis and strength hardening.

Hysteresis

Hysteresis is a phenomenon encountered in many disciplines, e.g., an electronic comparator, a beam in a magnetic field, and an inelastic spring [37]. In the broadest sense, hysteresis means that there is a looping relationship between the input of a system and its output. Figure 3.3 shows an example of a hysteresis loop.

In structural dynamics, hysteresis loops can be found when plotting a system's force (input) versus displacement (output) over time. Each enclosed loop has an area with units N · m, which equates to work (or energy). This energy is dissipated from the system and explains why hysteresis acts as a restoring force.

The parameters related to the hysteresis loops are unique for every system and should be derived from tests. The dissipated energy highly depends on the chosen parameters. If, for example, the (un)loading stiffness is equal to the secant stiffness[1], the hysteresis loop would be a line. As a result, no area is enclosed by the loop, and no energy is dissipated from the system.

[1] Secant stiffness means that the unloading pattern goes directly to the origin, which means that no permanent plastic deformation occurs.

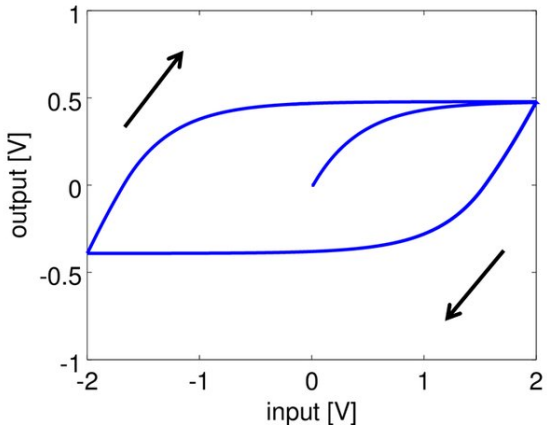

Figure 3.3: An example of a hysteresis loop. Image is taken from Tatebatake et al. [3].

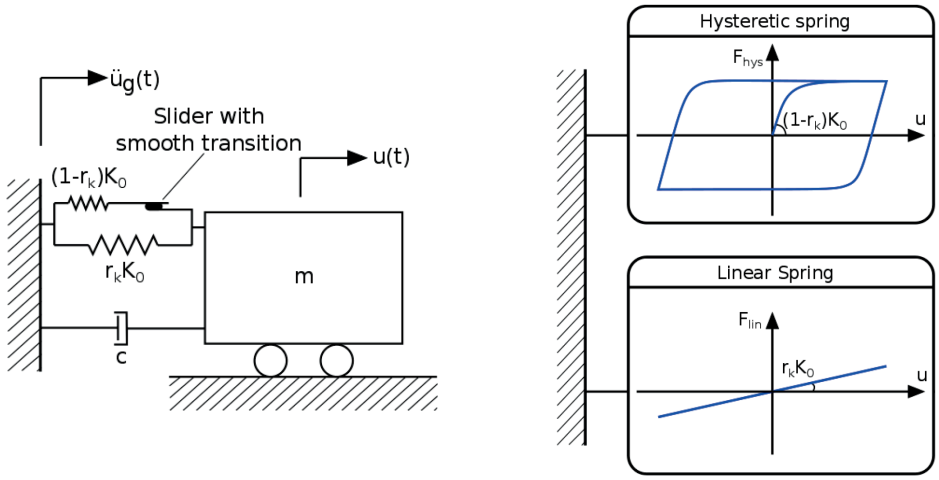

Figure 3.4: An example of a model with hysteresis and a bi-linear strength hardening, used for earthquake analysis. Image is taken from Tsouvalas [4].

Strength hardening

Strength hardening is a concept that has been handled before: figure 3.2 shows an example of (bi-linear) strength hardening. When the yield resistance of a system is exceeded, if beyond yielding, its resistance keeps increasing for increasing deformations, then the system possesses strength hardening. This system becomes stronger through plastic deformations.

The stiffness beyond the yield point is (almost always) lower than the initial stiffness. In reality, the transition from the linear to the non-linear phase follows a more smooth curve. Typical values for strength hardening in concrete structures are about 5% [38].

A combined system including hysteresis and strength hardening

Figure 3.4 shows a non-linear system subjected to hysteresis and strength hardening. In this figure, r_k is the ratio between the pre-yield and post-yield stiffness. From the force-displacement plots on the right, it follows that if $r_k = 0$, there is no additional capacity beyond the point of yielding, and if $r_k = 1$, the system behaves elastically.

The combination of these two phenomena can be modelled as two springs in parallel (as is shown in figure 3.4). It is well known that for a system with springs in parallel, the equivalent stiffness of a system is equal to the summation of all individual spring stiffnesses:

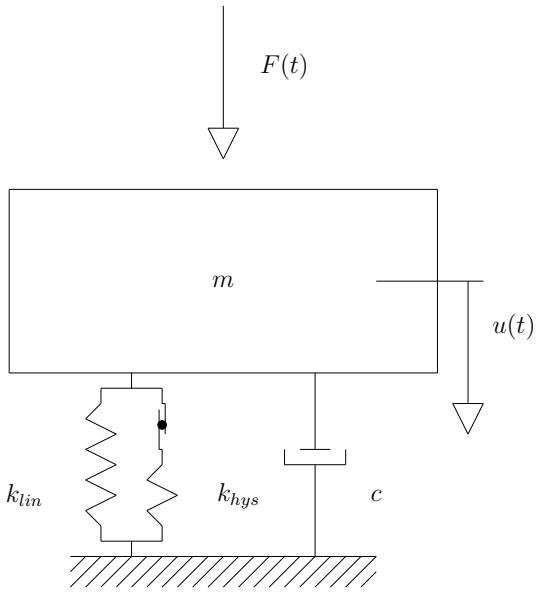

Figure 3.5: The equivalent mass-damper-spring system of the concrete structure, suitable for non-linear analyses.

$$k_{\text{eq}} = \sum_{i=1}^{n} k_i \tag{3.7}$$

Sivalsevan [39] proposed the following equation for the hysteretic spring:

$$k_{\text{hys}} = (1 - r_k)k_0 \left(1 - \left|\frac{F^*}{F_y^*}\right|^N (\eta_1 \text{sgn}\left(F^* \dot{u}\right) + \eta_2)\right) \tag{3.8}$$

where:

k_0	is the elastic stiffness of the system;
F^*	is the portion of applied force shared by the hysteretic spring;
F_y^*	is the yield force of the hysteretic spring;
N	is a parameter controlling the smoothness of the transition from elastic to inelastic;
$\eta_1 \ (0 < \eta_1 < 1)$	= η, a parameter controlling the shape of the unloading curve;
η_2	= 1 - η_1.

This gives a combined stiffness of:

$$k_{\text{sys}} = k_{\text{lin}} + k_{\text{hys}} = r_k k_0 + (1 - r_k)k_0 \left(1 - \left|\frac{F^*}{F_y^*}\right|^N (\eta_1 \text{sgn}\left(F^* \dot{u}\right) + \eta_2)\right) \tag{3.9}$$

In figure 3.5, the mechanical model of the system is presented. This model is suited for non-linear analyses.

Newmark-β integration scheme

Under certain conditions, such as a harmonic excitation, equation (3.6) can be solved semi-analytically. However, this is impossible for more complex excitation signals, e.g., randomly generated signals. Numerical integration methods are required. A commonly used numerical integration method in structural dynamics is called the Newmark-β method [40]. This is an implicit numerical integration method based on the assumption that the acceleration varies linearly over the timestep. The Newmark-β method discretizes equation (3.6) in the following manner:

$$\dot{u}_{n+1} = \dot{u}_n + (1-\gamma)\Delta t\ddot{u}_n + \gamma\Delta t\ddot{u}_{n+1} \tag{3.10a}$$

$$u_{n+1} = u_n + \Delta t\dot{u}_n + \frac{\Delta t^2}{2}\left((1-2\beta)\ddot{u}_n + 2\beta\ddot{u}_{n+1}\right) \tag{3.10b}$$

$$m\ddot{u}_{n+1} + c\dot{u}_{n+1} + f_s(u_{n+1}) = F_{n+1} \tag{3.10c}$$

where:

$\square_n$ is a quantity at timestep *n*;
$\square_{n+1}$ is the to solve for quantity at timestep *n+1*;
$\beta,\ \gamma$ are parameters that determine the stability and accuracy of the solution;
Δt is the timestamp.

These equations can be solved iteratively. The parameters γ and β can be freely chosen between 0 and 1. However, they do influence the result. If, for example, γ = 0.5, β = 0.25, are taken, the integration scheme becomes unconditionally stable.

3.2. The OpenSEES model

Section 3.1.1 described the non-linear differential equation that can describe the grandstand element's dynamical behaviour. The equation for the non-linear stiffness was also presented. Figure 3.5 showed the dynamical schematization of the element. This subsection deals with solving the EOM of the element.

The problem is solved using OpenSEES [41], developed by Berkeley University of California. It stands for Open System for Earthquake Engineering Simulation. OpenSEES is an open-source, object-oriented software package. It is used to calculate the structural and geotechnical response to earthquakes. It can be used for several types of calculations, ranging from simple mass-damper-spring systems to large systems that are solved using FEM.

In OpenSEES, a non-linear SDOF is recreated. Tables 3.1 and 3.2 present both the model parameters and calculation parameters that are required to solve this system. How the structure is excited is shown in section 3.4.

3.2.1. Model parameters

Table 3.1 shows the model parameters required to perform the dynamical analysis. These parameters are material- or structure dependent and should be derived from measurements or tests.

3.2.2. Calculation parameters

Table 3.2 presents the parameters used in the calculation. Here, the earlier mentioned Newmark-β parameters are presented. Additionally, the time step of the calculation is shown, as well as the convergence criteria. Convergence is based on an energy norm. Both the tolerance and the maximum number of iterations are given. A minimum tolerance of $\epsilon_{tol} = 10^{-4}$ is advised [42]. Smaller tolerances lead to more accurate results at the cost of increased computational time. Inversely, larger tolerances lead to faster solutions at the cost of accuracy.

3.2.3. The final mechanical model

OpenSEES is mainly used in the domain of earthquake engineering. The program requires a horizontal acceleration signal as input instead of a vertical force signal, as shown in figure 3.5. Therefore, the system is rotated. This is merely a mathematical operation: it does not influence the underlying physical interpretation - apart from the gravity, which is handled in section 3.4. The horizontal displacement of

Table 3.1 An overview of the model parameters.

Parameter	Symbol	Units
Mass	m	kg
Yield force	F_y	N
Yield displacement	u_y	m
Elastic stiffness	k_0	N/m
Ultimate force	F_u	N
Ultimate displacement	u_u	m
Post-yield stiffness	k_{nl}	N/m
Stiffness ratio	r_k	-
Damping ratio	ζ	-
Stiffness-proportional damping coefficient	α	-
Mass-proportional damping coefficient	β	-
Smoothness parameter	N	-
Unloading shape parameter	η_1	-
Unloading shape parameter	η_2	-

Table 3.2 An overview of the calculation parameters.

Parameter	Symbol	Value	Units
Time step	Δt	0.01	s
Newmark parameter	γ	0.5	-
Newmark parameter	β	0.25	-
Energy - tolerance	ϵ_{tol}	1.0 x 10^{-10}	Nm
Energy - max iterations	i	10	-

this system is thus equal to the vertical displacement in reality. Figure 3.6 shows the system that is created in OpenSEES. Equations (3.11) to (3.15) show how to go from a force signal $F(t)$, to an acceleration signal $\ddot{u}_{gr}(t)$. The basic equation of motion is:

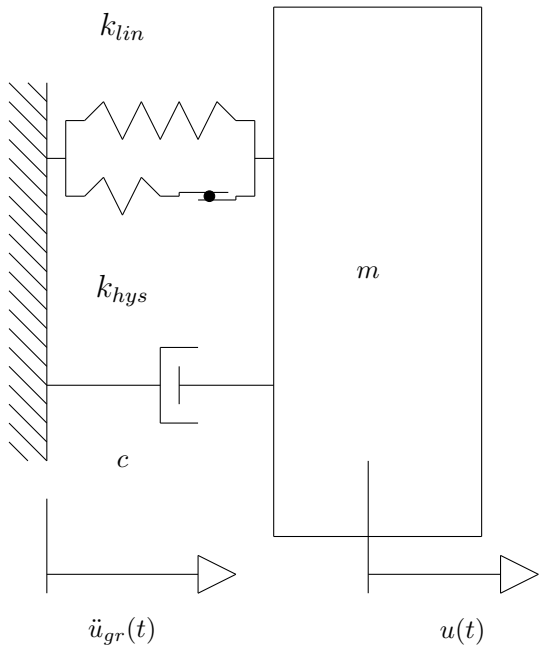

Figure 3.6: The mass-damper-spring system used for the non-linear analysis in OpenSEES.

$$m\ddot{u} + c\dot{u} + ku = F(t) \tag{3.11}$$

The equation of motion of a system excited by a ground acceleration $\ddot{u}_{gr}(t)$ is:

$$m(\ddot{u} + \ddot{u}_{gr}) + c\dot{u} + ku = 0 \tag{3.12}$$

Where u is the displacement of the structure relative to the ground. Moving the excitation of equation (3.12) to the right-hand side results in:

$$m\ddot{u} + c\dot{u} + ku = -m\ddot{u}_g \tag{3.13}$$

Comparison of the right hand sides of equation (3.11) and equation (3.13) yields:

$$F(t) = -m\ddot{u}_g \tag{3.14}$$

Therefore, the factor f between the force and the acceleration is:

$$f = -\frac{1}{m} \tag{3.15}$$

3.3. Analysis of a data set of jumping individuals and crowds

The previous two subsections describe how the dynamical system is derived, what the underlying equations are and how the system can be solved. An excitation signal - $F(t)$, or $\ddot{u}_{gr}(t)$ - needs to be introduced to perform the analysis. The creation of this signal is based on the analysis of the data set of jumping individuals and crowds.

This section shows the outcome of the data analysis. Distribution types and parameters for the most influential random variables required to create the signals are presented here. Correlations are also determined and, when reasonably present, incorporated into the signal. The outcomes of the data set are compared to what was stated in the literature. The next section explains how a signal is created using these variables. With these signals, a reliability assessment can be performed.

This section discusses forces in terms of the normalized force signal $\tilde{F}(t)$, which is equal to the jump factor in the case of an individual. In the case of a crowd, individual signals are added up and divided by the number of people in the crowd.

The notation used for distribution parameters is in line with the scipy library. For more information regarding the parameters, please consult [43].

3.3.1. Data cleaning

Before starting the analysis of the data set, the data sets are cleaned, as not all data sets turned out to be usable. This could be because people were unable to execute the task correctly, e.g., by not being able to jump for 30 seconds. Numerical errors are also present. First, the data cleaning for individuals is explained. Secondly, the cleaning for groups is handled. The test setup is first described.

Jumping individuals

Individuals were given the task to jump at four different frequencies: 1.5 Hz, 2.0 Hz, 2.67 Hz, and 3.5 Hz. A metronome guiding beat aided them. An additional test was also executed: participants were allowed to jump at their own will. In total, 334 tests were conducted. The tests were performed on a force plate. This plate directly measured the force people exerted on it. The shared data, therefore, is also the measured data.

Although this thesis focuses on jumping at 2 Hz, for this thesis it is assumed that the data from all jumping frequencies can be used to determine the statistical properties related to jumping. The non-guided

signals were excluded. All jumping peaks of each individual were determined using the find_peaks method from the scipy.signal library [44]. Visual verification showed that this method was robust: fewer than 5% of the metronome-guided signals were excluded from further investigations.

A set was discarded if three or more peaks were falsely determined. Most errors happened at the lowest (1.5 Hz) and highest (3.5 Hz) frequencies. At 1.5 Hz, the double-peaked impulse shape made the method more prone to errors. At 3.5 Hz, participants had trouble finishing the test. The unguided tests were discarded as well. 79 of the 334 signals were discarded: six at 1.5 Hz, five at 2.0 Hz, zero at 2.67 Hz, two at 3.5 Hz, and 66 because there was no metronome beat guiding the participants.

Besides judging the suitability of a signal based on the determination of the jump factor, requirements were also put on determining the contact ratio. If fewer than 90 % of the required contact ratios were determined, the set was discarded from further examination. In total, 19 data sets were discarded: zero at 1.5 Hz, two at 2 Hz, three at 2.67 Hz and sixteen at 3.5 Hz. Ginty et al. [27] have shown that individuals can jump comfortably up to 2.8 Hz, which is in line with what is found here, where a frequency of 3.5 Hz seems to be too high for a large group, and 2.67 Hz already seems uncomfortably fast for some.

After removing the unusable data sets, 236 unique signals remain. This number is considered enough for determining the distribution types and parameters for this study.

Jumping crowds

Crowds of up to 48 people were asked to jump between 1.5 Hz - 3.5 Hz, with 0.1 Hz intervals. 3D motion capture technology (MCT) was deployed to observe their movement. Each participant had three reflective markers around the clavicle area, which cameras in the room could measure. This resulted in three different displacement signals, which were averaged and translated to accelerations by taking its derivative with respect to time twice. These accelerations are translated to forces by using equation (3.16), under the assumption that a test subject can be seen as a rigid body.

$$\tilde{F}(t) = \frac{\ddot{u}_{ma}(t)}{g} + 1 \tag{3.16}$$

where:

$\ddot{x}_{ma}(t)$ is the second time derivative of the displacement at time t;
g = 9.81 m/s^2, is the gravitational constant.

Logically, this method is more prone to errors than using a force plate: one person could block another person's markers, for example. Furthermore, equation (3.16) is a simplification of reality, although it is supported by Racic et al. [45].

To clean the data; first, all measured values below 0 were set equal to 0. Due to the measuring technique, negative values for the displacement could be observed, and thus also for the accelerations. This is are not possible when jumping on a structure. For information regarding the measuring technique, it is referred to [17].

The data set requires an upper bound for the measurements: in some test cases, jump factors of over 70 were found. These are apparent measurement errors: the highest jump factor found for all individuals was lower than 6. To account for this, all jump factors higher than 8 are truncated.

Starting the truncation at 8 is a conservative take when the maximum value for an individual is below 6. However, Li et al. [46] have shown that a discrepancy in forces exists between using a force plate and 3D MCT. The pseudo loads, in general, were higher than that of the force plate. For 2 Hz, the ratio between the actual load and the pseudo load is 1.265. Including this factor would yield a maximum jump factor of about 6.3. Furthermore, the sum of up to 48 reaction forces is taken, so it is assumed

that potential errors are averaged out.

In order to be able to sum up the data of each individual, the records should start at the same time. Although not explicitly mentioned in their paper, Xiong confirmed this was the case through e-mail contact.

3.3.2. Analysis of jumping individuals

This section analyses the data set of jumping individuals. Figure 3.7 shows a visualization of an excitation signal of an individual jumping at 2 Hz. 2 Hz is chosen because this is the focus of this thesis. Evaluation of the data set should lead to suitable distributions of two random variables: (1) the jump factor $\tilde{F}$; and (2) the contact ratio α.

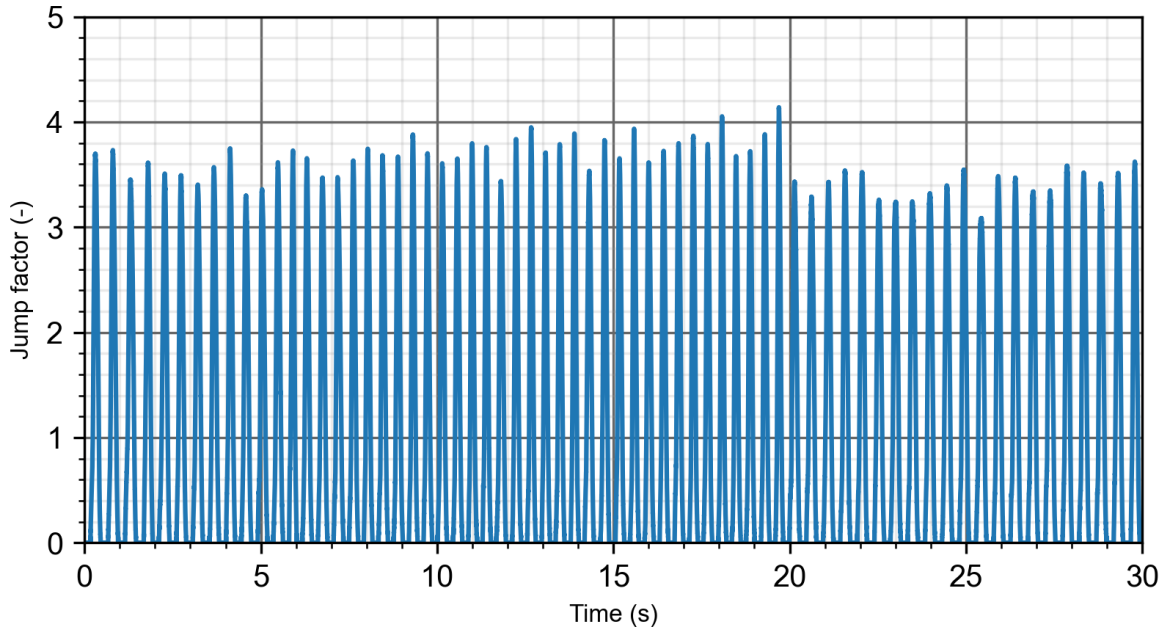

Figure 3.7: VisualizationVisualization of an excitation signal of the jump factor of an individual, jumping at 2 Hz.

The jump factor $\tilde{F}$

Each individual's peaks are determined. Then, their mean and standard deviation are calculated. The results are shown in figure 3.8. This figure shows that the mean jump factor for each individual shows a large variability, while everybody's standard deviation is more or less equal. Therefore, the distribution of the jump factor is split up in two: the joint distribution $\tilde{F}$ consists of two random variables, namely: (1) a marginal distribution that describes the series-to-series (sts) variation (i.e., between persons) $\tilde{F}_{sts}$; and (2) a marginal distribution that describes the within-series (ws) variation (i.e., for one person) $\tilde{F}_{ws}$:

$$\tilde{F} = \tilde{F}_{sts} + \tilde{F}_{ws} \tag{3.17}$$

The series-to-series variation of the jump factor $\tilde{F}_{sts}$

The distribution of the sts jump factor $\tilde{F}_{sts}$ is fitted using a normal distribution and a lognormal distribution. The result is shown in figure 3.9. Table 3.3 presents the parameters of the distributions.

The values in the data set correspond with what is found in the literature, which states values between 2.3 and 4.8. Both distributions seem almost equally suited to fit the data points. However, looking at

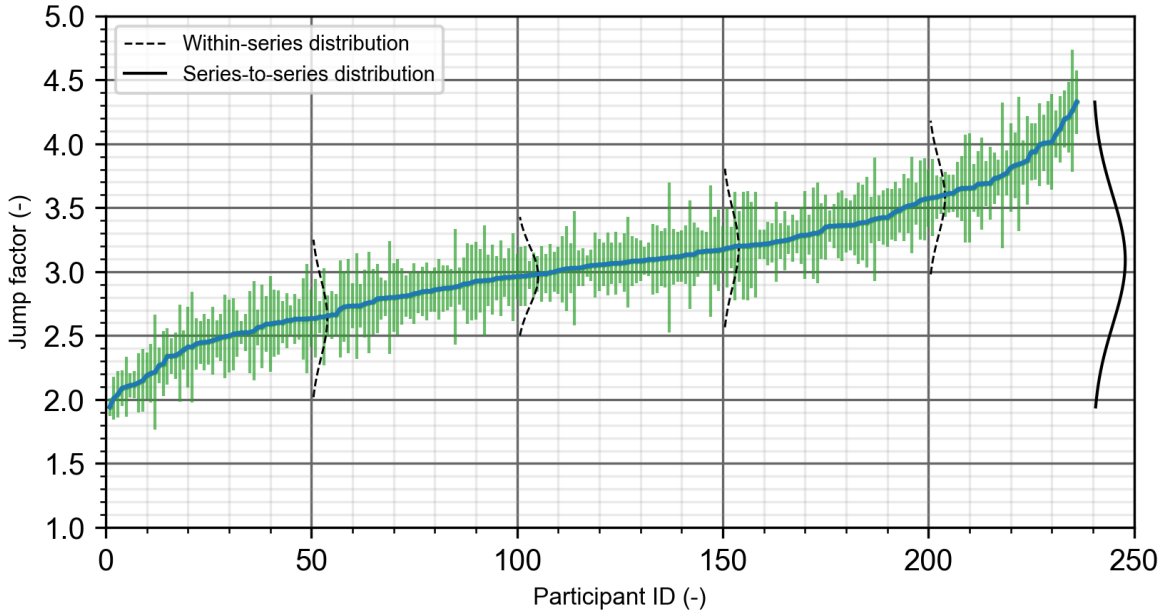

Figure 3.8: 30-second mean (blue) ± 1 standard deviation (green) of all peaks of the jump factor of each individual (n = 236). Two different distributions arise: (1) a series-to-series distribution; (2) a within-series distribution.

figure 3.9, the normal distribution seems to be the better fit in the tail of the distribution. Therefore, for the distribution of the sts jump factor, a normal distribution is taken with the parameters as given in table 3.3.

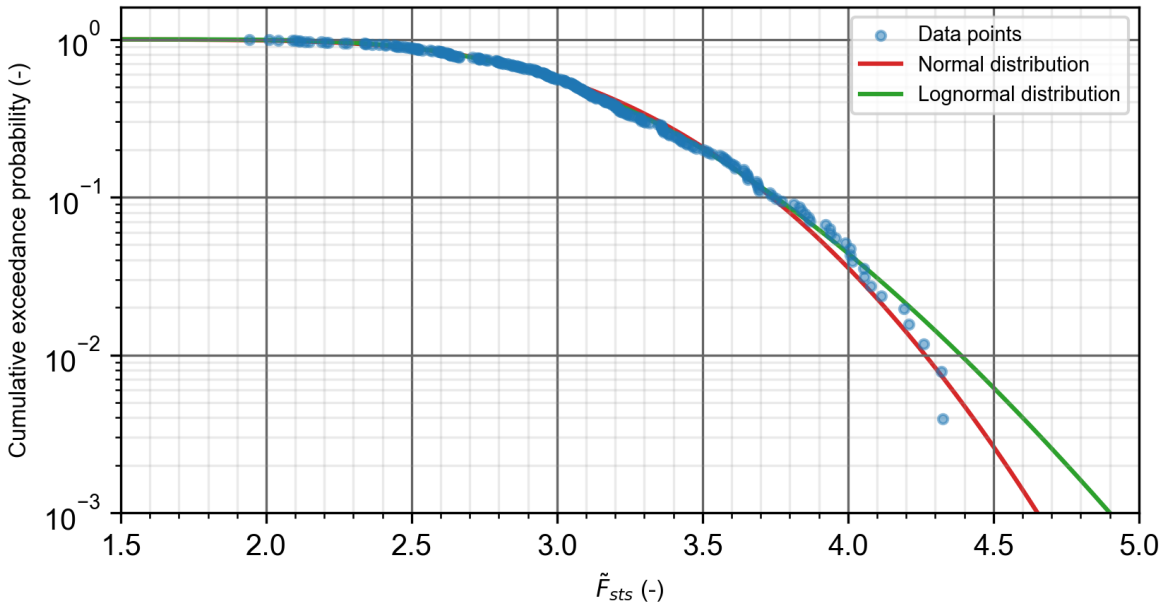

Figure 3.9: Data points of the sts jump factor $\tilde{F}_{sts}$ and a fitted normal and lognormal distribution.

The within-series variation of the jump factor $\tilde{F}_{ws}$

The distribution of the ws jump factor $\tilde{F}_{ws}$ is fitted using a normal, a lognormal, and a Weibull distribution. The result is shown in figure 3.10. Table 3.4 shows the parameters of the distributions.

Table 3.3 The parameters of the distribution of the sts jump factor. The parameters are in accordance with the SciPy library.

	Normal distribution	Lognormal distribution
shape	-	0.11
loc	3.09	-1.60
scale	0.51	4.66

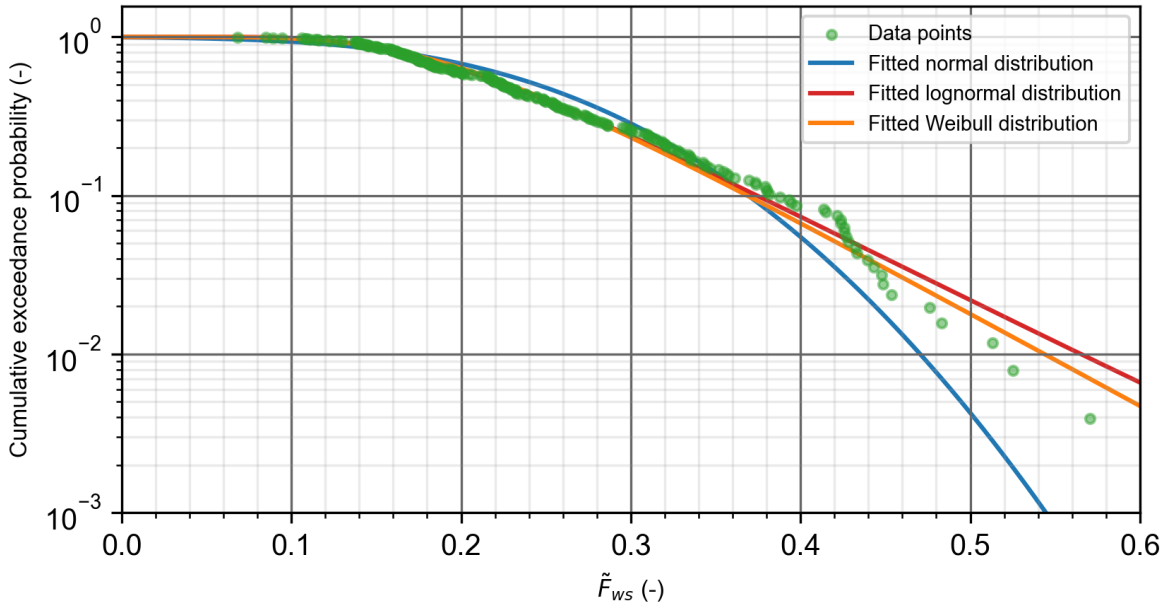

Figure 3.10: Data points of the ws jump factor $\tilde{F}_{ws}$ and a fitted normal, lognormal, and Weibull distribution.

Table 3.4 The parameters of the fitted distributions for the ws jump factor. The parameters are in accordance with the SciPy library.

	Normal distribution	Lognormal distribution	Weibull distribution	
shape	-	0.40	68.9	x 10^6
loc	0.24	0.01	51.3	x 10^6
scale	0.10	0.22	51.3	x 10^6

Equation (3.18) shows how to calculate the coefficient of variation (CoV). The CoV of the ws jump factor is about 0.4, which is high. This means that the data has a fat tail. A distribution that best fits the fail is therefore required. Since the Weibull distribution fits the data points best in the tail, this distribution is taken to describe the ws jump factor.

$$V = \frac{\sigma}{\mu} \tag{3.18}$$

where:

V is the coefficient of variation;
σ is the standard deviation of a random variable;
μ is the mean of a random variable.

Correlation between $\tilde{F}_{sts}$ and $\tilde{F}_{ws}$

The two marginal distributions, $\tilde{F}_{sts}$ and $\tilde{F}_{ws}$, are now defined. To describe the joint distribution $\tilde{F}$, the correlation coefficient $\rho_{\tilde{F}_{sts},\tilde{F}_{ws}}$ needs to be defined. The correlation between samples of two random variables, X and Y, can be determined using equation (3.19).

$$\rho_{x,y} = \frac{\sum_{i=1}^{n}(x_i - \bar{x})(y_i - \bar{y})}{\sqrt{\sum_{i=1}^{n}(x_i - \bar{x})^2}\sqrt{\sum_{i=1}^{n}(y_i - \bar{y})^2}} \tag{3.19}$$

where:

$\rho_{x,y}$	is the correlation coefficient;
n	is the sample size
x_i, y_i	are the sample points of random variables X and Y;
$\bar{x} = \frac{1}{n}\sum_{i=1}^{n} x_i$	is the sampled mean of variable X;
$\bar{y} = \frac{1}{n}\sum_{i=1}^{n} y_i$	is the sampled mean of variable Y.

The correlation coefficient takes on values between -1 and 1. A way to quantify the correlation is [47]:

- Perfect: $|\rho| = 1$;
- High: $0.5 \leq |\rho| < 1$;
- Moderate: $0.30 \leq |\rho| < 0.50$;
- Low: $|\rho| < 0.30$;
- No correlation: $|\rho| = 0$;

The correlation between $\tilde{F}_{sts}$ and $\tilde{F}_{ws}$ is equal to $\rho_{\tilde{F}_{sts},\tilde{F}_{ws}} = 0.20$. This means that a low correlation exists between the two variables. A quick look at figure 3.8 also suggests that the sts variation is unrelated to the ws variation, as the bandwidth of the ws jump factor stays somewhat constant. For future calculations, the two random variables are therefore assumed to be uncorrelated.

The contact ratio α

The contact ratio is the contact duration between the person and the ground relative to the jump period (see equation (2.4)). The average contact ratio of the 30-second excitation signal of each participant is calculated. Only values larger than a certain value are considered. This threshold is based on Bachmann and Ammann [16], who state that, from a psychological point of view, it is hardly possible to achieve a contact duration smaller than 0.15 s.

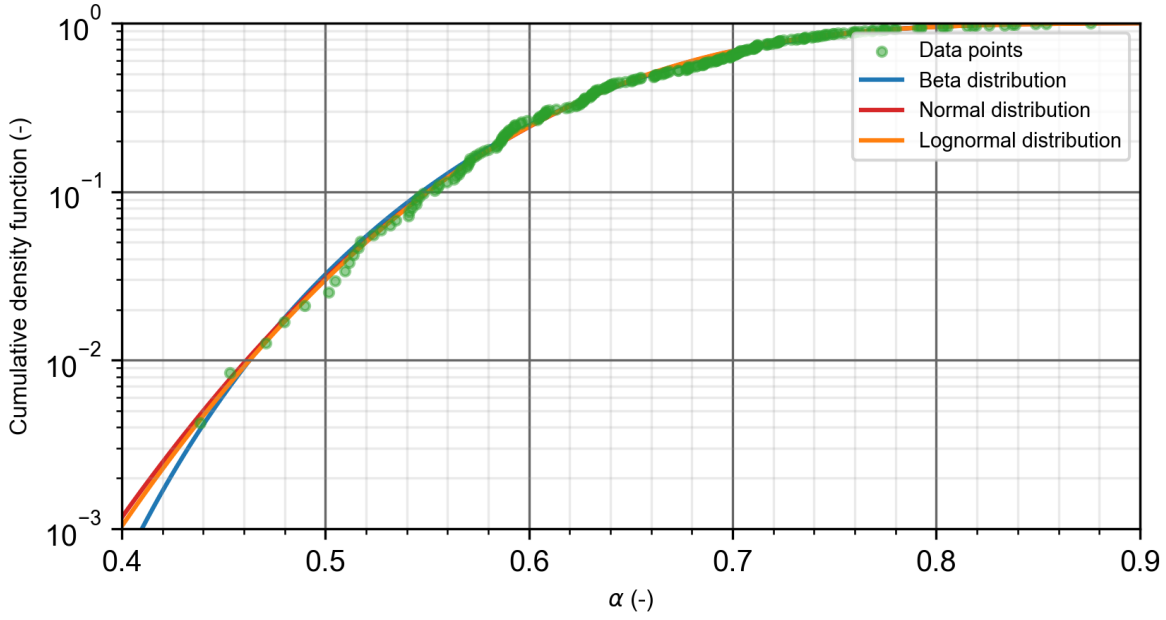

Figure 3.11: Data points of the contact ratio α and a fitted normal-, lognormal-, and beta distribution.

A normal, lognormal and beta distribution have been fitted on the data points. Figure 3.11 shows the result. Here, all are a good fit. Although the data points seem to wiggle up and down, all three fitted distributions can follow the slope. Table 3.5 shows the parameters of the distribution.

The following subsection shows that a low contact ratio is related to a high jump factor. This is unfavourable. Therefore, the contact ratio should fit the left tail the best. Although the differences are minor when looking at figure 3.11, the normal distribution best fits the left-most points. Therefore, a normal distribution with parameters as given in table 3.5 is taken.

Table 3.5 The parameters of the fitted distributions for the contact ratio. The parameters are in accordance with the SciPy library.

	Normal distribution	Lognormal distribution	Beta distribution
shape (s or a)	-	0.01	9.24
shape (b)	-	-	7.70
loc	0.66	- 9.61	0.26
scale	0.08	10.27	0.73

The expected value of the contact ratio, according to the data set, is 0.66. Compared to most literature, e.g., Ellis et al. [48], this is on the high side. In literature, the following three contact ratios are used almost exclusively: α = $\frac{1}{3}$, $\frac{1}{2}$, $\frac{2}{3}$, which represent normal jumping, rhythmic exercise and high-impact aerobics, and low-impact aerobics, respectively.

A sensitivity study has been performed on, among other things, the influence of the expected value of the contact ratio on the excitation signal. This study is shown in appendix B. The study has shown that a contact ratio of $\alpha = 0.33$ gives a better recreation of the excitation signal than the value found in the data analysis. Additionally, this ratio is related to normal jumping, which is in accordance with what is being modelled. Therefore, in further analyses, $\alpha = 0.33$ is applied.

Correlation between the jump factor $\tilde{F}$ and the contact ratio α

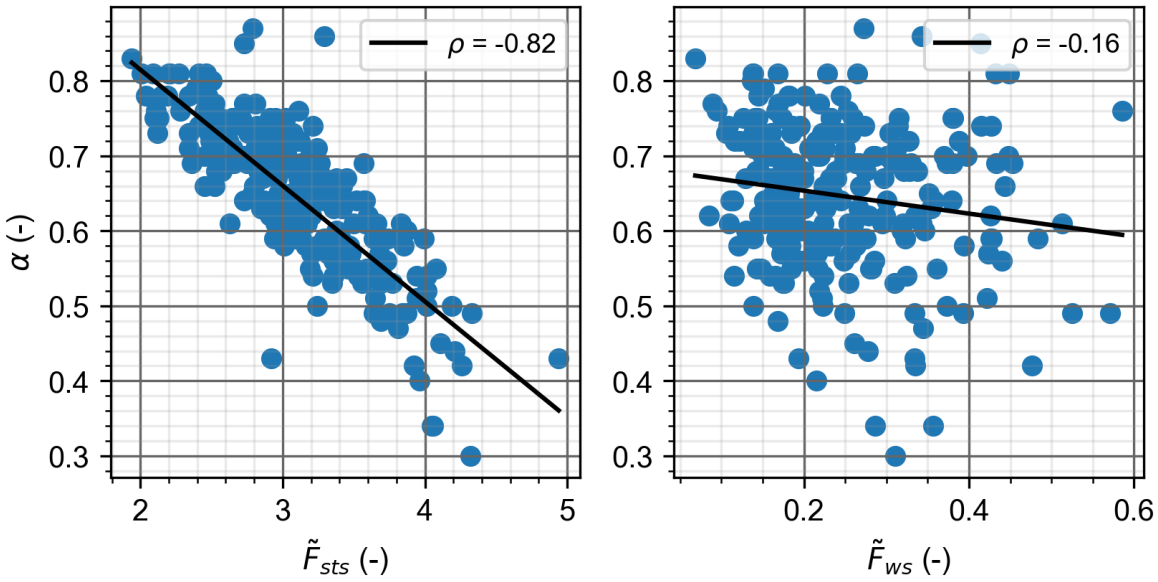

Figure 3.12: Correlation analysis between the contact ratio α and the sts jump factor $\tilde{F}_{sts}$ and the ws jump factor $\tilde{F}_{ws}$, respectively.

As mentioned in section 2.2, the jump factor and the contact ratio are negatively correlated. In this paragraph, the correlation between the contact ratio α is compared with both the sts jump factor $\tilde{F}_{sts}$ and the ws jump factor $\tilde{F}_{ws}$.

Figure 3.12 shows the contact ratio versus the sts jump factor and ws jump factor, respectively. It is visible that a high negative correlation indeed exists between the contact ratio and the sts jump factor. There is little to no correlation between the contact ratio and the ws jump factor. Evaluation leads to the following values: $\rho_{\alpha,\tilde{F}_{sts}} = -0.82$; $\rho_{\alpha,\tilde{F}_{ws}} = -0.16$. Therefore, the former is included when creating an excitation signal, and the latter is left out.

Autocorrelation

The autocorrelation between consecutive values is checked for both random variables. Autocorrelation is a way to measure the dependence of a random variable with a lagged version of itself, where the lag is either a time or a spatial lag. Since the signals are a function of time, in this case, the autocorrelation is temporal. The peak values from the data set are a realization of the two marginal distributions of the jump factor $\tilde{F}_{stS}$ and $\tilde{F}_{ws}$. Only the temporal autocorrelation for $\tilde{F}$ itself can be determined since the peak values are realizations of $\tilde{F}$. For the contact ratio α, this is no limitation.

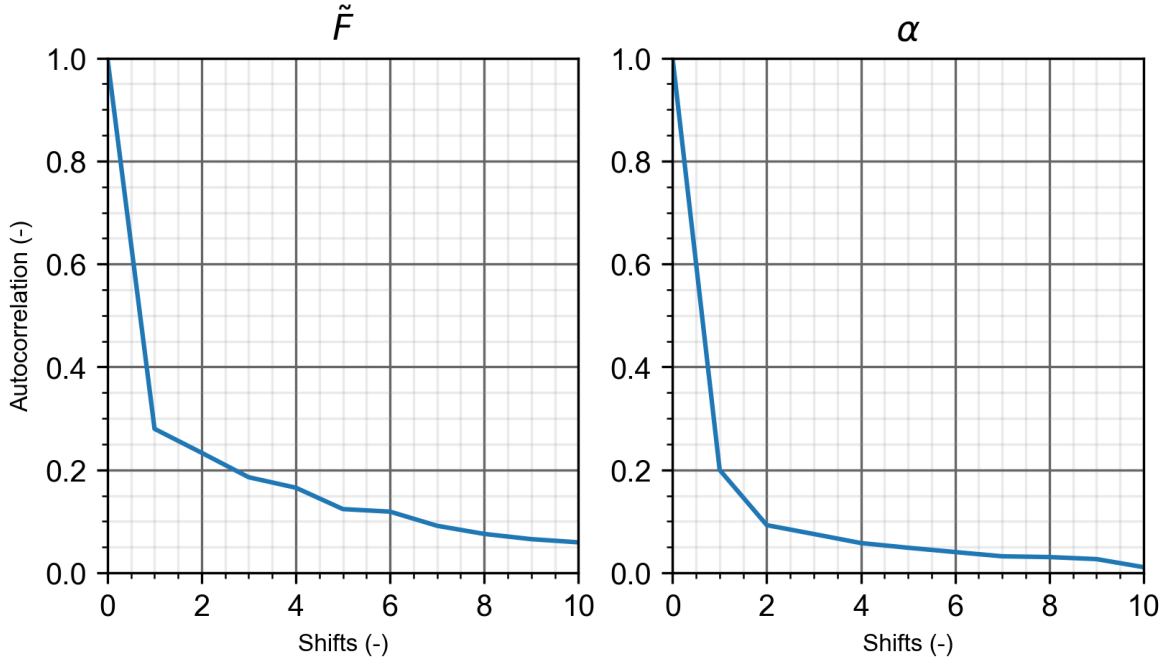

Figure 3.13: Temporal autocorrelation between the jump factor $\tilde{F}$ and the contact ratio α

Figure 3.13 shows the autocorrelation for both random variables, up to 10 lags away. Both random variables show a quick, steep drop in autocorrelation for their adjacent values.

The drop is more evident in the contact ratio, which shows an autocorrelation coefficient of only $\rho_{\alpha_i,\alpha_{i+1}} = 0.20$ after one shift, which gradually goes to almost zero after ten shifts. The jump factor shows a slightly higher autocorrelation. This one drops to $\rho_{\tilde{F}_i,\tilde{F}_{i+1}} = 0.28$ after one shift and goes well below 0.1 after ten shifts. Although one shift already results in a low autocorrelation, they are included in creating a signal. Higher shifts could also be included, but they are assumed insignificant due to the low autocorrelation.

3.3.3. Analysis of jumping crowds

This section analyses the data set of jumping crowds. Figure 3.14 shows the normalized jump factor of an arbitrarily chosen data set of people jumping at 2 Hz, both in the time and frequency domain. This figure demonstrates that the jump factor reduces significantly when going from an individual to a group. Evaluation of the data set should lead to suitable distributions of two random variables: (1) the period of each jump T_p; and (2) the phase lag between individuals ϕ. Combined, they should have an equivalent result on the force signal of a group as the application of a coordination factor does, which, according to the literature, can be as low as 0.5 or as high as 0.9.

The random nature of jumping is best illustrated in the frequency domain. There is quite some spread around its central frequency. Brownjohn et al. [19] showed that, for walking, the leakage of energy becomes more profound for higher harmonics. This figure shows that the same holds for jumping. Incorporating this in the excitation signal will result in a lower resonant response of the structure when the eigenfrequency corresponds with one of the harmonics of the excitation frequency.

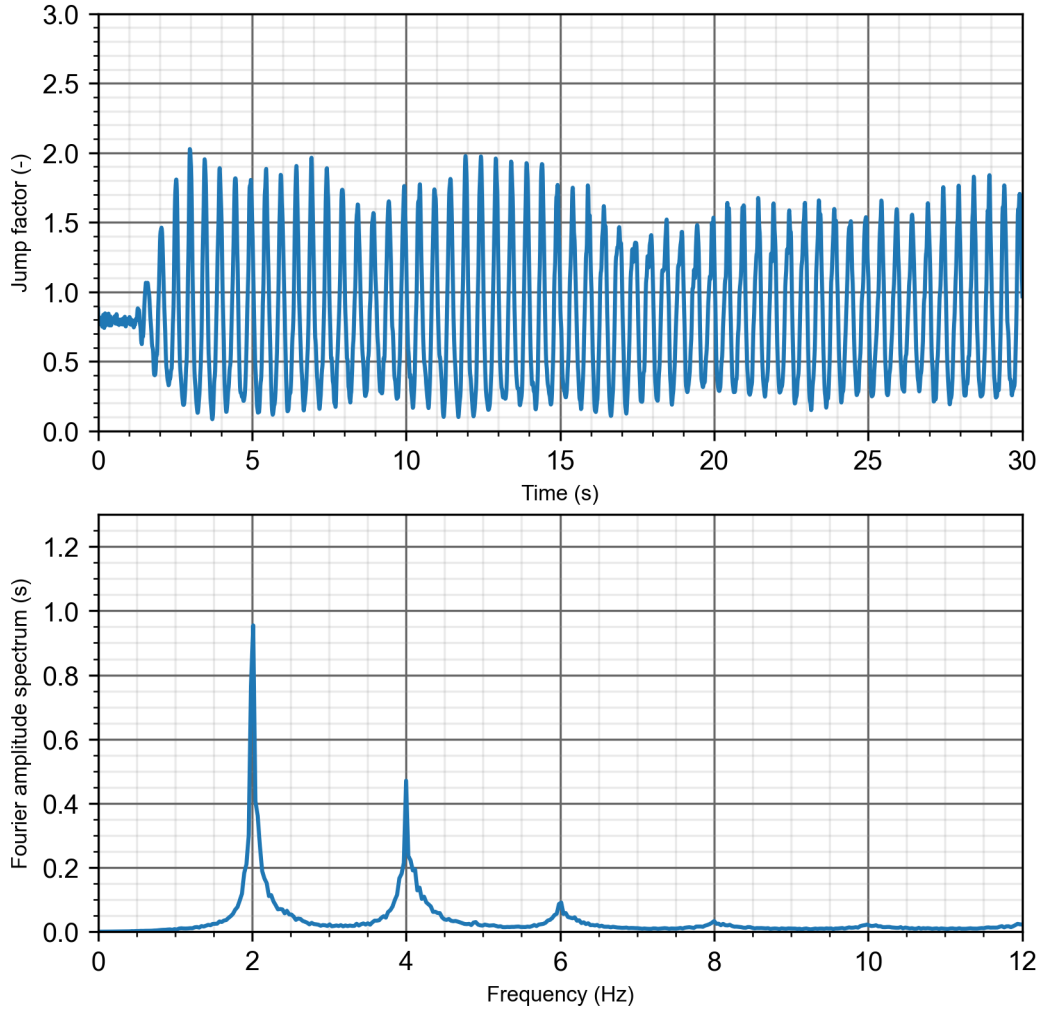

Figure 3.14: NormalizedNormalized jump factor of people jumping at 2 Hz, shown in the time and frequency domain, respectively.

A distribution for the period T_p

Ellis and Ji [23] suggested that the jumping period at moment *i*, $T_{p,i}$, depends on the previous $i-1$ realisations. Other studies (e.g., Pavic and Racic [26]) came to the same conclusions. If a person jumped too slowly on the previous step, they want to adjust their next jump by decreasing the period between them to keep up with the guiding beat. The distribution can be assumed to be normal.

The literature review has shown that no unequivocal answer exists regarding the distribution of the period of each jump. Evaluation of the individual jump data of the data set shows that the coefficient of variation of the jumping period reaches about 0.08 for increasing frequency. At 2.0 Hz, the coefficient of variation is about 0.10, which means that the standard deviation is $\sigma_{T_P} = 0.05$ s. This corresponds with what is found by Chen et al. [25].

In order to find a suitable parameter for the standard deviation of the period, several values around 0.05 s were tried, ranging from 0.01 s to 0.10 s, with 0.01 s intervals. The outcome is compared with figure 3.14. This sensitivity study is combined with the phase lag ϕ and the contact ratio α and is shown in appendix B. Based on visual inspection, a standard deviation of $\sigma_{T_P} = 0.02$ s turned out to be the best fit for jumping at 2 Hz. Other jumping frequencies have not been investigated. This results in the following distribution for the period at peak *n*:

$$T_{p,n} \sim N\left(\sum_{i=1}^{n}\left(n\cdot\mu - T_{p,i}\right), 0.02^2\right) \tag{3.20}$$

where:

n is the total number of peaks in the excitation signal at time moment *i*;
$T_{p,i}$ is realization *i* of the random variable;
σ = 0.02 s is the standard deviation.

A distribution for the phase lag ϕ

Parameters for the phase lag ϕ are also determined based on visual inspection. Several values are tried, ranging from 0.01 s to 0.1 s, with 0.01 s intervals. The result is shown in appendix B. Based on visual inspection, a standard deviation of $\sigma_\phi = 0.05$ s was the best fit for jumping at 2 Hz. The distribution type is assumed to be normal, resulting in the following equation:

$$\phi \sim N\left(0, 0.05^2\right) \tag{3.21}$$

3.3.4. Conclusion

Tables 3.6 to 3.8 show the distribution types, parameters, and correlations that resulted from the analysis of the data set and the comparison with the literature.

Table 3.6 Overview of the random variables' distribution types and parameter values.

Variable	Distribution type	c	loc	scale
$\tilde{F}_{sts}$	Normal	-	3.09	0.51
$\tilde{F}_{ws}$	Weibull	68.9 x 10^6	51.3 x 10^6	51.3 x 10^6
α	Normal	-	0.33	0.08
T_p	Normal	-	T_p	0.02
ϕ	Normal	-	0	0.05

Table 3.7 Correlation table.

	$\tilde{F}_{sts}$	$\tilde{F}_{ws}$	α
$\tilde{F}_{sts}$	1	0	- 0.82
$\tilde{F}_{ws}$	0	1	0
α	- 0.82	0	1

Table 3.8 Temporal autocorrelation table.

	$\tilde{F}_i$	α_i
$\tilde{F}_{i+1}$	0.28	n.a.
α_{i+1}	n.a.	0.20

3.4. Constructing a random excitation signal of a crowd jumping on a grandstand element

The analysis of the data set has led to distribution types and parameters for random variables. With these variables, an excitation signal can be generated. This can be done for each person. Figure 3.15 shows the first peak of two possible realizations, where the random variables are also presented. The jumping frequency in this figure is 2 Hz.
a
To obtain a force signal, the jump factor is multiplied by every person's static weight $G = m_p g$. The average mass of a Dutch male is $m_p = 85$ kg [49]. This value is used for every person in this thesis. The following subsection describes how this signal, on a rigid body, is translated to a signal that can be put on a grandstand element. Additionally, verification analyses of the method are introduced.

3.4.1. From a force on a rigid body to a force on a flexible body

The position where people are jumping on the element highly influences their contribution to the midspan displacement. It follows from logic that people jumping near midspan contribute more to the midspan displacement than people jumping on the edges. To determine the influence of one's location, the influence line is introduced.

An influence line shows the value of a quantity in a certain point as a function of the spatial coordinate of a unity load [50]. This concept is visualized in figure 3.16. In this case, the quantity of interest is the DOF of the mass-spring-damper system, i.e., the midspan displacement. The unity load is a force resulting from people jumping on the structure.

The Maxwell–Betti reciprocal work theorem states that the influence line of the displacement at midspan of a structure, given the spatial coordinate of the unity load, is equal to the displacement line of the structure, given a midspan unity load. By assuming that the grandstand element can be modelled as a simply supported, slender beam with a constant bending stiffness (see figure 3.16), the displacement line of the structure given a midspan load can easily be calculated using the Euler-Bernoulli beam theory:

$$EI\frac{d^4u(x)}{dx^4} = q(x) \tag{3.22}$$

where:

EI is the bending stiffness of the structure at position x;
$u(x)$ is the displacement of the structure at position x;
$q(x)$ is the applied lateral load at position x.

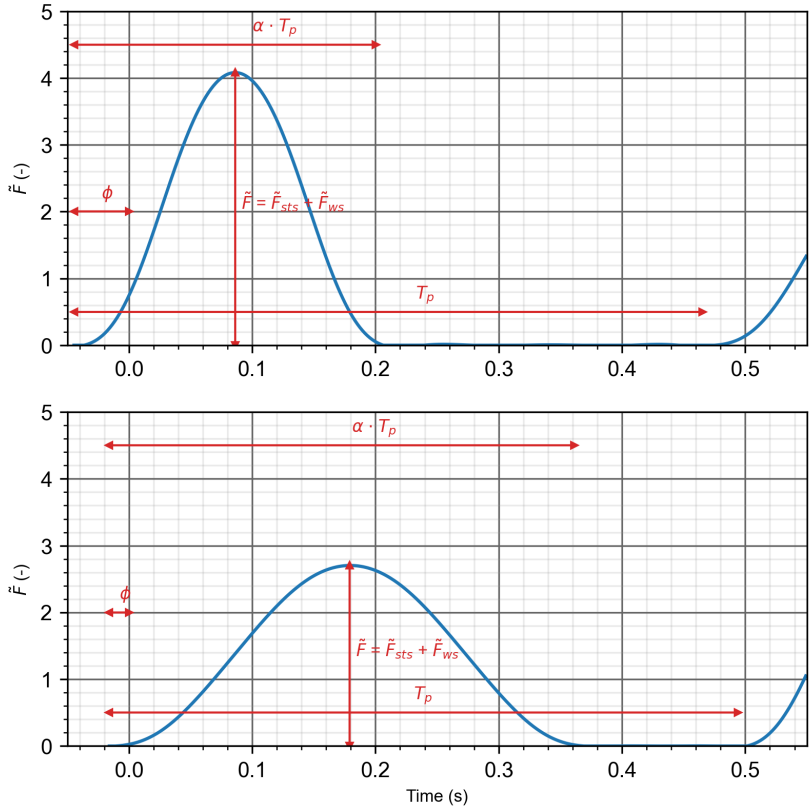

Figure 3.15: Two possible realizations of the generated excitation signal.

Equation (3.22) is a fourth-order linear differential equation and thus requires four boundary conditions to be solved. They are shown in equation (3.23).

$$u(0) = 0 \tag{3.23a}$$

$$\frac{d^2u(0)}{dx^2} = 0 \tag{3.23b}$$

$$u(L) = 0 \tag{3.23c}$$

$$\frac{d^2u(L)}{dx^2} = 0 \tag{3.23d}$$

Solving yields the following equation for the displacement of the beam as a function of its spatial coordinate:

$$\frac{u(x)}{EI} = \frac{Fx(3L^2 - 4x^2)}{48}, \qquad 0 < x < \frac{L}{2} \tag{3.24}$$

Dynamical influence lines also exist: they are better known as mode shapes. Instead of a fourth-order polynomial, a mode shape takes a sine-shaped form to describe the displacement of a beam. The difference between a static and dynamical influence line depends on the length of the beam and the number of people. In the case of the Goffert stadium, the difference is marginal. A dynamical influence line results in a 2% more extreme condition compared to a static influence line (only the first mode shape is considered).

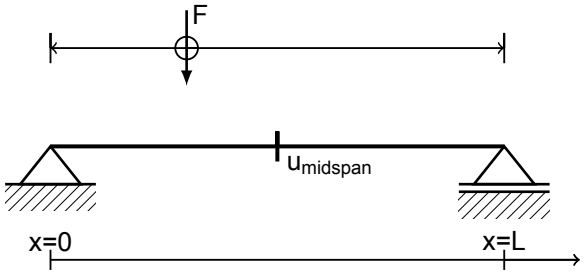

Figure 3.16: The mechanical schematization of a simply supported beam.

Crowds are reasonably uniformly distributed [51], indicating that the number of people can be placed uniformly over the grandstand element. The middle of the span is the most severe condition. In the modelling of the force, the placing of people starts from the middle. Additionally, people are assumed to be standing within the supports: cantilevers are not occupied by people. Multiplicating a force signal with a person's influence factor leads to a force signal on the grandstand. Doing this process for every individual results in an equivalent force signal. Dividing this force signal by the mass m_s of the structure results in the acceleration signal $\ddot{u}_{gr}(t)$. In total, almost 100,000 30-second acceleration signals are created.

3.4.2. Gravity

An additional acceleration signal is superimposed on this signal. This second signal has a constant value representing the static displacement due to the structure's weight. This second signal is superimposed on the other signal. The combined acceleration signal is used as input for the OpenSEES model.

3.4.3. Verification analyses

In order to verify the OpenSEES model, its output is compared to another solver: the linear equation of motion is also solved using Duhamel's integral. This solution procedure accepts the force signal as input. Both methods should lead to a similar displacement when executing a linear elastic dynamical analysis.

3.5. The reliability analysis

This section describes how the reliability of the grandstand element is determined. First, the limit state function is presented. The second subsection discusses a model uncertainty parameter for the resistance of the structure, which, thus far, has yet to be introduced. The solution procedure follows this section: a Monte Carlo simulation is proposed. The last section discusses the maximum load expected during a structure's lifetime.

3.5.1. The Limit State Function

Failure of a structure can be described by introducing a limit state function (LSF):

$$Z = R - S \tag{3.25}$$

where:

Z is the limit state function;
R is the resistance;
S is the solicitation.

Failure occurs when the solicitation is larger than the resistance, i.e., when $Z < 0$. Section 3.1.2 discussed that for non-linear analyses, a displacement-based criterion is often used. The LSF, therefore, is a function of the system's displacement.

The solicitation is the displacement of the grandstand element resulting from the non-linear dynamical analysis. It is a function of time. The resistance of the structure is the maximum allowable displacement, u_u. This point is time-independent. Failure happens when the systems' displacement exceeds the ultimate displacement capacity.

3.5.2. Model uncertainty in the resistance model

The acceleration signal is constructed by using multiple random variables. Thus far, no uncertainties have been introduced on the resistance function of the structure. This subsection presents the model uncertainty parameter θ that is used as a multiplier for the force-displacement relationship.

For concrete structures subjected to bending, the Joint Committee on Structural Safety (JCSS) probabilistic model code [52] proposes a lognormal distributed model uncertainty parameter, with a mean of 1.2 and a coefficient of variation of 0.15. This parameter is based on static analyses. The mean value of 1.2 suggests that additional capacity is hidden inside the structure. However, the numerical model is assumed to be true; thus, there is no reason to assume additional strength beyond the ultimate point. Therefore, this model is deemed unsuitable for this analysis.

Schlune et al. [53] conducted a study on the safety format for non-linear analysis of concrete structures. Their key motivation was that all model uncertainty parameters are based on beams and columns, which lack the suitability for more complex models. They concluded that for beams in bending, the coefficient of variation lies somewhere in the region of 5%-30%. Lower values are related to the yielding of the reinforcing steel, which is what happened in the Goffert stadium. This parameter is also based on static analyses. Casas et al. [54] suggest a coefficient of variation of 6%, which is in line with what Schlune et al. propose in the case that yielding of the reinforcement is expected.

At least two studies propose a coefficient of variation of around 5% for concrete structures. Unfortunately, no literature regarding the model uncertainty of concrete structures for dynamical analyses is found. For this, a penalty of 5% is added to the model uncertainty. This makes the resistance model's total coefficient of variation equal to 10%. The resistance function has two points: an elastic limit - and a plastic limit point. Both points are multiplied with the model uncertainty parameter. The values, obtained by the numerical model, of the yield- and ultimate force and displacement are found in table 3.1. In the limit state function, the resistance thus becomes:

$$R = \theta \; R_{\text{nm}} \tag{3.26}$$

where:

θ $\sim$ N(0, 0.1^2), is the model uncertainty parameter that is multiplied by the force and the displacement;
R_{nm} is the force-displacement relationship determined by a numerical model.

3.5.3. A Monte-Carlo simulation

The reliability analysis can be performed with the limit state function completely defined. Due to the complexity of the function (non-linear, time-dependent), a Monte Carlo simulation is proposed.

Monte Carlo is categorized as a type III reliability method, indicating that it can be deployed to determine the true probability of failure (in contradiction to approximation- or semi-probabilistic methods). A Monte Carlo simulation is an easy-to-implement method, making it a favourable method for this complex analysis. Each simulation is different from the others. By conducting this experiment multiple

times, some might lead to failure, while others do not. The probability of failure is then equal to the ratio between the number of failed simulations and the total number of simulations (see equation (3.27).

$$P_f = \frac{n_f}{n} \tag{3.27}$$

where:

P_f is the probability of failure;
n_f is the number of failed simulations;
n is the total number of simulations.

The reliability β of a structure is related to the probability of failure through equation (1.1).

3.5.4. The lifetime maximum load

In multiple studies, blocks of around 30 seconds are taken. The database also consists of signals that last for about 30 seconds. However, EN 1990 Table B2 [55] states that the 50-year extreme load condition should be put on the system. The determination of the lifetime maximum load conditions is complicated. First, it is unknown if the 30-second maximum jump factor is equal to the lifetime maximum jump factor. Secondly, when people jump longer than 30 seconds, more energy is put into the system. If the system cannot dissipate this energy, displacements will increase, and the structure will eventually collapse.

There are two signs that the 30-second maximum is also close to the lifetime maximum. The first argument is related to fatigue. In studies, the exercise duration was limited to prevent symptoms of fatigue, e.g., Sim et al. (30-35 seconds), Racic & Pavic (30 seconds, where the middle 25 seconds were recorded), Chen et al. (slightly over 25 seconds), Li et al. (30 seconds) [6, 21, 46, 56]. Li et al. gave the participants a 60-second rest period after each jumping test and 20 minutes after four tests, ensuring the participants from staying energetic. This indicates that jumping for more than 30 seconds likely does not lead to larger forces.

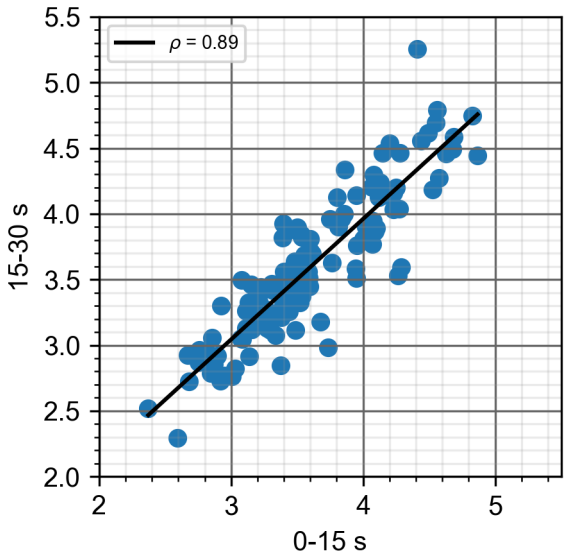

Figure 3.17: Correlation between the 0-15 s block maximum and the 15-30 s block maximum of each participant.

The second indication that the 30-second maximum is a reasonable assumption for its lifetime maximum is found by splitting up the signal in 15-second blocks. A correlation analysis between the 0-15 s maxima and the 15-30 s maxima shows that a very high correlation exists between the two. In figure 3.17, the correlation between the two blocks is shown. The correlation coefficient is $\rho = 0.89$.

Larger time intervals lead to a higher correlation. This study assumes that the correlation approaches 1 at 30 seconds, indicating that longer signals will not result in higher forces. When enough signals are generated, 30-second signals should include all possible scenarios on the grandstand element.

It is plausible that people jump longer than 30 seconds. This means that more energy is put into the system. If, after 30 seconds of jumping, a dynamic equilibrium is not yet found, this could still lead to collapse. To investigate this phenomenon, longer time series are created. Since the 30-second maxima of each signal are assumed to be completely dependent, longer series can be generated using concatenated 30-second signals. Almost 100,000 30-second signals should include (almost) all possible jumping scenarios on a grandstand element. The analyses should thus give a proper estimation of the probability of failure after 30 seconds. In order to see the influence of jumping for more than 30 seconds, about 23,500 excitation signals with a duration of 120 seconds and over 9,400 300-second signals are put on the system as well.

3.6. A case study: the Goffert stadium

Sections 3.1 to 3.5 presented a method to determine the reliability of a grandstand element. In this section, a case study is introduced. The reliability of the collapsed grandstand element of the Goffert stadium is assessed. First, a short description of the situation at the moment of collapse is given. Second, the model parameters of the grandstand are presented. This section is followed by the influence factor of each person, which is required to generate the excitation signal. The fourth section discusses the duration of the excitation signals. Finally, a sensitivity study on the non-linear stiffness is presented.

3.6.1. A description of the situation at the moment of collapse

Figure 3.18: The grandstand element, photographed at the moment of collapse. Image is taken from RTLnieuws.nl [5].

At the moment of collapse, there were 93 people present on the grandstand element, divided over three rows. They were either jumping, bobbing, or standing still. Football players guided the jumping or bobbing frequency by waving their hands up and down. They did this with a frequency of around 2 Hz. The 8.5 m long element failed after about eight seconds of this rhythmic activity. Figure 3.18 shows the grandstand at the moment of collapse.

3.6.2. Model parameters

The model parameters used for the calculation are based on the engineering firm's report, who created a numerical model in DIANA of the grandstand element, based on technical drawings. Table 3.9 shows all relevant model parameters for the calculation. For more information, please consult [7]. Only some of the values of the parameters can be found in this report; for these, assumptions have been made. This applies to the smoothness parameter N, and both unloading shape parameters η_1 and η_2. Given these parameters, the hysteretic loops barely dissipate any energy. This is a conservative approach.

Table 3.9 An overview of the model parameters.

Parameter	Symbol	Value		Units
Mass	m	14.2	x 10^3	kg
Yield force	F_y	249	x 10^3	N
Yield displacement	u_y	6	x 10^{-3}	m
Elastic stiffness	k_0	41.5	x 10^6	N/m
Ultimate force	F_u	376	x 10^3	N
Ultimate displacement	u_u	40	x 10^{-3}	m
Post-yield stiffness	k_{nl}	3.74	x 10^6	N/m
Stiffness ratio	r_k	0.09		-
Damping ratio	ζ	0.05		-
Stiffness-proportional damping coefficient	α	1.86	x 10^{-3}	-
Mass-proportional damping coefficient	β	0		-
Gravity constant	g	9.81		m/s^2
Smoothness parameter	N	10		-
Unloading shape parameter	η_1	0.5		-
Unloading shape parameter	η_2	0.5		-

The random variable T_p ensures that the jumping behaviour becomes increasingly more random, as each jumping period is randomly drawn from this variable. However, it takes some time to develop this randomness. In order to overcome a too periodic response in the first seconds, the synthetic signal is gradually put on the structure over 2 seconds. This ensures that initial effects are not dominating the response. The excitation signal will therefore be 32 seconds. However, the first two seconds are not considered in the discussion of the results: this signal will still be treated as a 30-second signal.

3.6.3. Influence factors

The element has three rows of standing places. This means that, on average, 31 people were standing on each element row. The element has a length of 8.5 m between the supports. This gives the influence factors as shown in table 3.10. Due to symmetry, standing at, e.g., the location $x = 1.7$ m means the same as standing at the location $x = 6.8$ m. Therefore, only half of the values are shown: twice as many people are standing here than the earlier mentioned three.

Although the database also includes sets of a crowd jumping at 2 Hz, these cannot be used for the reliability assessment. There are two main reasons why they cannot be used: (1) there are only a handful of sets of a crowd jumping at 2 Hz. These are not enough for a probabilistic calculation; and (2) the sets contain up to 48 people, whereas there were 93 people on the grandstand element at the moment of collapse. 93 people represent a more extreme situation.

3.6.4. 30-second signals to determine the reliability

The grandstand element collapsed after only 8 seconds of rhythmic jumping. Therefore, shorter signals are required than the 30-second excitation signals at hand. However, 30 seconds of jumping represent a more severe situation than 8 seconds: if failure happens within 8 seconds, it also happens within 30

Table 3.10 Influence factors.

# of people	x (m)	$u(x)/EI$	u_{max}/EI	Influence factor
6	0.00	0.00	12.79	0.000
6	0.28	1.28	12.79	0.100
6	0.57	2.54	12.79	0.199
6	0.85	3.79	12.79	0.296
6	1.13	5.00	12.79	0.391
6	1.42	6.16	12.79	0.481
6	1.70	7.27	12.79	0.568
6	1.98	8.31	12.79	0.649
6	2.27	9.26	12.79	0.724
6	2.55	10.13	12.79	0.792
6	2.83	10.90	12.79	0.852
6	3.12	11.55	12.79	0.903
6	3.40	12.08	12.79	0.944
6	3.68	12.47	12.79	0.975
6	3.97	12.71	12.79	0.993
3	4.25	12.79	12.79	1.000
93				

seconds; if failure happens within 30 seconds, it does not necessarily happen within 8 seconds. The probability of failure after 8 seconds will be lower or equal to the failure probability after 30 seconds. The result of the 30-second reliability analysis can therefore be seen as an upper bound to the probability of failure of the grandstand element.

3.6.5. Expressing doubts about the correctness of the structure's resistance

A concrete structure's ultimate bending moment capacity is linearly related to the internal lever arm between the concrete compressive force and the steel tensile force. The steel tensile force is found at the location of the reinforcement. Discrepancies between the technical drawing and the as-built reinforcement location can result in significant changes in the ultimate bending capacity.

Although the location of the reinforcement of the collapsed grandstand element has not been measured, there is cause to perform a sensitivity study on the bending moment capacity of the structure. Measurements on 23 other elements in the stadium have been performed. The result of each measurement is presented in appendix C and summarized in table 3.11. The highest deviations are, on average, 41% or 16 mm higher than the mean, with an extreme case of 103% or 35 mm. The lowest deviations are, on average, 24% or 10 mm lower than the mean, with an extreme case of 50% or 19 mm. The collapsed element had a total height of 120 mm: a deviation of 16 mm would be very significant.

Table 3.11 Results of measurements of the concrete cove on other grandstand elements in the Goffert stadium [7].

	Deviation high		Deviation low	
	(%)	(mm)	(%)	(mm)
Average	41	16	-24	-10
Extreme	103	35	-50	-19

A higher concrete cover result in a lower internal lever arm, thus reducing the ultimate bending moment capacity. It does, however, not influence the initial strength of the structure: the concrete tensile strength is mainly responsible for this part, and that has not changed. This means that only the non-elastic resistance of the structure is subjected to these changes.

Table 3.12 presents the parameters used for the sensitivity study. In figure 3.19, they are visualized. This study is performed using the 30-second excitation signals. Only the ultimate force is reduced, with a percentage of the difference between the ultimate and yield force. The influence of the actual location of the reinforcement is much more complicated than presented in this study. A complete study on this phenomenon better indicates the sensitivity of the concrete cover on the ultimate resistance. The sensitivity study presented in this thesis can be used to indicate its influence on the probability of failure.

Table 3.12 Calculation parameters used for the sensitivity study.

Weakened	u_y (mm)	F_y (kN)	u_u (mm)	F_u (kN)
0%	6	249	40	376
10%	6	249	40	363.3
20%	6	249	40	350.6

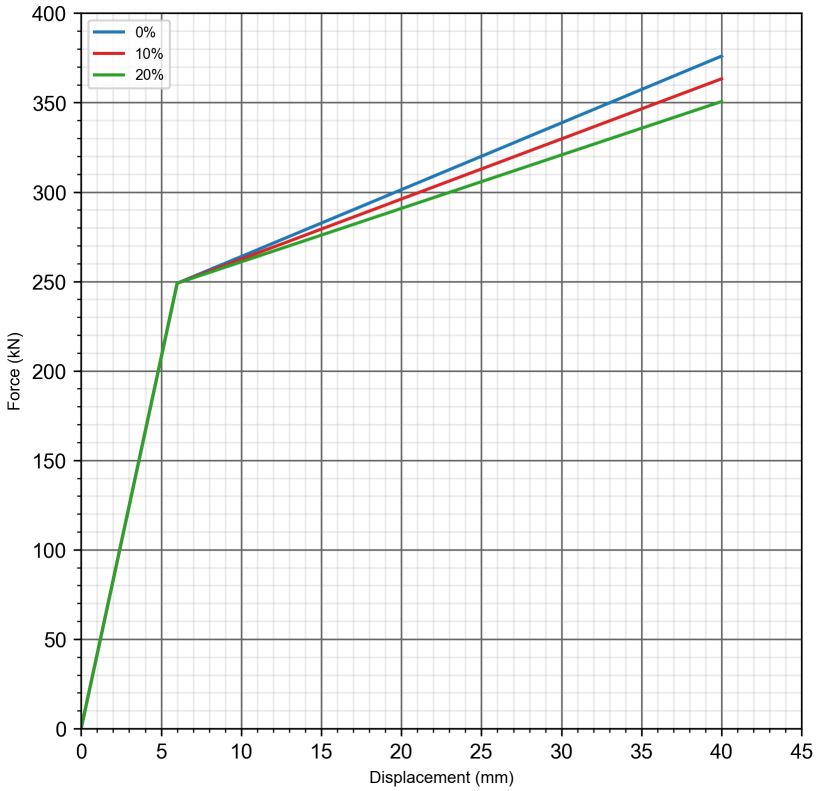

Figure 3.19: The weakened force-displacement relationships used for the sensitivity analysis.

4 Results

This thesis aimed to develop a method to perform a reliability assessment on concrete grandstand elements. The method has been applied to a case study. This chapter presents five results: (1) the generation of the synthetic excitation signal; (2) A verification analysis of the OpenSEES model ; (3) the probability of failure[1] of a concrete grandstand element subjected to 30-second acceleration signals; (4) the probability of failure[1] of a weakened concrete grandstand element; and (5) the probability of failure[1] of a concrete grandstand element subjected to 120-second, and 300-second acceleration signals.

4.1. The synthetic excitation signal

Synthetic excitation signals are required to perform the reliability analyses. Section 3.4 described the method used to generate synthetic excitation signals. Figure 4.1 portrays a randomly generated normalized ground reaction force for 93 persons in both the time and frequency domains, with a realization of a signal from the data set. Influence factors have not been introduced at this stage.

4.2. The OpenSEES verification analysis

Section 3.2 discussed the need for acceleration signals contrary to force signals. Therefore, the force signal was transformed into an acceleration signal. In order to verify this transformation, the solution to the linear elastic equation of motion in OpenSEES (using the acceleration signal) was compared to the solution using Duhamel's integral (using the force signal). The applied load is a step force. Figure 4.2 shows the result of the two calculations.

The translation of a force signal to an acceleration signal has proven successful. The response of the OpenSEES solver to the acceleration signals and the Duhamel's integral solver to the force signal are identical. As the linear elastic analysis of OpenSEES resulted in the expected outcome, it is assumed that it can also be used for non-linear analyses. The results presented in the next sections are outcomes of the non-linear dynamical analysis in OpenSEES.

[1]The failure probabilities presented in this chapter are estimates due to the limited sample size (10,000-100,000), but large enough to make conclusions.

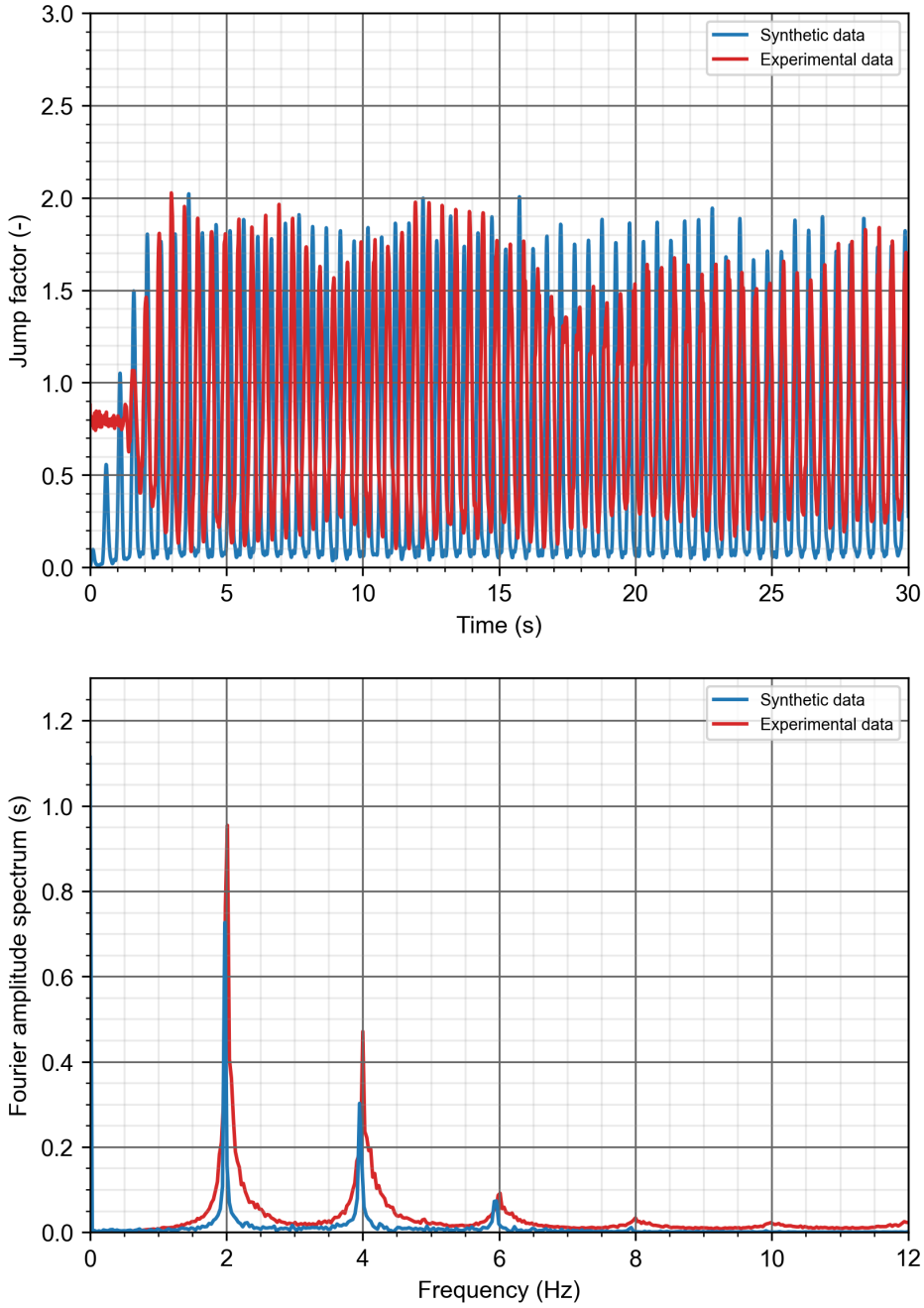

Figure 4.1: An example of a normalized ground reaction force for 93 jumping persons in the time domain (top) and frequency domain (bottom). Blue denotes the synthetically generated data. Red shows the experimentally obtained data.

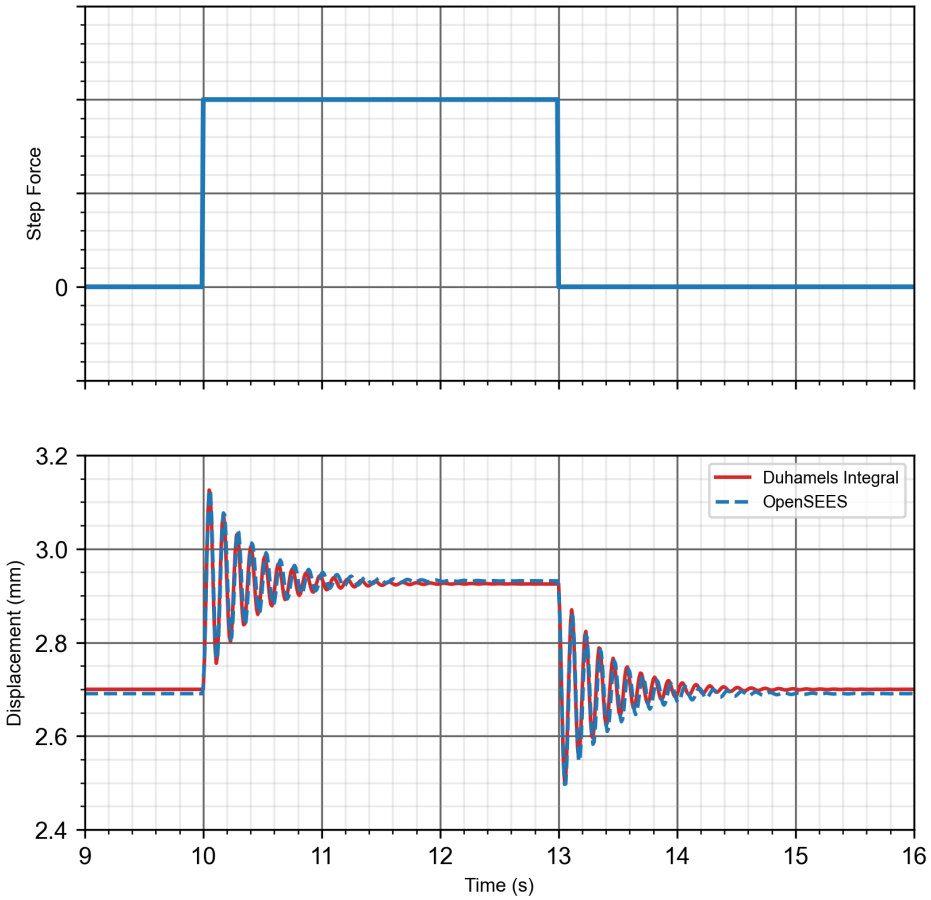

Figure 4.2: Linear elastic response of the system, subjected to a step force.

4.3. The probability of failure of the concrete grandstand element after 30 seconds of jumping

Synthetic acceleration signals are required to perform the non-linear dynamical reliability analyses. Section 3.4 explained how these are generated. Depending on the computational power of a device, generating an acceleration signal takes about 140 seconds per core per processor, resulting in over 9,000 signals per day. Given the time frame of this thesis, in total, 94,221 signals were generated. The maximum occurred displacement in the system was measured and compared to the ultimate displacement of the system. If the ratio between the maximum occurred displacement and the ultimate displacement was smaller than 1, the structure did not fail. If the ratio was higher than 1, the structure did collapse. This ratio is called a unity check:

$$uc = \frac{u_{max}}{u_u} \tag{4.1}$$

where:

uc	is the unity check;
u_{max}	is maximum displacement of the structure found during the analysis;
u_u	is the ultimate displacement allowed by the system.

Figure 4.3 presents the result of the Monte Carlo simulation. Out of 94,221 simulations, 0 failed. The probability of failure of the concrete grandstand element after 30 seconds of jumping is equal to $P_{f,30} = 0.0$. This is an unexpected result, given that the actual element failed. This assessment does not explain

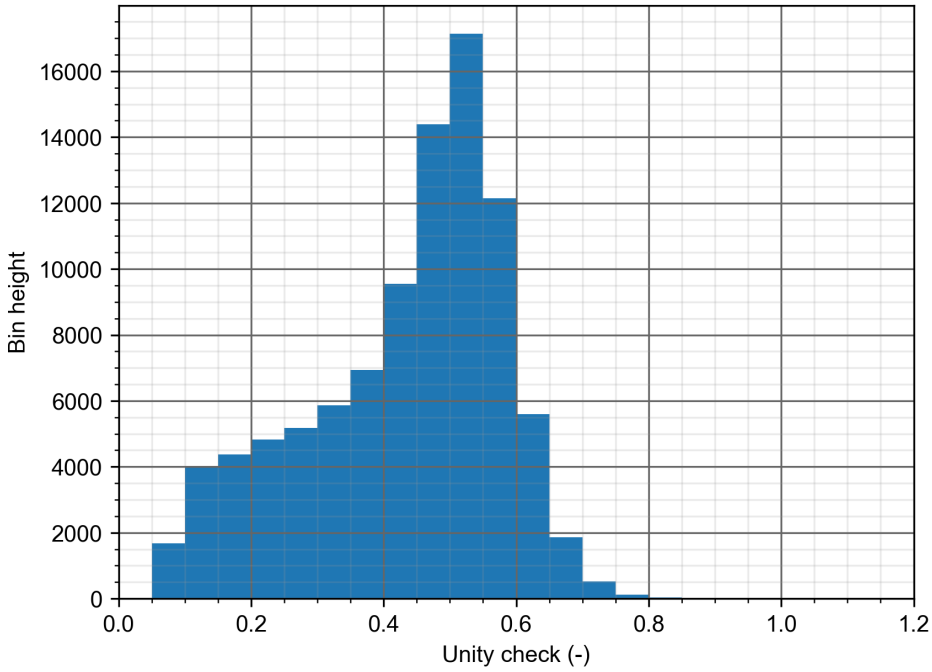

Figure 4.3: The result of the Monte Carlo simulation of the 30-second excitation signals.

why that element should have failed with such a high probability as it did. The following section presents additional assessments, which explain a more plausible cause of the failure of the collapsed element.

4.4. The probability of failure of the weakened concrete grandstand element

Section 3.6 expressed doubts regarding the correctness of the resistance of the grandstand element. This resistance is numerically determined based on the technical drawings. However, as measurements of the concrete cover on 23 other grandstand elements have shown, high variety in the concrete cover exists. These measurements can be found in appendix C. When the concrete cover on the bottom reinforcement increases, the post-yielding strength of the structure decreases. This raised a cause to perform a sensitivity analysis on the non-linear resistance of the grandstand element. Therefore, two additional simulations were performed, where this resistance was weakened. The ratio between the ultimate force and the yield force had been reduced by 10% and 20%, respectively. The results of these assessments are displayed in Figure 4.4.

When the non-linear resistance was reduced by 10%, 6 out of the 94,221 simulations failed. The probability of failure of the concrete grandstand element after 30 seconds of jumping is equal to $P_{f,10\%} = 6.4 \cdot 10^{-5}$. When the non-linear resistance was reduced by 20%, 219 out of the 94,221 simulations failed. The probability of failure of the concrete grandstand element after 30 seconds of jumping is equal to $P_{f,20\%} = 2.3 \cdot 10^{-3}$.

4.5. The probability of failure of the concrete grandstand element after 120 and 300 seconds of jumping

Section 3.5.4 presented two potential flaws of using 30-second signals, namely that 30-second signals might not contain all variability that can be expected during its lifetime and that energy could be put into the system for more than 30 seconds. The first problem was already discussed in section 3.5.4. Based on a high correlation between 15-second maxima ($\rho = 0.89$) and other studies that limited the duration

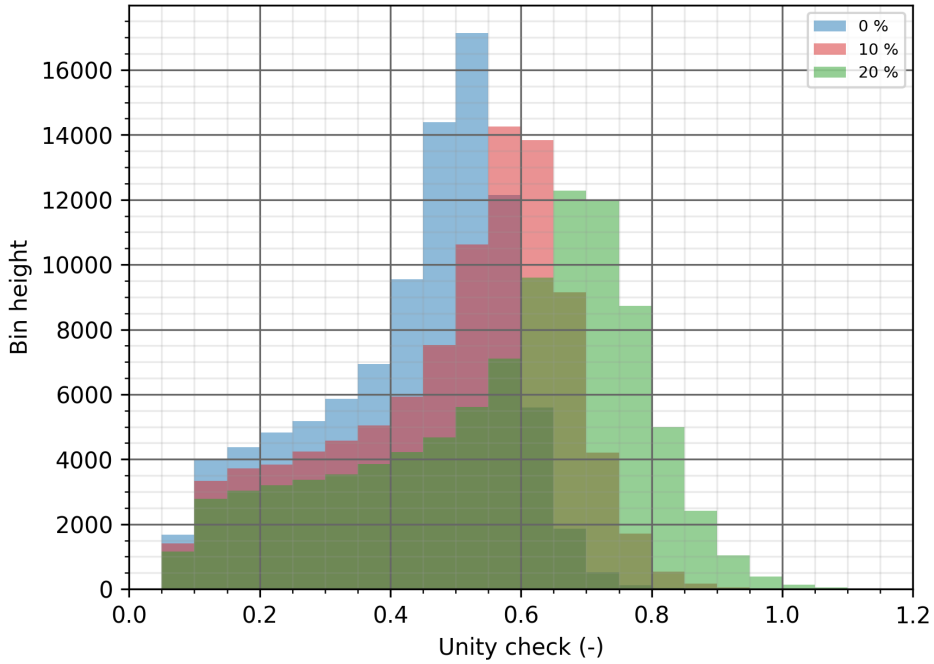

Figure 4.4: The result of the Monte Carlo simulation of the 30-second excitation signals for the 10% and 20% weakened case. The results of the 30-second excitation signals are also presented as a reference.

to 30 seconds for fatigue reasons among the participants, it is assumed that 30-second signals are approximately fully correlated. The phenomenon related to the increased energy input was tested by performing 23,554 additional tests with 120-second excitation signals and 9,421 tests with 300-second excitation signals. Figure 4.5 illustrates the result of this analysis.

80 out of the 23,554 simulations failed. The probability of failure of the concrete grandstand element after 120 seconds of jumping is equal to $P_{f,120} = 3.4 \cdot 10^{-3}$. 19 out of the 9,421 simulations failed. The probability of failure of the concrete grandstand element after 120 seconds of jumping is equal to $P_{f,300} = 2.0 \cdot 10^{-3}$.

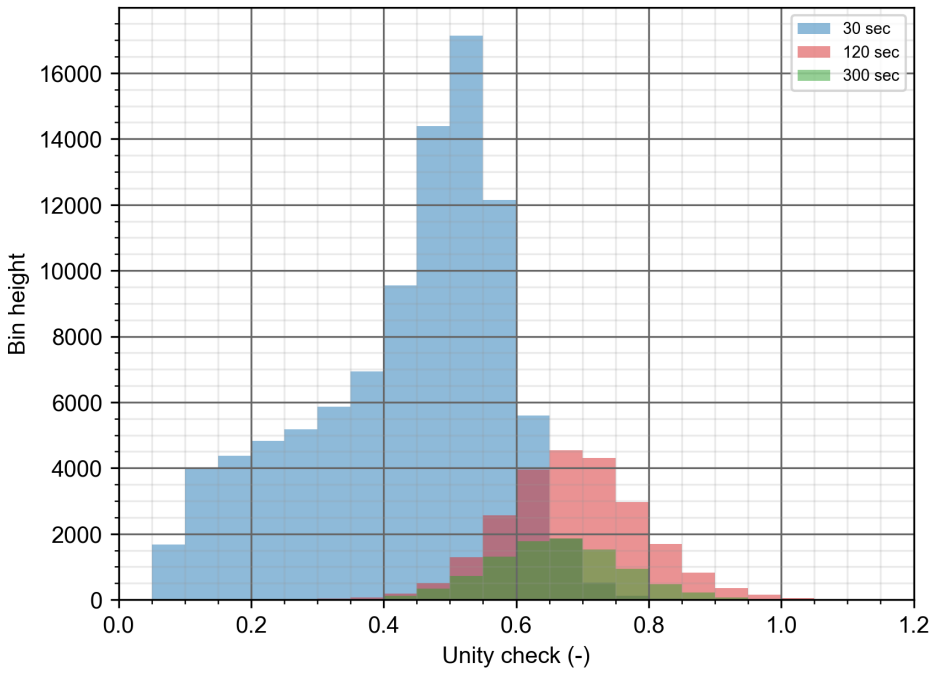

Figure 4.5: The result of the Monte Carlo simulation of the 120- and 300-second excitation signals. The results of the 30-second excitation signals are also presented as a reference.

5 Discussion

This thesis described a method to perform a reliability assessment of concrete grandstand elements subjected to jumping loads. This method was applied to a case study: football stadium the Goffert in the Netherlands. First, synthetic excitation signals were generated. These signals were required to perform Monte Carlo simulations, which was the proposed method to determine the reliability of the structure. None of the 30-second signals led to the failure of the system. Longer signals and weakened resistance models did lead to failure in some cases. This chapter discusses the results presented in chapter 4.

5.1. Randomly generated excitation signals

This section discusses the creation of synthetically generated excitation signals. The results presented a realization of the normalized ground reaction force. Given the distributions and parameters for the random variables, the peaks of this signal were, on average, between 1.6 and 2.1. The expected peak value of the sts jump factor was determined at 3.1. This results in a coordination factor between 0.52 and 0.68. The lower bound supports the lowest values found in the literature [24]. Values up to 0.90 [12] are found in other studies: therefore, the upper bound of the randomly generated signals is also accepted.

The database showed that, for crowds, there is always someone in contact with the floor. This is also the case for synthetic signals: the normalized force never reaches zero. However, the force's lowest magnitude is lower in the synthetic signal than in the experimentally obtained signal. The synthetic signal yields values around 0.1, whereas the data set is closer to 0.25. This indicates that the random variables used for this study alone are insufficient to describe the actual jumping behavior accurately. In addition, experimentally obtained signals show a wavy pattern, both on the top and bottom sides. The synthetically obtained signals only have this on the top side.

Further comparison of the two signals in their frequency domains shows that both are narrow-banded signals. This was the goal of randomizing the parameters T_p and ϕ. Narrow-banded processes prevent possible artificial resonances in numerical models and lead to a better reconstruction of the actual situation.

The magnitude of the first (2 Hz) harmonic is slightly underrepresented in the synthetic signal: around 0.75 versus 0.9 for the experimental data. For the second harmonic, the difference is larger: around 0.30 versus 0.45. The third harmonics are more or less equally represented. The experimental data shows significant contributions at frequencies other than the harmonics, which the synthetic data lacks. This indicates that more parameters are required to recreate a signal than used in this thesis accurately.

To investigate the influence of the differences between the two signals, three linear elastic dynamical analyses are performed to show the different responses to the two excitation signals. Figure 5.1

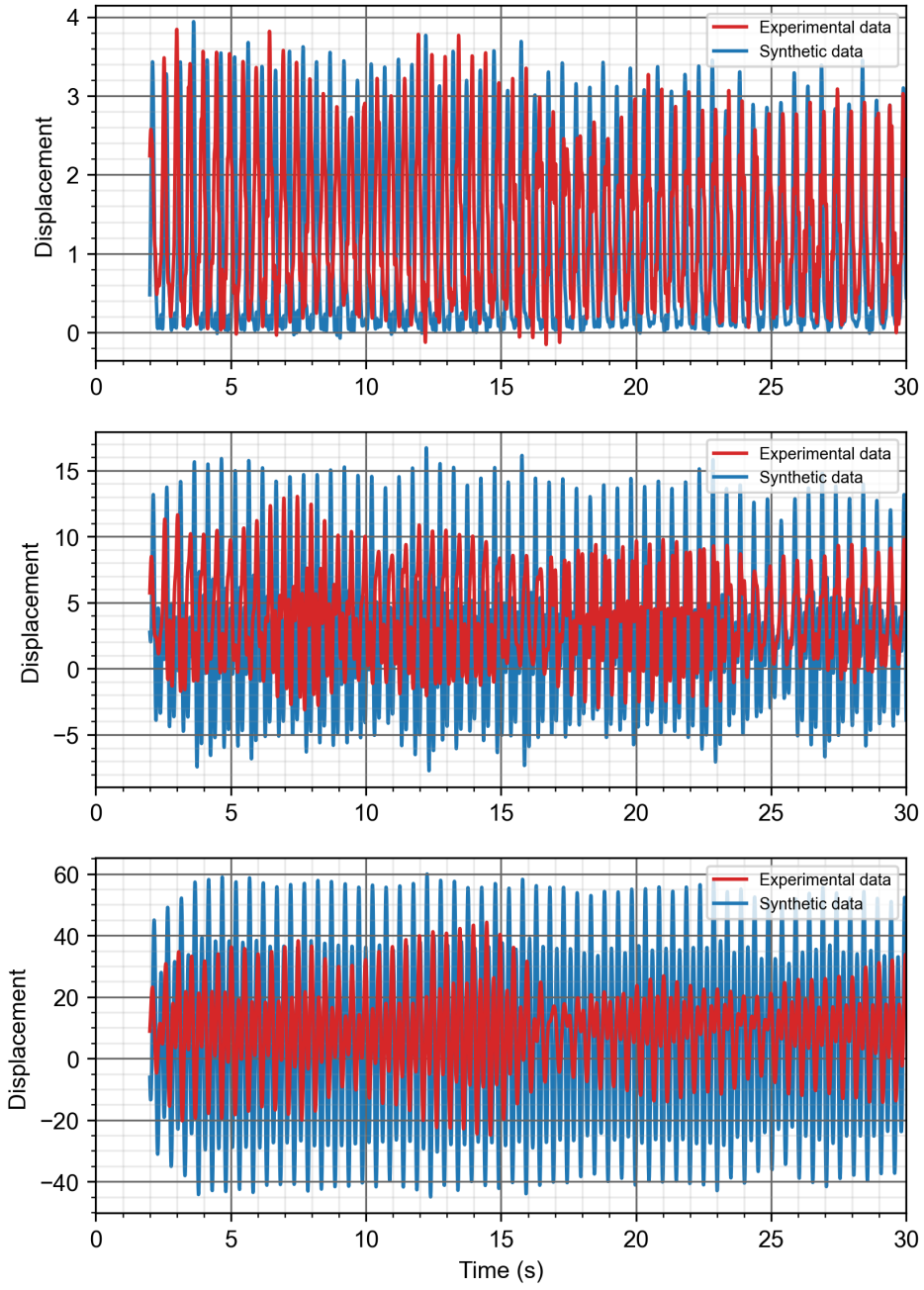

Figure 5.1: Linear elastic response of the system to an experimental (red) and a synthetic (blue) excitation signal. The structure's eigenfrequency is either 10 Hz (top), 6 Hz (middle), or 4 Hz (bottom).

presents the results. The eigenfrequencies of the system are 10 Hz, 6 Hz, and 4 Hz, respectively. The first eigenfrequency represents the linear elastic situation. The 6 and 4 Hz eigenfrequencies are chosen because resonant effects could occur at these frequencies.

Figure 5.1 shows that the synthetic signals lead to a larger response when the eigenfrequency is 6 Hz or 4 Hz. This is an unexpected result, especially when the eigenfrequency is 4 Hz because the experimentally obtained signal shows much more energy around this frequency than the synthetically obtained signal. However, the response is lower than the experimentally obtained signal. Further investigation is required to explain the reasoning behind this result. Nevertheless, the synthetically generated signals do not underestimate the structural response when the eigenfrequency reduces.

Therefore, the proposed method is suited to generate excitation signals of jumping crowds.

5.2. The reliability level of a grandstand element

Chapter 4 presented two different types of reliability analyses. The first type investigated the Goffert stadium case study and tried to explain the failure of this element. The second type examined the reliability of grandstand elements in general, subjected to a jumping crowd. Here, failure is not expected after 8 seconds of jumping. In total, this resulted in five different reliability assessments: a basic analysis, where 30 seconds of jumping was simulated; two sensitivity studies where the non-linear resistance of the grandstand element was weakened by 10 or 20%; and two studies where longer (120 s and 300 s) excitation signals were put on the system. This section discusses the results of these reliability analyses.

5.2.1. The reliability of the Goffert stadium grandstand element

Table 5.1 presents the reliability assessment results of the first assessment. The first assessment represents the bi-linear force-displacement relationship as determined by a numerical model of the technical drawings of the grandstand element.

Assessment	n_f	n	n_f / n*	β*	Average uc
1	0	94,221	0	-	0.43

Table 5.1 The estimated probability of failure of the grandstand element after 30 seconds of jumping, where the resistance is based on a numerical model recreated in DIANA, which is based on the technical drawings of the grandstand element.

* The results presented in this table are estimates of the true probability of failure of the grandstand element. The sample size in this study is too small to obtain a converged probability of failure P_f, or reliability level β, but it is large enough to draw conclusions. To achieve converged values, 1-10 million simulations are required.

After 30 seconds of jumping, 0 failed simulations out of the 94,221 were noted. These results are based on an as accurate as possible description of the force a crowd generates by jumping on 2 Hz and a force-displacement relationship as determined by the numerical model reconstructed by the engineering consultancy firm in DIANA based on the technical drawings of the grandstand element. However, after only eight seconds of jumping, the element collapsed. There is a discrepancy between the failure probability of the real structure and the failure probability of the assessment: a much higher probability of failure of the assessment was expected as it collapsed after only 8 seconds of jumping. This indicates that either the model or the input is incorrect. The input can be divided into the load and the resistance. All these topics are now examined in greater detail.

The way the grandstand element is modelled is a very commonly used method. Some studies have proposed a 2DOF system to model the element that can include HSI, but in most cases, an SDOF system is sufficient. An SDOF system is likely to overestimate the structural response when excited at resonance, as was concluded by the literature study. The numerical solver of the system (i.e., OpenSEES) has been compared to another method (i.e., Duhamel's integral) in a linear elastic comparison, and the results were equal, indicating that numerical errors are also unexpected. The proposed method is therefore judged to lead to unbiased results for this analysis.

The synthetically generated excitation signals are based on the analysis of a data set of jumping crowds. The values of the data set generally compared well with what is stated in the literature: especially the magnitude of the forces exerted by jumping was perfectly in line with what is found there. The contact ratio was overestimated, but values from the literature were adopted when generating the signals. Because the force signals of the data set looked comparable to what other literature has stated, the data set is assumed to be reliable.

Section 5.1 has shown that the synthetic signals look similar to the experimental signals in the time domain. The response to these signals in these three cases was larger when the system was subjected

to a synthetic signal. The structure's response in the non-linear analysis is most likely overestimated when the system's eigenfrequency gets close to one of the harmonics of the excitation frequency. The excitation signals are based on state-of-the-art literature and random variables obtained from the analysis of a data set. Thus, the discrepancy cannot be explained by the excitation signals.

The numerical resistance model created by the engineering firm has not been verified, but the grandstand element is not complex to model. The engineering firm should be more than capable of creating such models. There is no reason to assume the DIANA model would be incorrect. Furthermore, the consultancy firm has also performed a numerical analysis of the grandstand element in Abaqus, increasing the trust in the correctness of the model. Therefore, there is no reason to assume that a falsely numerically determined resistance model is the basis of the discrepancy.

Measurements of 23 other grandstand elements in the Goffert stadium portrayed high variations of the concrete cover (see appendix C). The highest measured cover in each element was, on average, 16 mm higher than the average concrete cover of that element. Although these measurements do not directly apply to the failed element, it is reasonable to assume that it was subjected to large variations in the concrete cover. Therefore, as described in section 3.6, additional reliability assessments were performed, where the structure's non-linear resistance was reduced. The results are presented in table 5.2, together with the unweakened resistance (assessment 1). The probability of failure ramps up when the non-linear capacity is reduced. A 10% weakened structure (assessment 2) results in a probability of failure in the order of magnitude of 10^{-5}. This goes up to 10^{-3} for 20% (assessment 3). Based on this sensitivity study, it can be concluded that the non-linear capacity of the structure is a key parameter when investigating the reliability of a grandstand element.

Assessment	Weakened	n_f	n	n_f / n*	β*	Average uc
1	0%	0	94,221	0	-	0.43
2	10%	6	94,221	6.4×10^{-5}	3.8	0.49
3	20%	219	94,221	2.3×10^{-3}	2.8	0.57

Table 5.2 The estimated probability of failure of the grandstand after 30 seconds of jumping for 10 and 20% weakened structures.

* The results presented in this table are estimates of the true probability of failure of the grandstand element. The sample size in this study is too small to obtain a converged probability of failure P_f, or reliability level β, but it is large enough to draw conclusions. To achieve converged values, 1-10 million simulations are required.

The first reliability assessment gave no indication that the grandstand element would have been unreliable if the design conformed to the technical drawings. A combination of state-of-the-art excitation signals combined with the model's resistance according to the structural drawing gives no cause for concern regarding the reliability of the element. A sensitivity study demonstrated that the non-linear capacity of a grandstand element is an important parameter when determining the probability of failure of the element. Concrete cover measurements of other elements in the stadium have shown large variations in the concrete cover. These two points combined indicate that the failed grandstand element in the Goffert stadium was likely subjected to large variations in the concrete cover. The three presented reliability assessments have shown that the collapse of the Goffert stadium grandstand element cannot be explained by the loads but rather by a likely weaker-than-intended resistance. This did not play a role in the investigation of the engineering consultancy firm.

5.2.2. The general reliability of a grandstand element

This section discusses the reliability of a grandstand element in general. For these elements, no failure is expected after 8 seconds of jumping but rather after 30 seconds or even longer. Therefore, longer signals are included. The reliability level in this section is related to the exceedance of the bending moment capacity of the structure, which is excited by a uniformly distributed crowd of 93 people jumping at a grandstand element of 8.5 m long at a frequency of 2 Hz.

Longer excitation signals are required as people can jump for over 30 seconds. Jumping for more than 30 seconds does not lead to a higher expected lifetime maximum load due to the very high correlation between the 15-second maxima ($\rho = 0.89$) and fatigue symptoms of the participants. These combined indicated that the 30-second maxima are approximately fully correlated, which means that no higher force peaks are expected to occur when jumping for more than 30 seconds compared to jumping for 30 seconds.

Jumping for a longer duration could lead to more energy being put into the system, which means that deformations also increase and, subsequently, the probability of failure would increase. However, at a certain point, a steady-state solution is reached. In the steady state, the energy put into the system equals what is dissipated from the system. This means that deformations do not increase anymore beyond the boundaries of the steady-state solution, thus leading to a bounded displacement. The bounded displacement means that it does not matter how long the crowd jumps after this is reached: the displacements will not increase beyond these bounds. This section investigates the required duration of excitation signals to achieve the steady-state solution. Table 5.3 shows the result of jumping for a prolonged duration (assessments 4 and 5). The initial assessment is also shown as a reference.

Assessment	Duration	n_f	n	n_f / n*	β*	Average uc
1	30 s	0	94,221	0	-	0.43
4	120 s	80	23,554	3.4×10^{-3}	2.7	0.69
5	300 s	19	9,421	2.0×10^{-3}	2.9	0.66

Table 5.3 The probability of failure of the grandstand after 30, 120, and 300 seconds of jumping.

* The results presented in this table are estimates of the true probability of failure of the grandstand element. The sample size in this study is too small to obtain a converged probability of failure P_f, or reliability level β, but it is large enough to draw conclusions. To achieve converged values, 1-10 million simulations are required.

The reliability of the structure, when people jump on it for 120 seconds, drops to $\beta = 2.7$. The decreased reliability indicates that a steady-state solution was not yet found after jumping for 30 seconds. Jumping for 300 seconds did not result in a larger probability of failure of the system. This indicates that a steady-state solution might be reached after 120 seconds. Furthermore, the average unity check does not increase either, suggesting that the structure does not oscillate beyond the boundaries of the steady-state solution: signs of a converged calculation are plausible at a probability of failure in the order of magnitude of magnitude 10^{-3}. Different jumping combinations for 120 seconds are thus not expected to result in a different reliability level: the 120-second reliability has become equal to the lifetime reliability.

NEN 8700 [57] explains how to judge the structural reliability of existing structures. In this Standard, the lifetime reliability for Consequence Class 2 structures (for a reference period of 15 years) should be larger than $\beta > 2.5$. Given the framework of this analysis, if the reliability of grandstand elements is to converge to $\beta = 2.7 - 2.9$, then there is no cause for concern regarding the safety of existing grandstand elements such as those found in the Goffert stadium if the element is designed according to the technical drawings. All the conclusions are based on a state-of-the-art numerical model. A model uncertainty parameter was incorporated to correct for potential errors, and damping parameters were chosen conservatively. Therefore, given the scope of this thesis, there is no reason to assume that the presented results would negatively deviate from the true probability of failure.

The proposed method this thesis presents is suited to model the dynamical behavior of a concrete grandstand element subjected to dynamical crowd loads. Given the boundaries of this thesis, it is expected that the proposed framework allows assessing the reliability of any grandstand element whose resistance can be modelled using one of the OpenSEES material models that allows a force-displacement relationship as input: it is thus not limited to concrete structures. A Monte Carlo simulation can be used to assess the element's reliability: 100,000 simulations can be performed in less than eight hours, depending on the calculation device's capacity. Therefore, this thesis has provided a quick and flexible framework to assess the reliability of a grandstand element.

6

Conclusions

This thesis presented a new method to assess the reliability of concrete grandstand elements. The study was motivated by the collapse of the Goffert stadium in Nijmegen, the Netherlands, caused by 8 seconds of rhythmic jumping at 2 Hz. Although dynamical models of grandstand elements exist, there is no model incorporating all the variability, allowing for a full probabilistic calculation of the failure probability.

In this reliability assessment, the element is modelled as a non-linear single-degree-of-freedom system, where the resistance of the structure was copied from a numerical model of the Goffert stadium grandstand element. State-of-the-art 30-second excitation signals were generated by combining what is found in the literature and by analyzing a data set of jumping people. A bi-linear force-displacement relationship based on technical drawings of the collapsed grandstand element is adopted and extended by a model uncertainty parameter which accounts for both the non-linearity of the analysis and the uncertainty related to the dynamical basis of the analysis. The response was determined through a non-linear dynamical analysis, and the reliability was determined using a Monte Carlo simulation.
This method was applied to a case study: the Goffert stadium in Nijmegen. The jumping behavior of the crowd was modelled as correctly as possible. When using the numerical resistance model based on technical drawings of the Goffert stadium grandstand element, 0 of almost 100,000 simulations failed. This assessment showed that if the structure's resistance conformed to the technical drawings, there would be no cause for concern regarding its reliability.

However, measurements on other grandstand elements in the Goffert showed a high variation on the concrete cover, suggesting that the failed grandstand element may also have been subjected to a wide variety of concrete cover. This presented a cause to perform additional analyses to quantify the influence of this phenomenon on the probability of failure. In these analyses, much larger failure probabilities were found. Since the initial assessment could not explain the collapse, whereas these two assessments could, it is more plausible that the failure of the Goffert stadium grandstand element is caused by the structure being weaker than intended rather than by the loads being too large.

In a second study, the influence of the excitation signals' duration on the grandstand element's reliability, based on the numerically determined resistance of the Goffert stadium element, was investigated. Longer excitation signals of 120 to 300 seconds are recommended to assess the grandstand elements' reliability fully. These durations indicated that the reliability level of these grandstand elements might converge to $\beta = 2.7 - 2.9$, which is acceptable by current Standards for existing structures (with a reference period of 15 years). Given the boundaries of this thesis, the proposed method allowed the determination of the lifetime reliability of a grandstand element. Therefore it can be concluded that the proposed method provides a valuable framework for evaluating the reliability of grandstand elements. With minor adaptations, the presented reliability assessment can be extrapolated to assessing any structure's reliability whose resistance can be modelled bi-linearly.

7

Recommendations

This thesis aimed to develop a method for the reliability assessment of concrete grandstand elements. While the study made considerable progress in this direction, there are still areas for improvement and further research. The following are some recommendations for future work.

The generation of synthetic excitation signals was a crucial part of the proposed method. However, these signals only approximate real-world excitations and may lead to slight overestimations of the response. A better recreation of the excitation signals leads to a lower response. This can be achieved by further analyzing the data set of jumping people and by conducting new experiments. Further research can be carried out in these two directions to improve the accuracy of recreating these signals and enhance the reliability assessment.

Further investigation into human-structure interaction is necessary to fully understand the dynamic interaction between jumping crowds and grandstands; incorporating human-structure interaction in the dynamic calculation results in a lower response. Although this thesis touched upon this aspect, it was limited in scope, and more research is needed to incorporate these effects in the model fully. Future studies could focus on the influence of the human-structure interaction of groups, as almost all literature is focused on the interaction between an individual and the structure.

The choice of damping parameters is a critical factor in determining the structure's response. Currently, there is not enough literature to support the selection of appropriate parameters for concrete grandstand elements. This thesis assumed that damping due to hysteresis is negligibly small, which is a conservative take. Further work can be carried out to obtain reliable damping parameters, e.g., by performing tests on grandstand elements, improving the model's accuracy.

Although the proposed method is expected to be flexibly constructed such that it can assess the reliability of any grandstand element - given the limitations of this thesis - this can only be concluded after more case studies are performed incorporating this method. A great addition would be to assess the reliability of a grandstand element composed of a different material and different supporting conditions, such as a steel cantilever grandstand element.

Finally, this thesis provided estimations of reliability levels based on a limited sample size. A larger sample size (1-10 million) and longer excitation signals are needed to achieve more accurate and converged results. Longer signals will also help verify if the steady-state solution is reached after 120 or 300 seconds, improving the proposed method's robustness.

References

[1] J. van der Plicht. *Tribune NEC-stadion ingestort door constructiefout en te veel springende fans*. NU.nl, https://www.nu.nl/binnenland/6166148/tribune-nec-stadion-ingestort-door-constructiefout-en-te-veel-springende-fans.html. Nov. 2021.

[2] M. Spanenburg. "Dynamische belasting op tribunes". In: *Cement* 2 (2022), pp. 36–46.

[3] Ken'ichi TATEBATAKE et al. "Modeling of hysteresis characteristics of the piezoelectric actuator using the bouc-wen model". In: *Transactions of the JSME (in Japanese)* advpub (2017), pp. 16–00462. DOI: 10.1299/transjsme.16-00462.

[4] A. Tsouvalas. *Structural Response to Earthquakes*. 2020.

[5] RTL. *Onderdelen tribunes stadion NEC moeten worden versterkt*. RTLnieuws.nl, https://www.rtlnieuws.nl/sport/voetbal/artikel/5272655/nec-kan-volle-goffert-blijven-spelen-na-versterken-tribunes. Dec. 2021.

[6] J Sim et al. "Statistical model of crowd jumping loads". In: *Journal of structural engineering* 134.12 (2008), pp. 1852–1861.

[7] Royal HaskoningDHV. *Onderzoek naar de technische oorzaken van het bezwijken van het tribune-element van het Goffertstadion te Nijmegen*. Gemeente Nijmegen, https://www.nijmegen.nl/nieuws/nieuwsdossiers/instorting-tribune-element-de-goffert. Feb. 2022.

[8] *Eurocode 1: Actions on structures - Part 1-1: General actions - Densities, self-weight, imposed loads for buildings*. Standard. European Committee for Standardization, Nov. 2007.

[9] Hugo Bachmann et al. *Vibration problems in structures: practical guidelines*. Springer Science & Business Media, 1995.

[10] JH Rainer, G Pernica, and David E Allen. "Dynamic loading and response of footbridges". In: *Canadian Journal of Civil Engineering* 15.1 (1988), pp. 66–71.

[11] T Ji and BR Ellis. "Floor vibration induced by dance-type loads: theory". In: *Structural Engineer* 72 (1994), pp. 37–37.

[12] *Bases for design of structures - Servicability of buildings and walkways against vibrations*. Standard. International Organization for Standardization, Nov. 2007.

[13] *Loading for buildings Part 1. Code of practice for dead and imposed loads*. Standard. British Standard, Sept. 1996.

[14] *National Building Code of Canada 2005 Volume 1*. Standard. Canadian Commission on Building and Fire Codes, 2005.

[15] *Trillingen van vloeren door lopen*. Standard. SBR, Sept. 2005.

[16] Hugo Bachmann and Walter Ammann. *Vibrations in structures: induced by man and machines*. Vol. 3. Iabse, 1987.

[17] Jiecheng Xiong and Jun Chen. "Open access and updated human-induced load data set". In: *Journal of Structural Engineering* 147.3 (2021), p. 04720003.

[18] Jackie HH Sim. "Human-structure interaction in cantilever grandstands". PhD thesis. University of Oxford, 2006.

[19] J MW Brownjohn, Aleksandar Pavic, and P Omenzetter. "A spectral density approach for modelling continuous vertical forces on pedestrian structures due to walking". In: *Canadian Journal of Civil Engineering* 31.1 (2004), pp. 65–77.

[20] Vitomir Racic and A Pavic. "Mathematical Model to Generate Asymmetric Pulses due to Human Jumping". In: *Journal of Engineering Mechanics* (2009).

[21] Vitomir Racic and A Pavic. “Stochastic approach to modelling of near-periodic jumping loads”. In: *Mechanical systems and signal processing* 24.8 (2010), pp. 3037–3059.

[22] A Ebrahimpour and RL Sack. “Modeling dynamic occupant loads”. In: *Journal of Structural Engineering* 115.6 (1989), pp. 1476–1496.

[23] BR Ellis and T Ji. “Loads generated by jumping crowds: numerical modelling”. In: *Structural Engineer* 82.17 (2004), pp. 35–40.

[24] Elsa Caetano, Álvaro Cunha, and Carlos Moutinho. “Vandal loads and induced vibrations on a footbridge”. In: *Journal of Bridge Engineering* 16.3 (2011), pp. 375–382.

[25] Jun Chen et al. “Data-driven synchronization analysis of a bouncing crowd”. In: *Shock and Vibration* 2019 (2019).

[26] Vitomir Racic and A Pavic. “Mathematical model to generate near-periodic human jumping force signals”. In: *Mechanical Systems and Signal Processing* 24.1 (2010), pp. 138–152.

[27] D Ginty, JM Derwent, and T Ji. “The frequency ranges of dance-type loads”. In: *Structural Engineer* 79.6 (2001), pp. 27–31.

[28] John D Littler. “Frequencies of synchronised human loading from jumping and stamping.” In: *Structural Engineer* 81.22 (2003), pp. 27–35.

[29] Puk (https://physics.stackexchange.com/users/171547/puk). *Why do higher harmonics have a lower amplitude than the fundamental frequency?* Physics Stack Exchange. URL: `https://physics.stackexchange.com/q/563773`.

[30] BR Ellis, T Ji, and BRE. “Human-structure interaction in vertical vibrations.” In: *Proceedings of the Institution of Civil Engineers-Structures and Buildings* 122.1 (1997), pp. 1–9.

[31] E Shahabpoor and Aleksandar Pavic. “Human-structure dynamic interaction during short-distance free falls”. In: *Shock and Vibration* 2016 (2016).

[32] S Yao et al. “Forces generated when bouncing or jumping on a flexible structure”. In: *Proceedings of the international conference on noise and vibration*. Vol. 2. 2002, pp. 563–572.

[33] Cássio Gaspar et al. “Active human-structure interaction during jumping on floors”. In: *Structural Control and Health Monitoring* 27.3 (2020), e2466.

[34] S. Appelman. “Dynamic Interaction Between Event Deck Structures and a Jumping Crowd”. MA thesis. Delft University of Technology, 2022.

[35] Spijkers, J.M.J., Vrouwenvelder, A.W.C.M., Klaver, E.C. *Structural Dynamics*. 2005.

[36] G. Giraldo. *How to Compute the Coefficients for Rayleigh Damping?* 2021.

[37] KA Morris. “What is hysteresis?” In: *Applied Mechanics Reviews* 64.5 (2011).

[38] Mervyn J Kowalsky, MJ Nigel Priestley, and Gregory A MacRae. “Displacement-based design of RC bridge columns in seismic regions”. In: *Earthquake engineering & structural dynamics* 24.12 (1995), pp. 1623–1643.

[39] Mettupalayam Veluswami Sivaselvan and Andrei M Reinhorn. *Hysteretic models for cyclic behavior of deteriorating inelastic structures*. Multidisciplinary Center for Earthquake Engineering Research Buffalo, NY, 1999.

[40] Nathan M Newmark. “A method of computation for structural dynamics”. In: *Journal of the engineering mechanics division* 85.3 (1959), pp. 67–94.

[41] Frank McKenna, Michael H Scott, and Gregory L Fenves. “Nonlinear finite-element analysis software architecture using object composition”. In: *Journal of Computing in Civil Engineering* 24.1 (2010), pp. 95–107.

[42] de Borst, Prof.dr.ir. R., Sluys, Prof.dr.ir. L.J. *Computational Methods in Non-linear Solid Mechanics*. 2015.

[43] SciPy. *Statistical functions*. Scipy, `https://docs.scipy.org/doc/scipy/reference/stats.html`. n.d.

[44] Pauli Virtanen et al. “SciPy 1.0: Fundamental Algorithms for Scientific Computing in Python”. In: *Nature Methods* 17 (2020), pp. 261–272. DOI: `10.1038/s41592-019-0686-2`.

[45] Vitomir Racic, JMW Brownjohn, and A Pavic. “Reproduction and application of human bouncing and jumping forces from visual marker data”. In: *Journal of Sound and Vibration* 329.16 (2010), pp. 3397–3416.

[46] Guo Li, Tianjian Ji, and Jun Chen. “Determination of the dynamic load factors for crowd jumping using motion capture technique”. In: *Engineering structures* 174 (2018), pp. 1–9.

[47] Statistics Solutions. *Pearson’s Correlation Coefficient*. Statistics Solutions, `https://www.statisticssolutions.com/free-resources/directory-of-statistical-analyses/pearsons-correlation-coefficient/`. n.d.

[48] Brian R Ellis, T Ji, and JD Littler. “The response of grandstands to dynamic crowd loads”. In: *Proceedings of the Institution of Civil Engineers-Structures and Buildings* 140.4 (2000), pp. 355–365.

[49] Algemeen Dagblad. *Nederlanders steeds langer én steeds zwaarder*. Algemeen Dagblad, `https://www.ad.nl/binnenland/nederlanders-steeds-langer-en-steeds-zwaarder~a3f876511/`. Nov. 2019.

[50] J.W. Welleman. *Module: Invloedslijnen*. June 2013.

[51] BR Ellis and T Ji. “Loads generated by jumping crowds: experimental assessment”. In: *BRE INFORMATION PAPER IP* 4 (2002).

[52] Joint Committee on Structural Safety. *JCSS PROBABILISTIC MODELCODE PART 3: RESISTANCE MODELS*. Joint Committee on Structural Safety, `https://www.jcss-lc.org/publications/jcsspmc/modeluncertainties.pdf`. Mar. 2001.

[53] Hendrik Schlune, Mario Plos, and Kent Gylltoft. “Safety formats for non-linear analysis of concrete structures”. In: *Magazine of Concrete Research* 64.7 (2012), pp. 563–574.

[54] Joan Ramon Casas et al. *Safety and Probabilistic Modelling: Sustainable Bridges Background document D4. 4*. 2007.

[55] *Eurocode - Basis of structural design*. Standard. European Committee for Standardization, Nov. 2001.

[56] Jun Chen, Guo Li, and Vitomir Racic. “Acceleration response spectrum for predicting floor vibration due to occupants jumping”. In: *Engineering Structures* 112 (2016), pp. 71–80.

[57] *NEN 8700+A1: Beoordeling van de constructieve veiligheid van een bestaand bouwwerk bij verbouw en afkeuren - Grondslagen*. Standard. Stichting Koninklijk Nederlands Normalisatie Instituut, Aug. 2020.

A

Extreme value theory

Appendix A describes the extreme value theory. EVT is used to describe extreme deviations from the median of a probability distribution. This theory allows for the extrapolation of exceedance probabilities of smaller and known time windows to more severe conditions. The theory knows many applications. Two examples are to determine the water level that occurs once every 1000 years or the maximum wind load that occurs once every 50 years.

A.1. Mathematics

EVT is based on the assumption that the random variables are independent and identically distributed (i.i.d.). If $X_1, ..., X_n$ are realizations of a random variable and the distribution of its maximum is the one of interest, then the following is searched for:

$$Z = \max\{X_1, ..., X_n\} \tag{A.1}$$

For a certain threshold ξ, it should hold that all realizations X_i are smaller than ξ:

$$F_Z(\xi) = P(Z < \xi) = P\left(\max\{X_1, ..., X_n\} < \xi\right) = P\left(X_1 < \xi, ..., X_n < \xi\right) \tag{A.2}$$

Under the assumption that all events X_i are independent, equation (A.2) can be rewritten into:

$$F_Z(\xi) = P\left(X_1 < \xi, ..., X_n < \xi\right) = P\left(X_1 < \xi\right) \cdot ... \cdot P\left(X_n < \xi\right) \tag{A.3}$$

If all realisations X_i are of the same distribution function $F_i = F$ for all i, then:

$$F_Z(\xi) = \left(F\left(\xi\right)\right)^n \tag{A.4}$$

A.2. Maximum value distributions

In general, there are two approaches to determine the maximum value distribution within a time interval. The first is called the block maxima method, and the second is called the peaks over threshold (POTS) method. The following two subsections will each briefly explain how the methods work and what distinguishes them.

A.2.1. Block maxima method

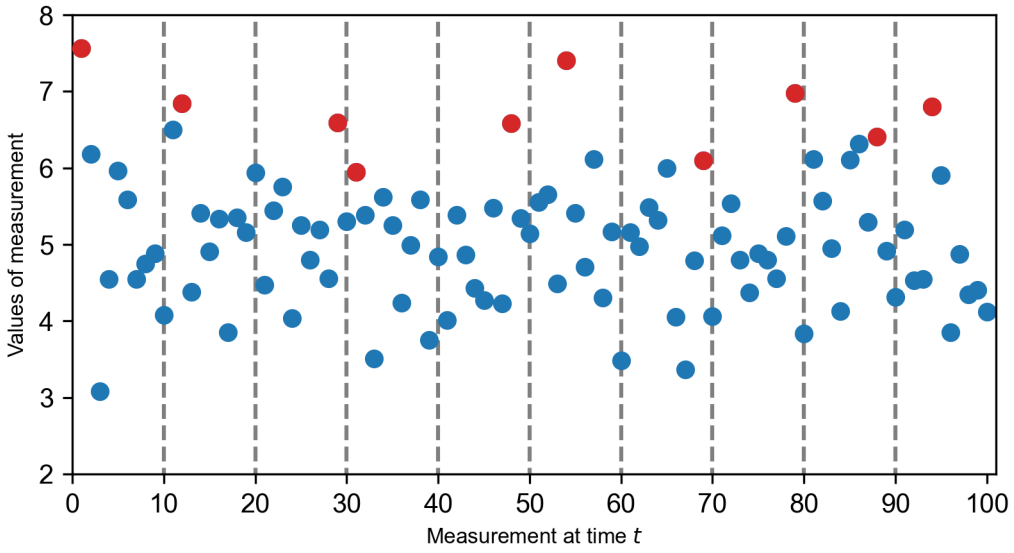

Figure A.1: An example of the block maxima method. Here, 100 samples are divided into blocks of 10. The 10-block maxima are denoted in red.

The block maxima method divides time into segments of a, to be determined, constant width, Δt. In each time block, the maximum value is taken. This is shown in figure A.1.

The Fisher–Tippett–Gnedenko theorem states that for a large enough sample size n, the distribution of its extremes converges to the generalized extreme value (GEV) family of distributions, denoted as $G(x)$. This is regardless of the distribution of X. The GEV family consists of three types of distributions, which can all be denoted with the following equation:

$$G(x) = \exp\left\{-\left(1+\xi\cdot\frac{x-\mu}{\sigma}\right)^{-\frac{1}{\xi}}\right\}, \qquad \left(1+\xi\cdot\frac{x-\mu}{\sigma}\right)>0 \tag{A.5}$$

where:

$G(x)$ is the cumulative density function of the extreme distribution;
μ is the location parameter ($-\infty < \mu < \infty$);
σ is the scale parameter ($\sigma > 0$);
ξ is the shape parameter ($-\infty < \xi < \infty$).

The shape parameters indicates the behavior of the tail of the distribution and is what distinguishes one type of the GEV family from the other two. Type I distributions are also known as Gumbel distributions. Their shape parameter approaches zero ($\xi \longrightarrow 0$), and the tail decays exponentially. Type II distributions are called Fréchet distributions. Here, the shape parameter is larger than zero ($\xi > 0$), and the right tail has a polynomial decay. The third distribution type, Type III, is called a Weibull distribution. The shape parameter is smaller than zero ($\xi < 0$), and the right tail is bounded. Figure A.2 shows the shape of the three distributions. In this figure, the different tail behaviors are visualized.

One of the challenges of using the block method is determining the correct width t of each block. On the one hand, each block should be chosen large enough to be considered independent of adjacent blocks, as this is one of the requirements of applying EVT (see equations (A.1) to (A.4)). Furthermore, it follows logically that if the blocks are taken too small, the extreme distribution type will be too similar to its momentary distribution type. Conversely, larger blocks lead to fewer data points of extremes, likely resulting in a poorer fit over the data. This makes extrapolation dangerous, as these uncertainties become more profound when looking at tiny probabilities. Additionally, if multiple extremes happen in the same block, this method would only take the highest of these values, which results in a loss of information.

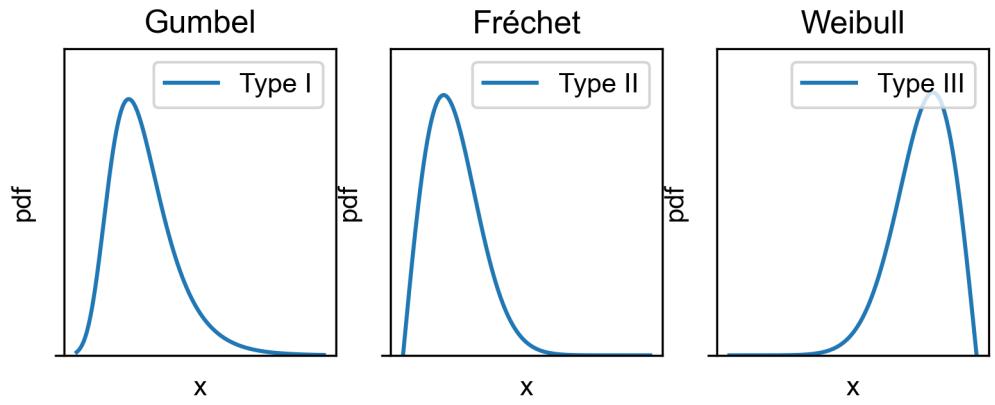

Figure A.2: The pdf of a Gumbel (left), Fréchet (middle), and Weibull (right) distribution. This figure clearly illustrates the differences in the tails.

A.2.2. Peaks over threshold method

In the POTS method, only values higher than a certain threshold are considered. An example of this is shown in figure A.3, where the same 100 samples as in figure A.1 are considered. For reference, the blocks are shown as well. Applying a threshold of 6.2 results in 10 extreme values, just like the block method did. However, as seen from figure A.3, some blocks have more than one value higher than the threshold, while others do not contribute any values.

The Pickands–Balkema–De Haan theorem states that for a large enough threshold u, the distribution of its extremes converges to the family of generalized Pareto distributions (GPD):

$$F_{(\mu,\sigma,\xi)}(x) = \begin{cases} 1 - \left(1 + \frac{\xi(x-\mu)}{\sigma}\right)^{-1/\xi} & \text{for } \xi \neq 0 \\ 1 - \exp\left(-\frac{x-\mu}{\sigma}\right) & \text{for } \xi = 0 \end{cases} \tag{A.6}$$

where:

$F_{(\mu,\sigma,\xi)}(x)$ is the cumulative density function of the extreme distribution;

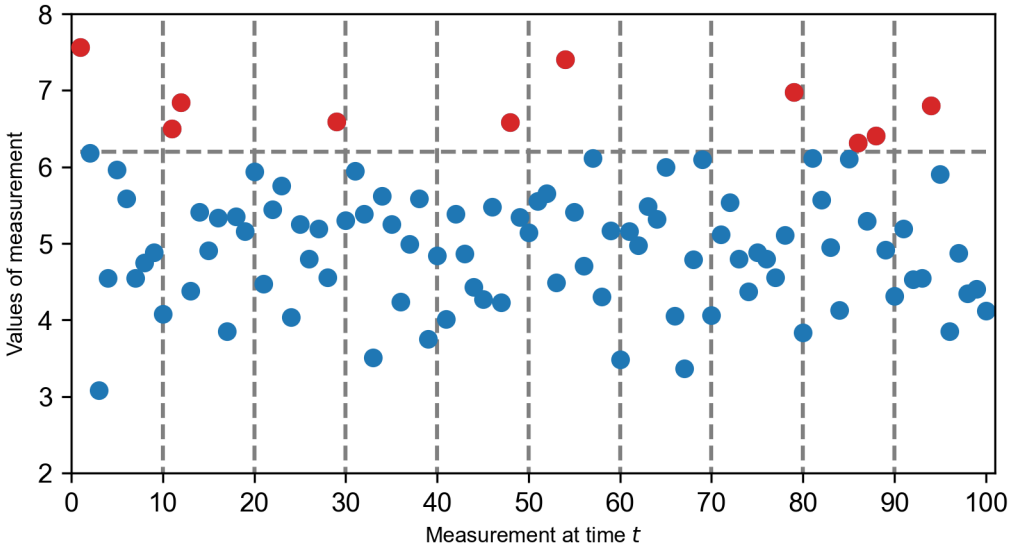

Figure A.3: An example of the POTS method. Here, the same 100 samples as in figure A.1 are taken. The threshold is put at 6.2. For reference, the blocks are shown as well.

μ is the location parameter;
σ is the scale parameter;
ξ is the shape parameter.

Similarly, like for the block method and the width t, the choice of the threshold u is essential for the wellness-of-fit of the GPD. Putting the threshold too low will result in a distribution that looks too much like the momentary distribution. Setting it too high results in a small sample to work with.

B

A sensitivity study on T_p, ϕ, and α on $\tilde{F}$

Appendix B presents the sensitivity study conducted on the period of each jump T_p, the phase lag ϕ, and the contact ratio α. Their influence on the normalized force $\tilde{F}$ was compared, and based on visual inspection, suitable parameters for the standard deviation of the period and phase lag were determined. According to the data set, the expect value for the contact ratio was $\alpha = 0.66$. This is not in line with what the literature states for normal jumping. Here, a value of $\alpha = 0.33$ is proposed. Both contact ratios are therefore included in the analysis.

Not all combinations that were tried are shown in this appendix, as they do not contribute to the result. The first subsection shows the result of varying the period and phase lag between 0.02 s and 0.05 s, with 0.01 s intervals, for a contact ratio of $\alpha = 0.66$. The second one shows the same combinations of the period and the phase lag, for a contact ratio of $\alpha = 0.33$.

Although the differences between some cases are minor, the combination of $T_p = 0.02$, $\phi = 0.05$, and $\alpha = 0.33$ shows the best result.

B.1. The influence of T_p and ϕ on $\tilde{F}$ with $\alpha = 0.66$

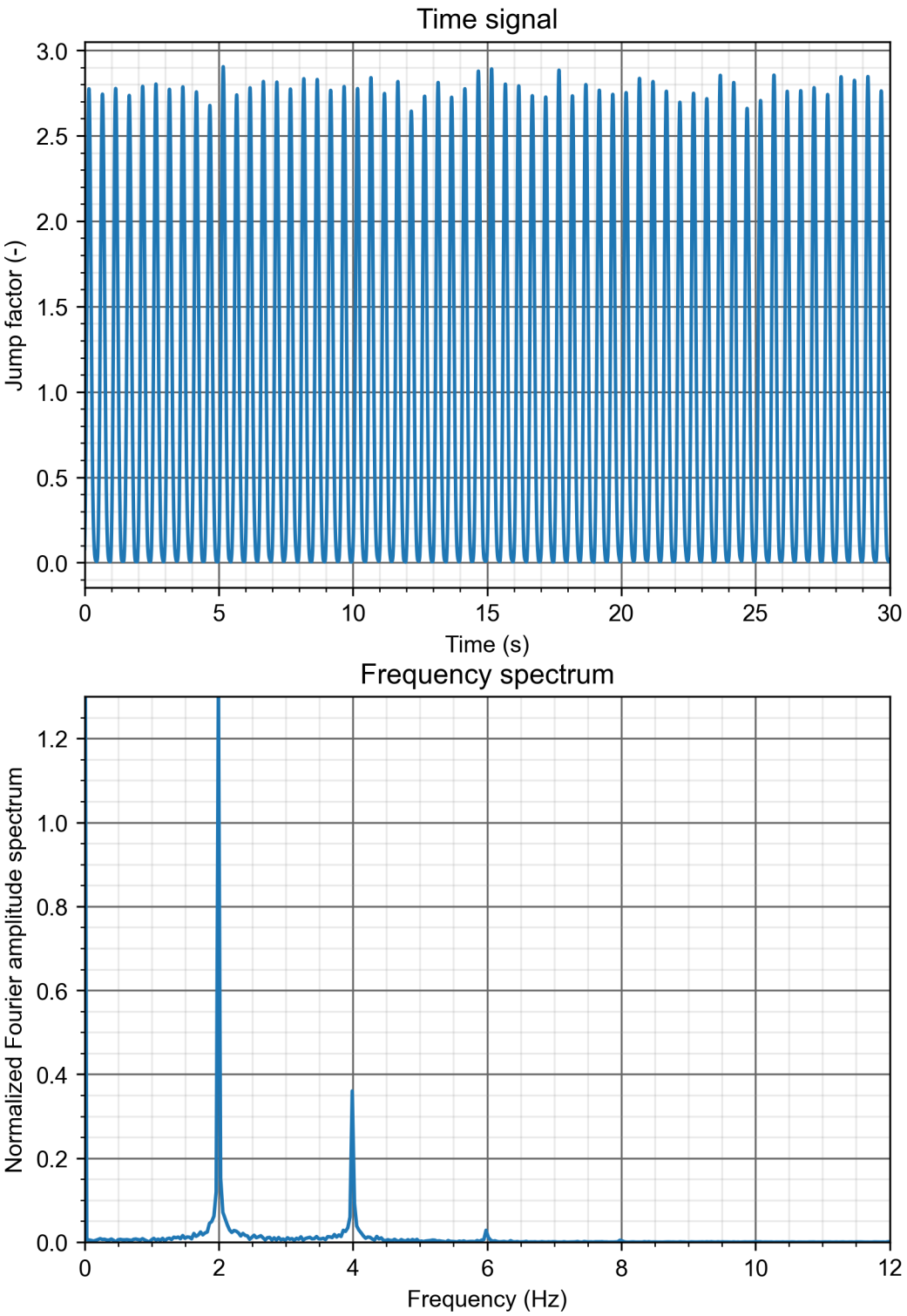

Figure B.1: $T_p = 0.02$, $\phi = 0.02$, $\alpha = 0.66$

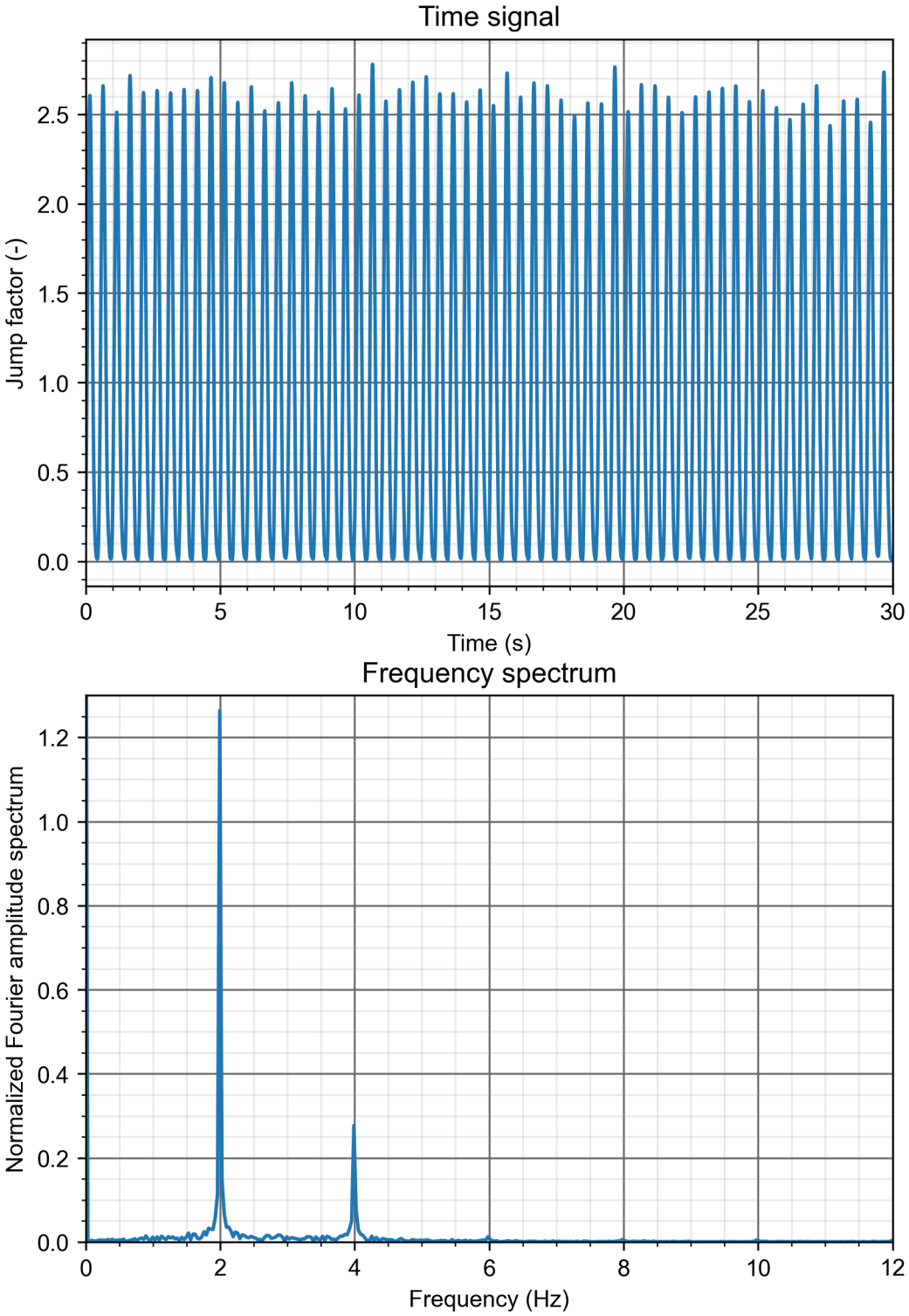

Figure B.2: $T_p = 0.02$, $\phi = 0.03$, $\alpha = 0.66$

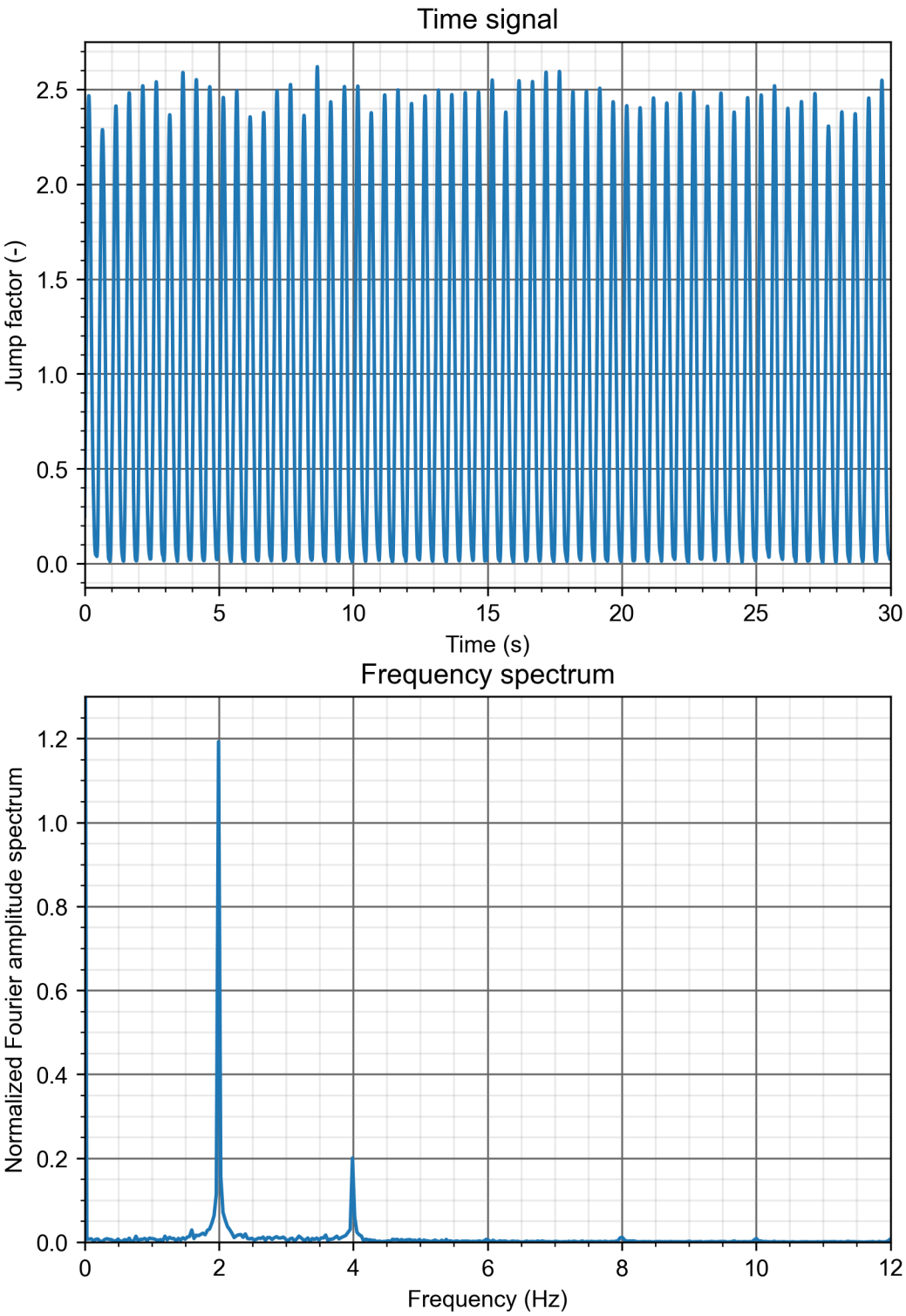

Figure B.3: $T_p = 0.02$, $\phi = 0.04$, $\alpha = 0.66$

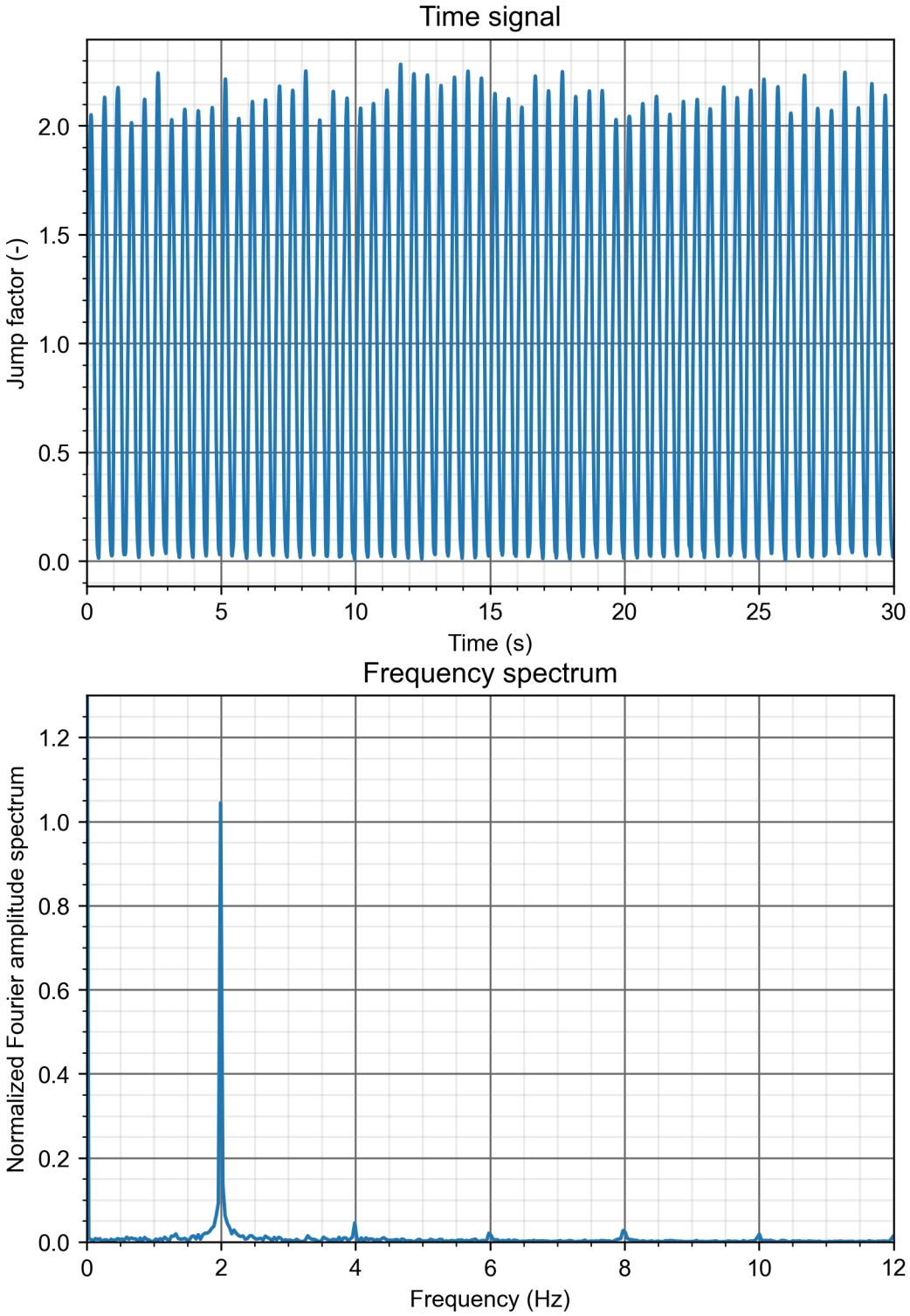

Figure B.4: $T_p = 0.02$, $\phi = 0.05$, $\alpha = 0.66$

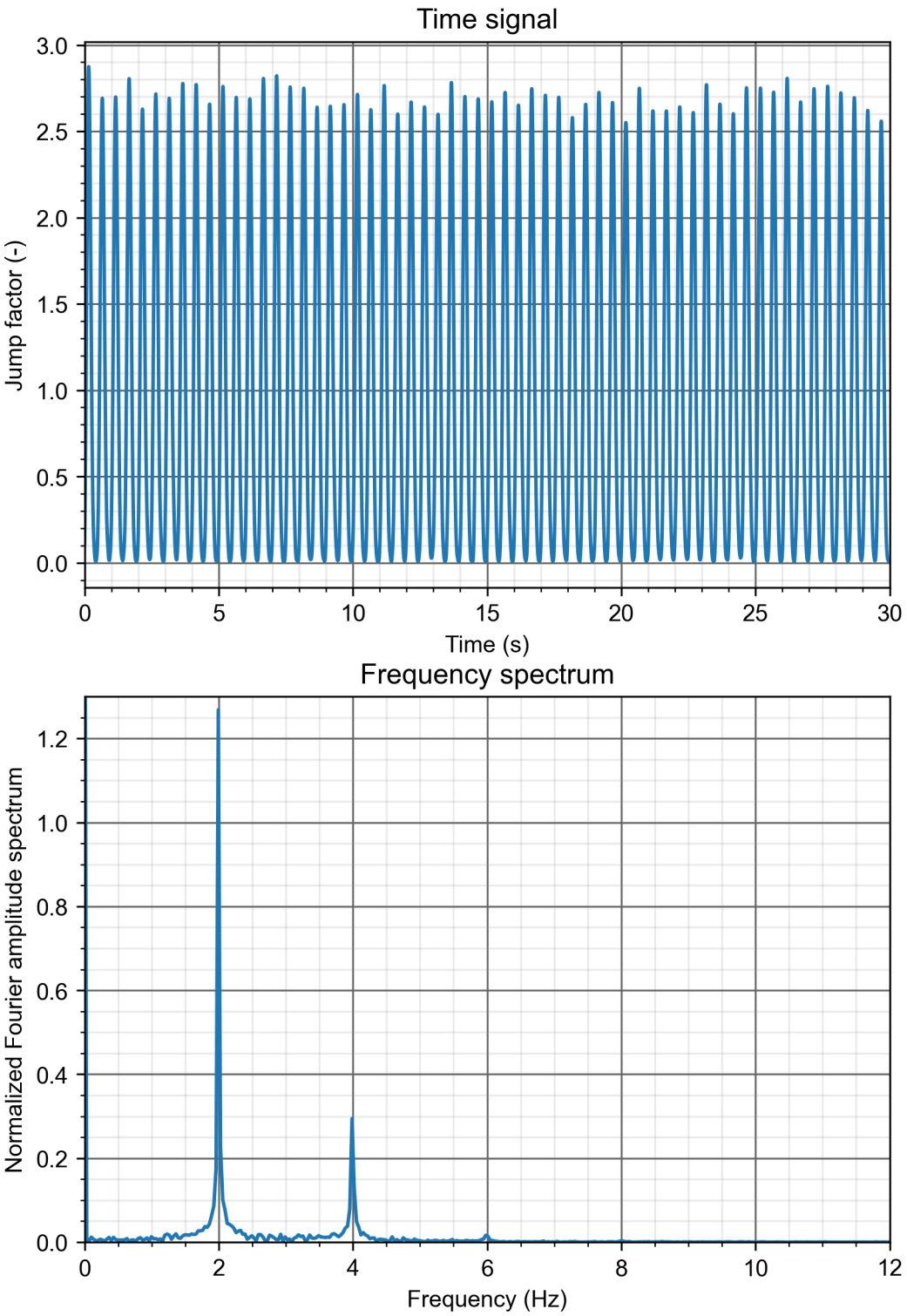

Figure B.5: $T_p = 0.03$, $\phi = 0.02$, $\alpha = 0.66$

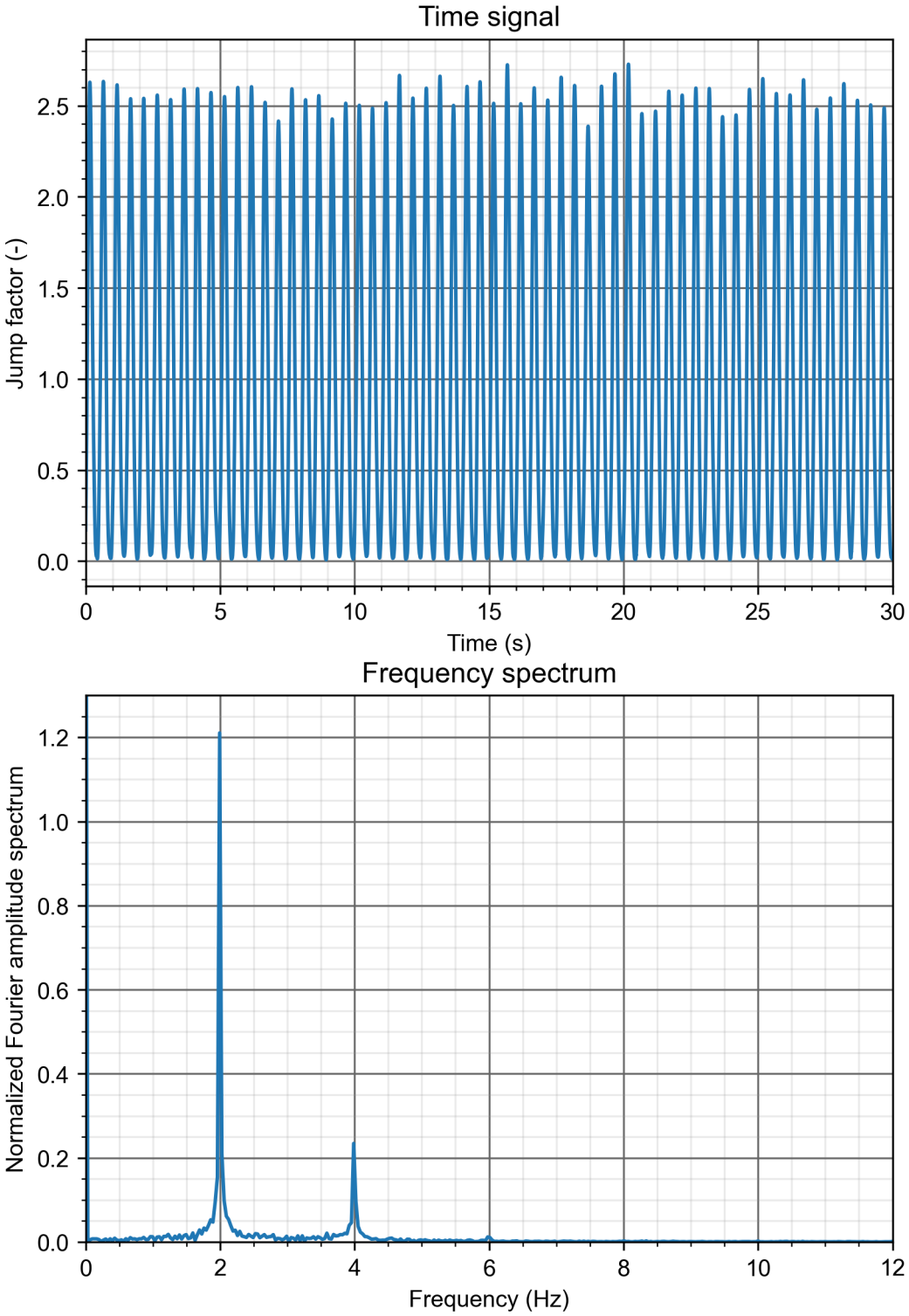

Figure B.6: $T_p = 0.03$, $\phi = 0.03$, $\alpha = 0.66$

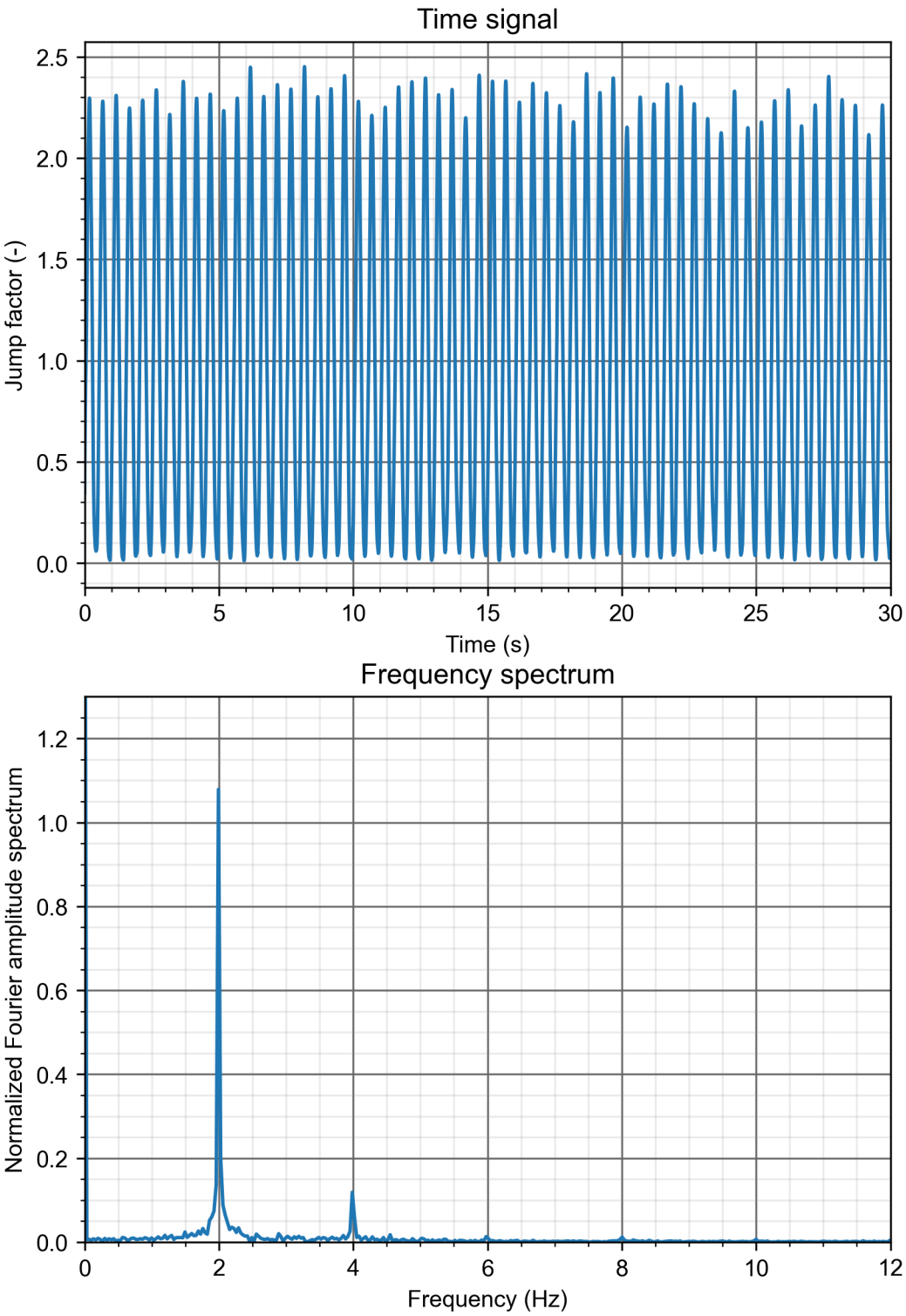

Figure B.7: $T_p = 0.03$, $\phi = 0.04$, $\alpha = 0.66$

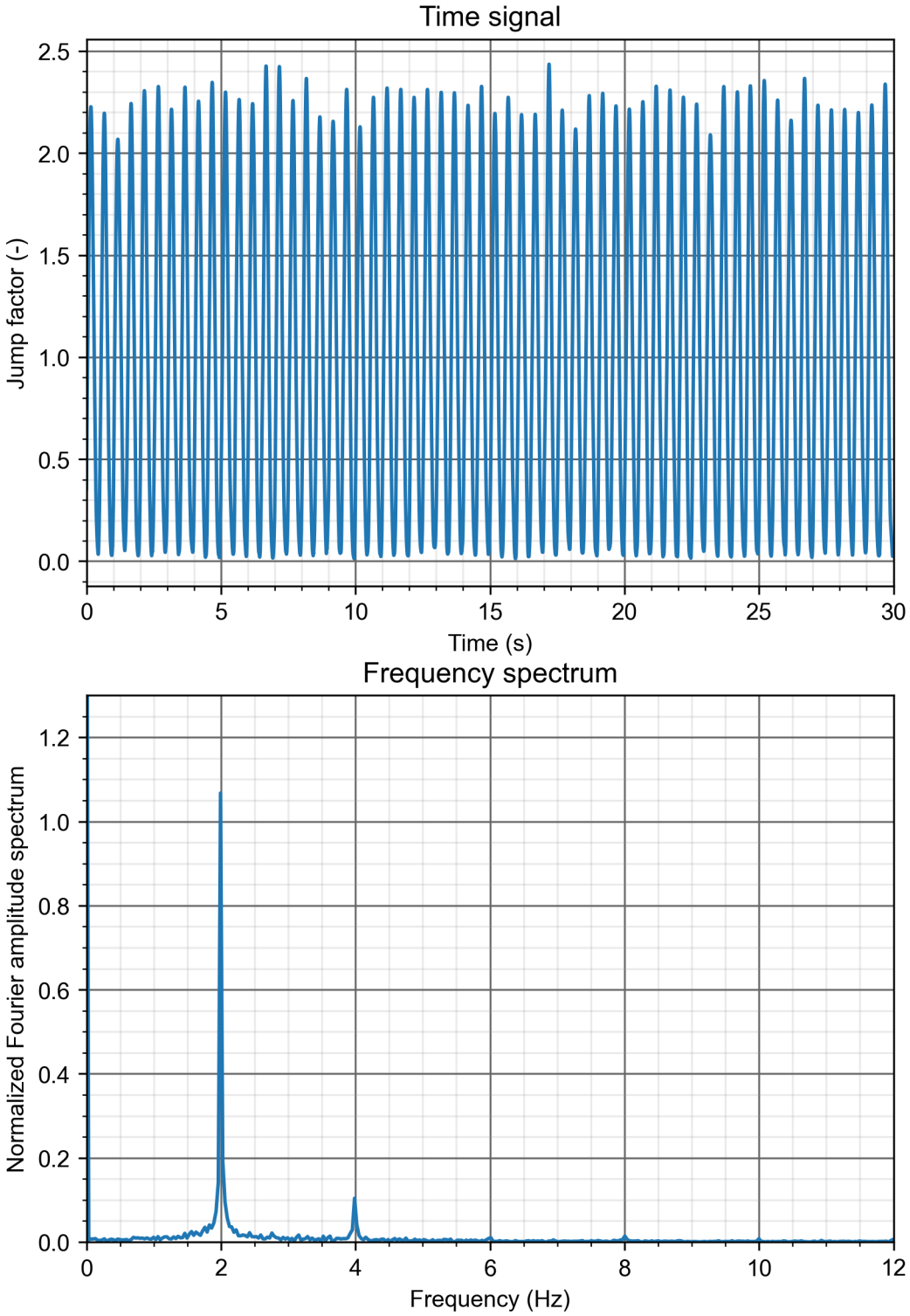

Figure B.8: $T_p = 0.03$, $\phi = 0.05$, $\alpha = 0.66$

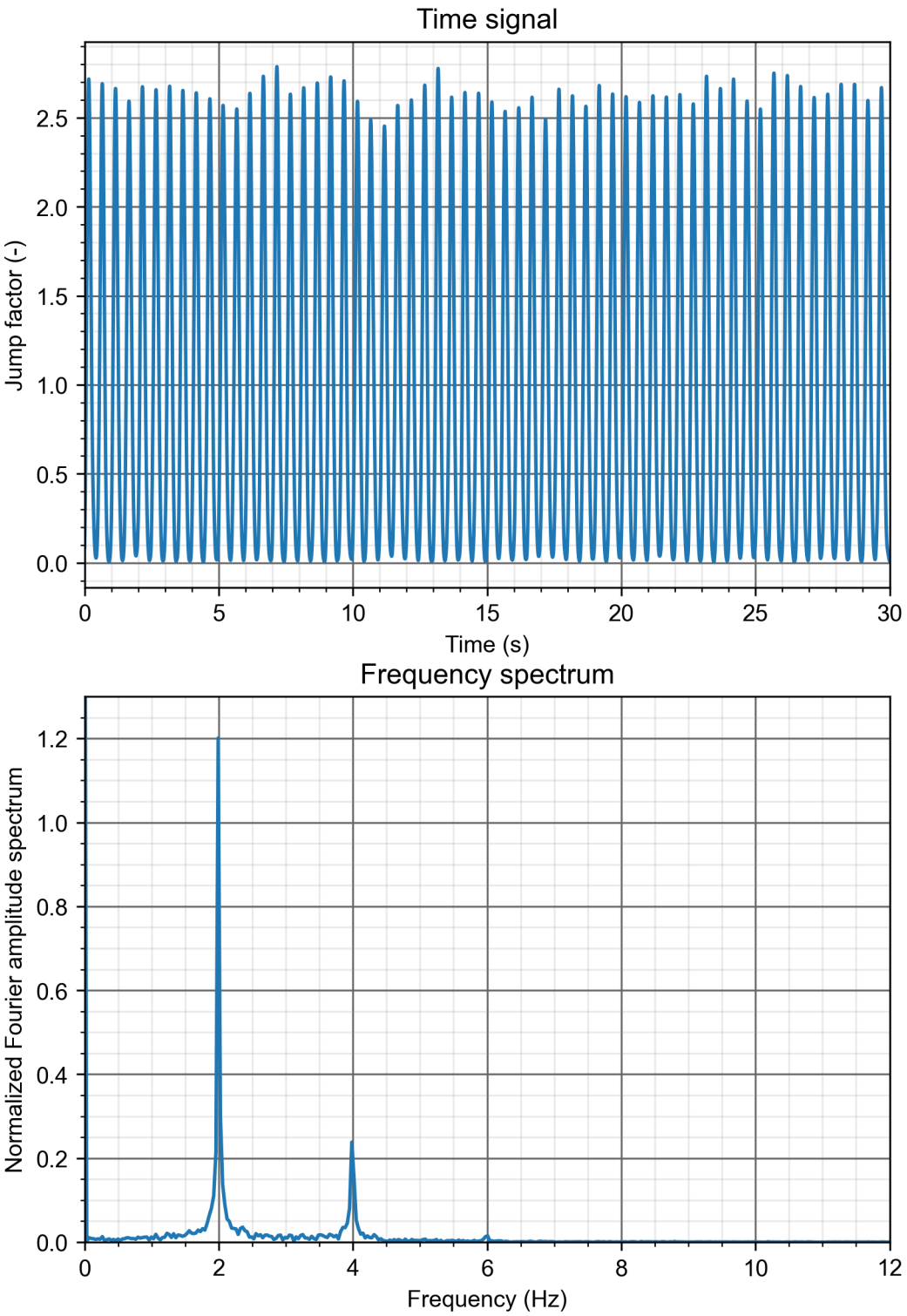

Figure B.9: $T_p = 0.04$, $\phi = 0.02$, $\alpha = 0.66$

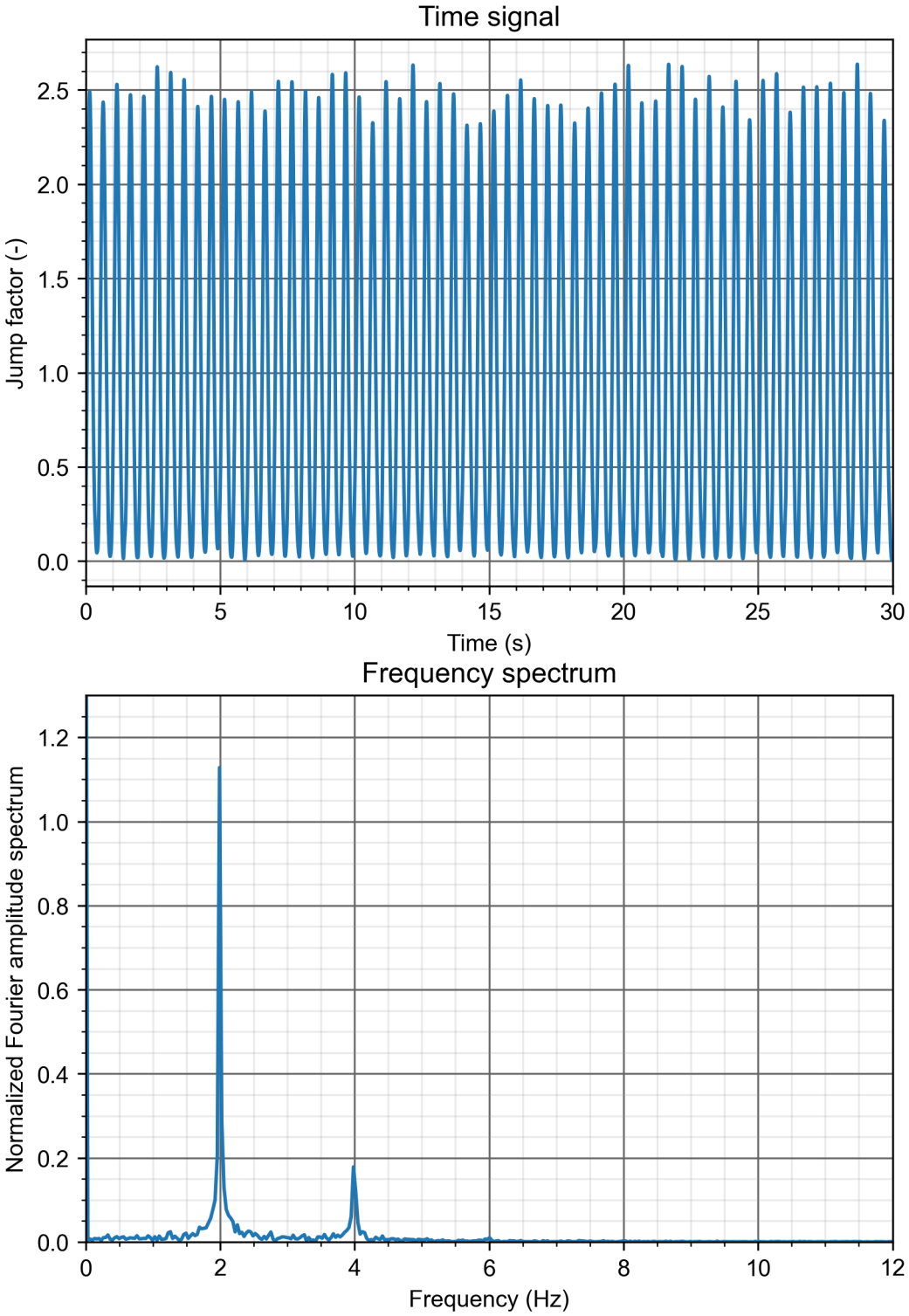

Figure B.10: $T_p = 0.04$, $\phi = 0.03$, $\alpha = 0.66$

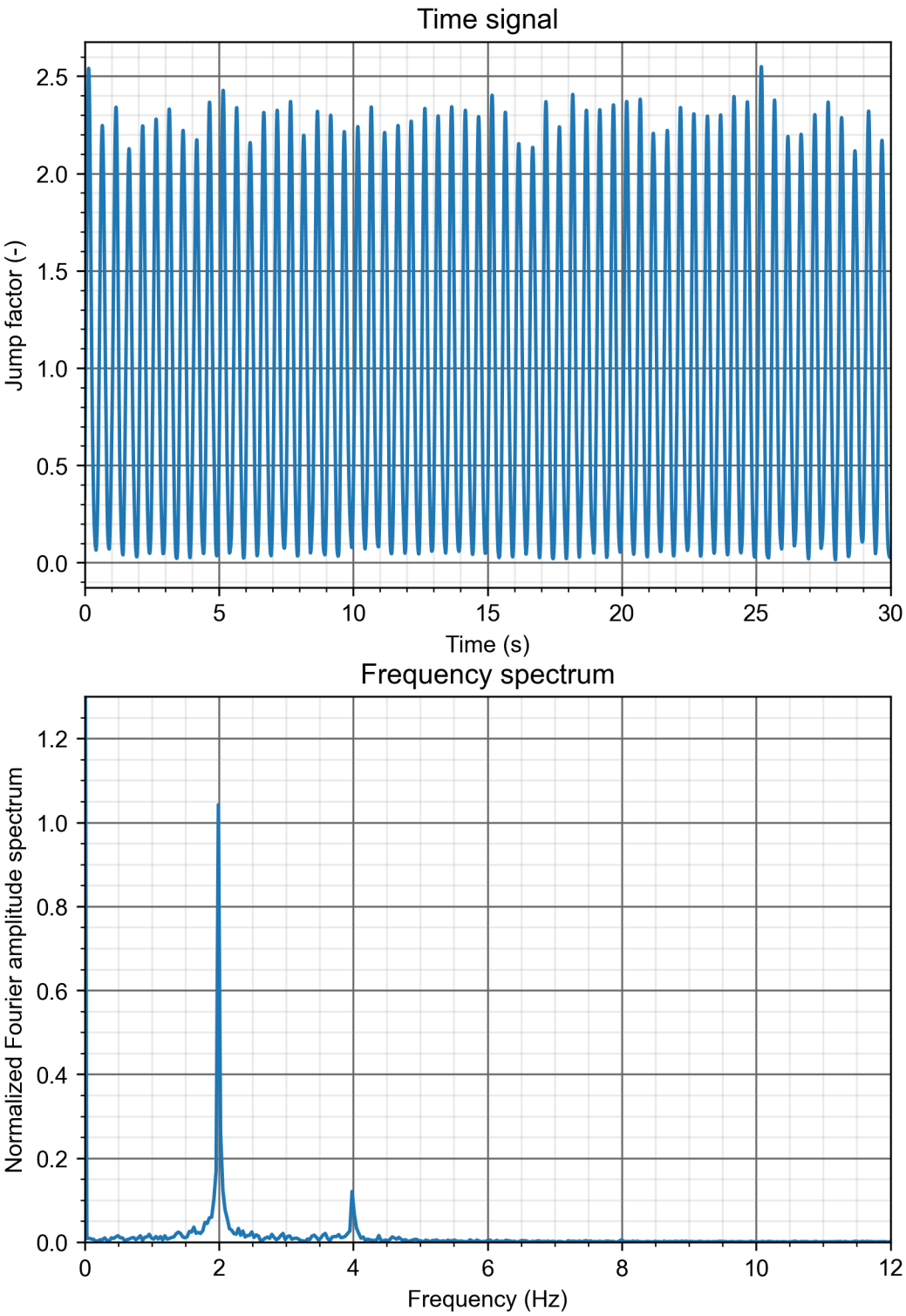

Figure B.11: $T_p = 0.04$, $\phi = 0.04$, $\alpha = 0.66$

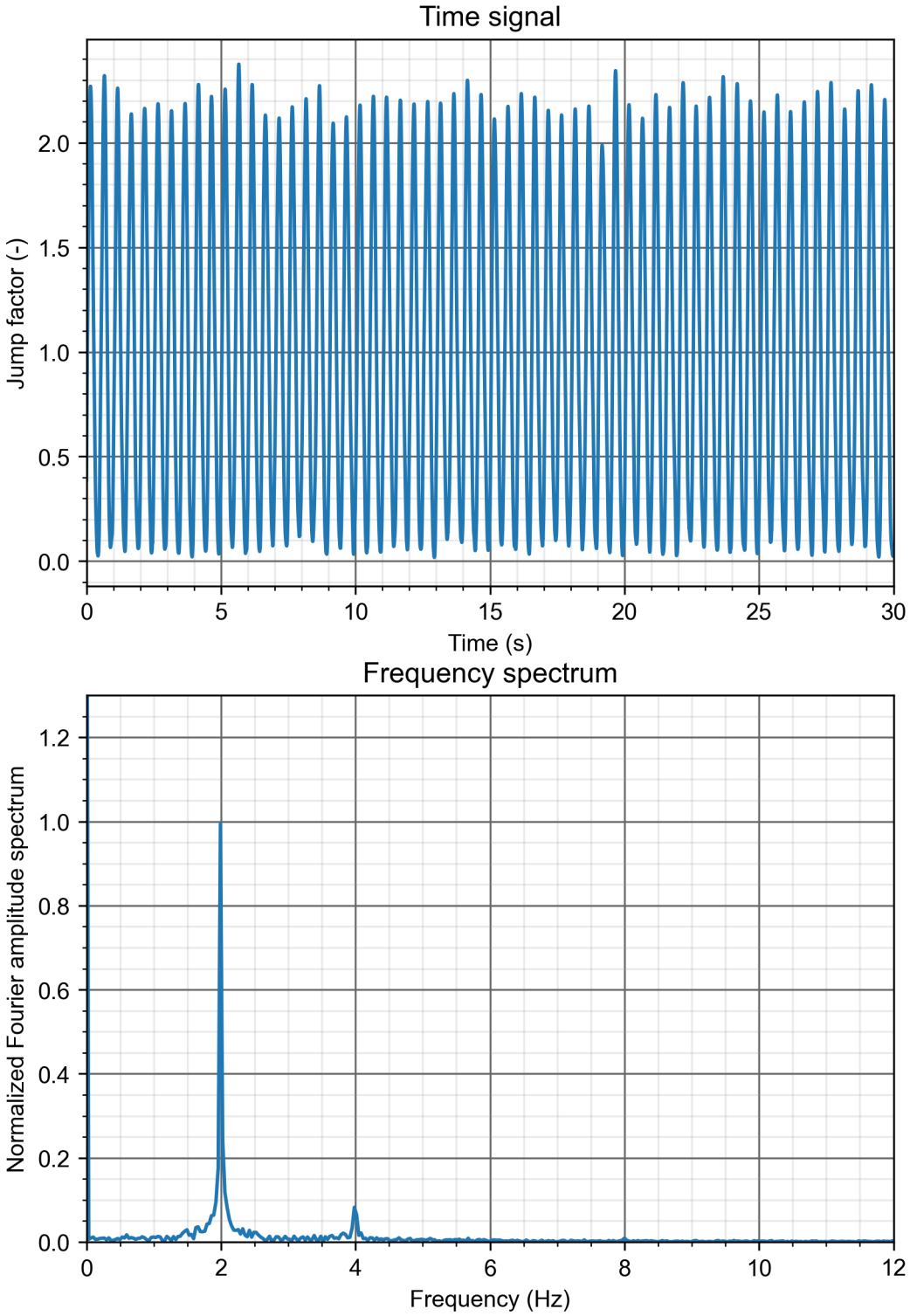

Figure B.12: $T_p = 0.04$, $\phi = 0.05$, $\alpha = 0.66$

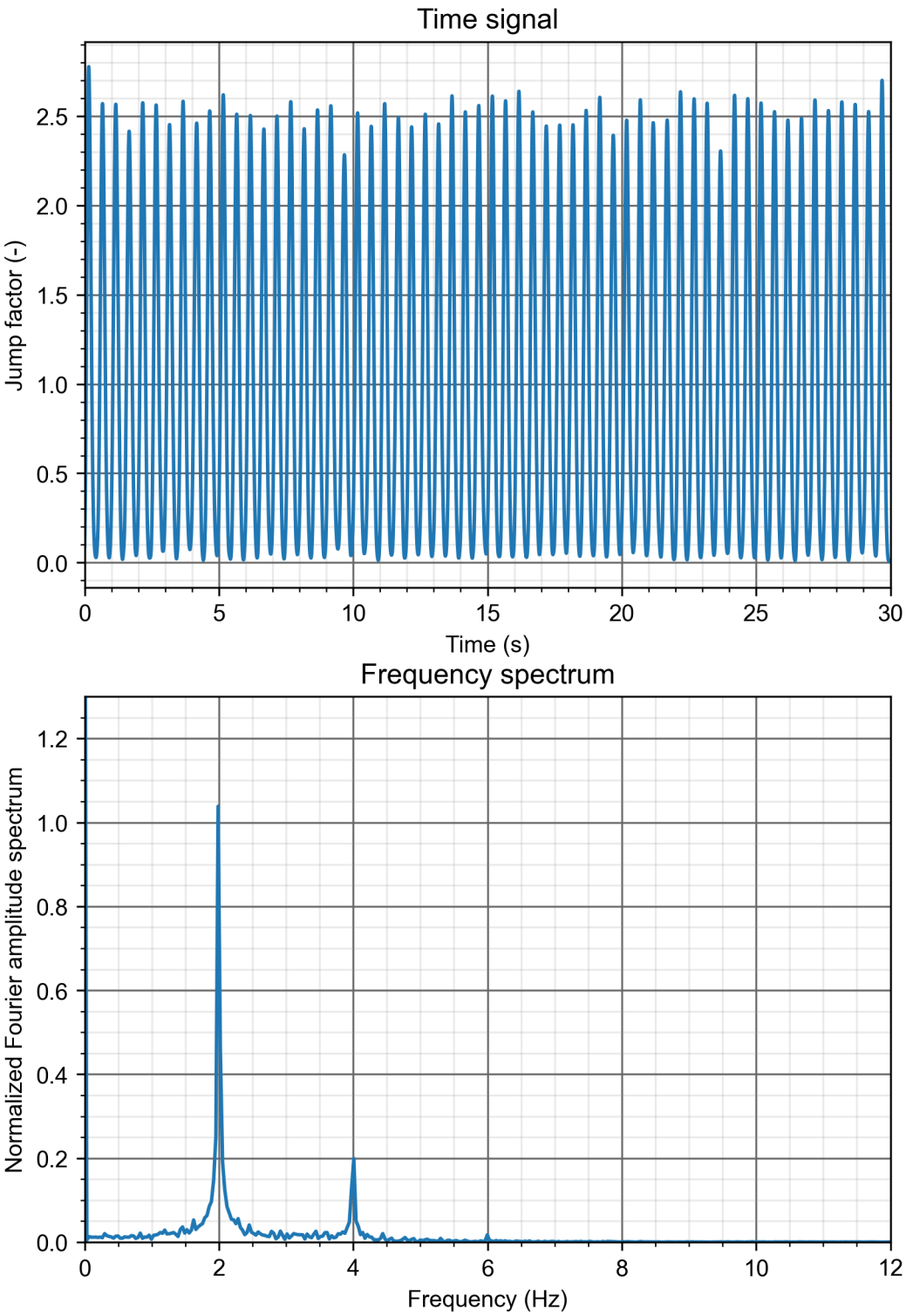

Figure B.13: $T_p = 0.05$, $\phi = 0.02$, $\alpha = 0.66$

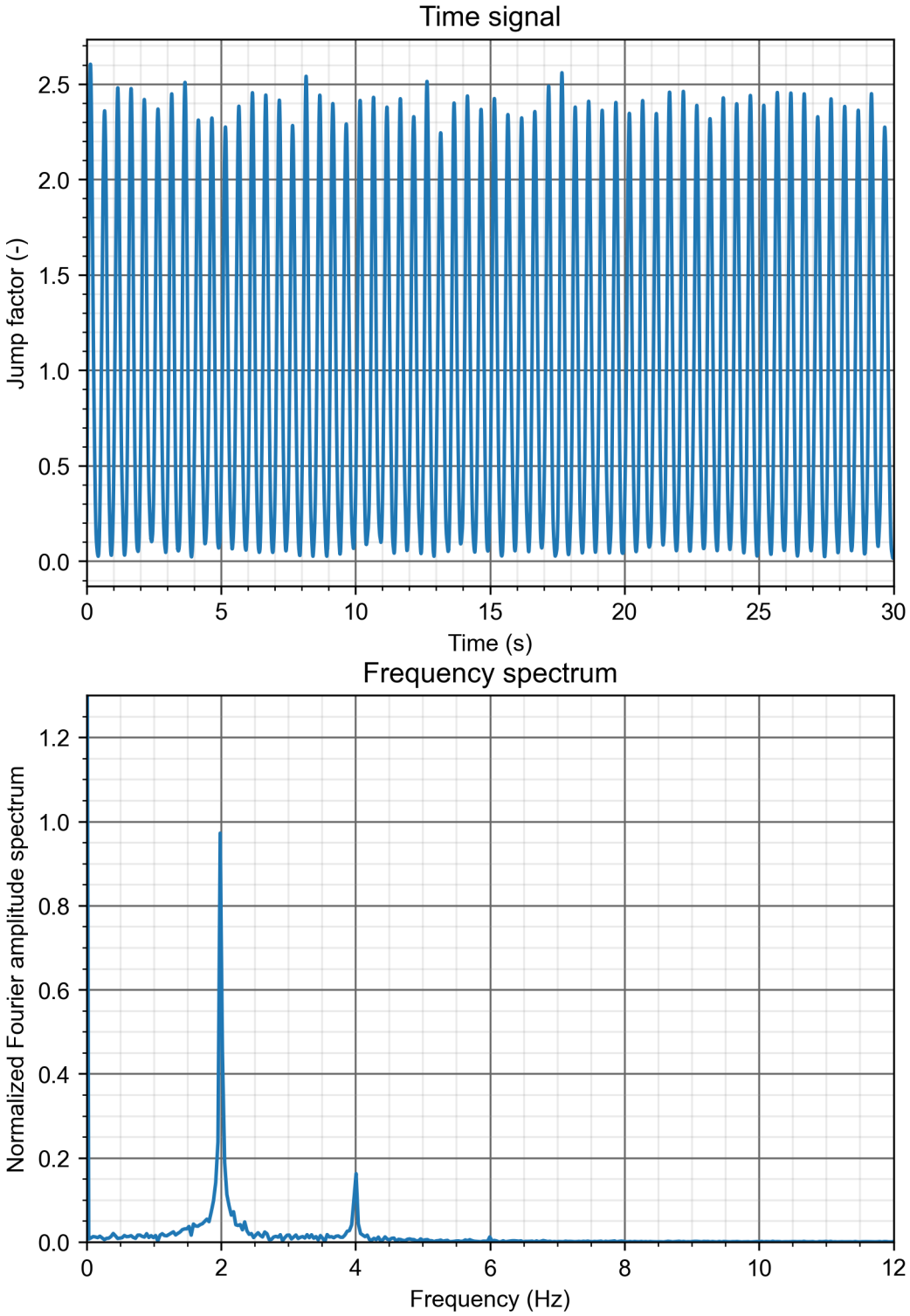

Figure B.14: $T_p = 0.05$, $\phi = 0.03$, $\alpha = 0.66$

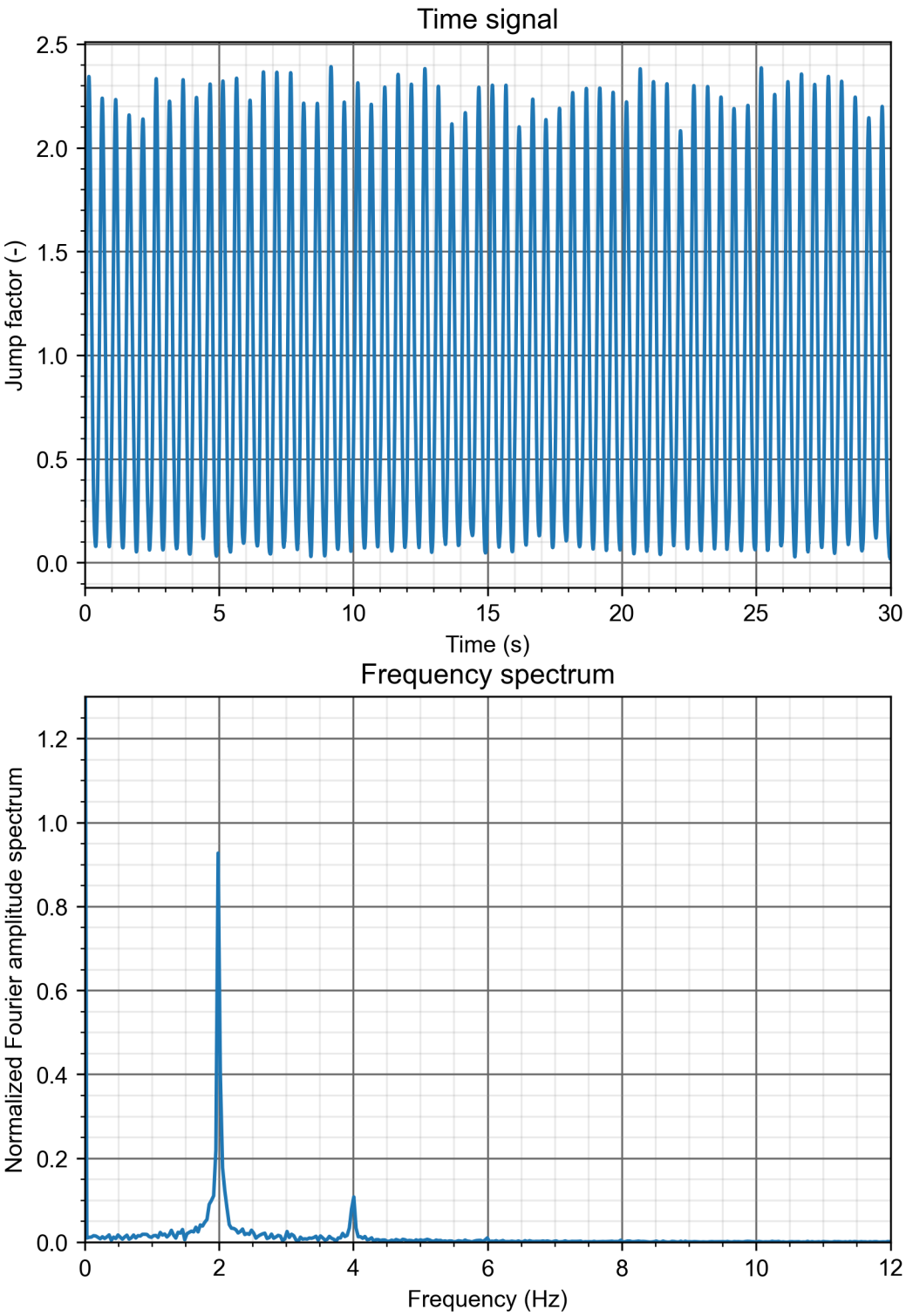

Figure B.15: $T_p = 0.05$, $\phi = 0.04$, $\alpha = 0.66$

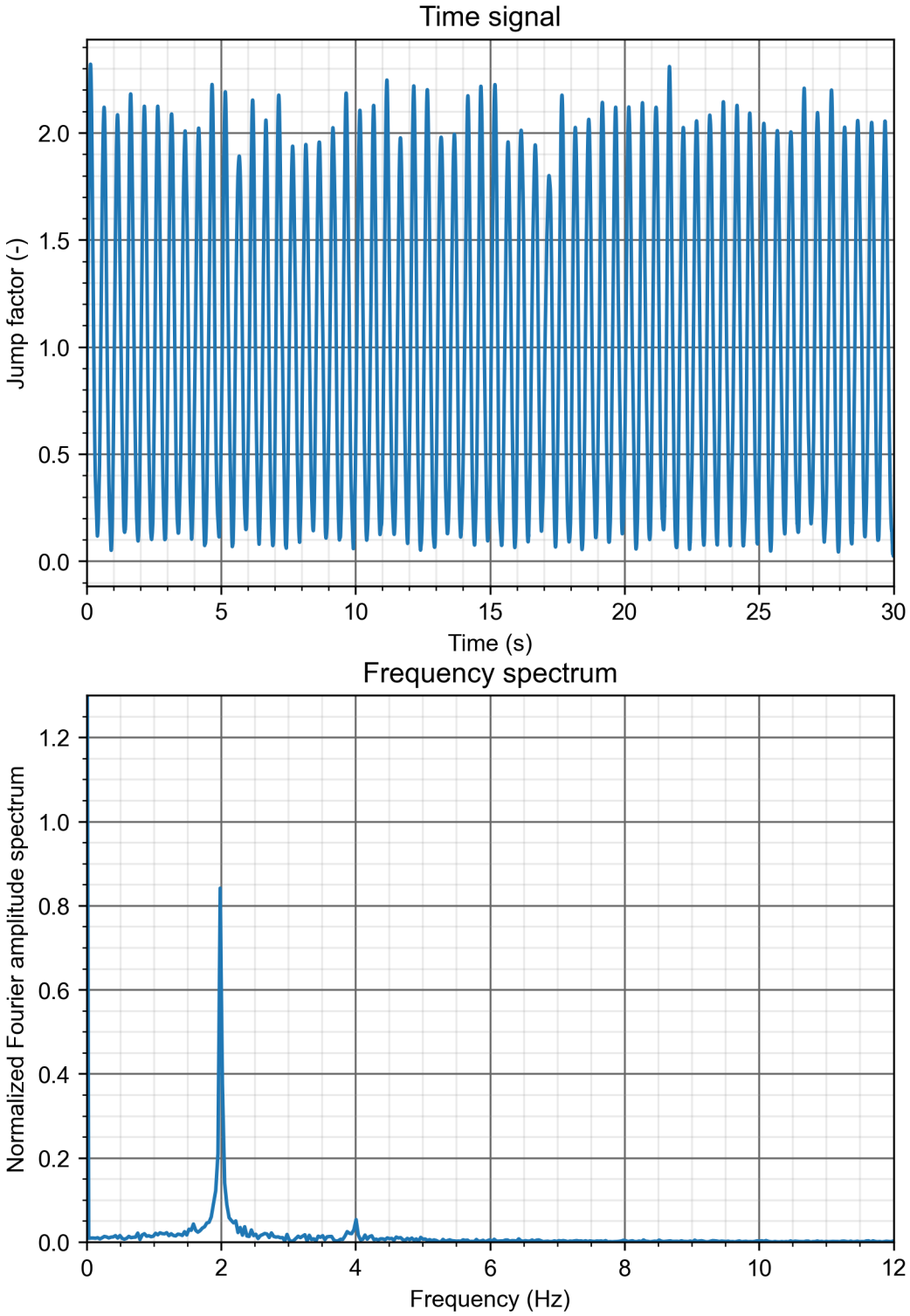

Figure B.16: $T_p = 0.05$, $\phi = 0.05$, $\alpha = 0.66$

B.2. The influence of T_p and ϕ on $\tilde{F}$ with $\alpha = 0.33$

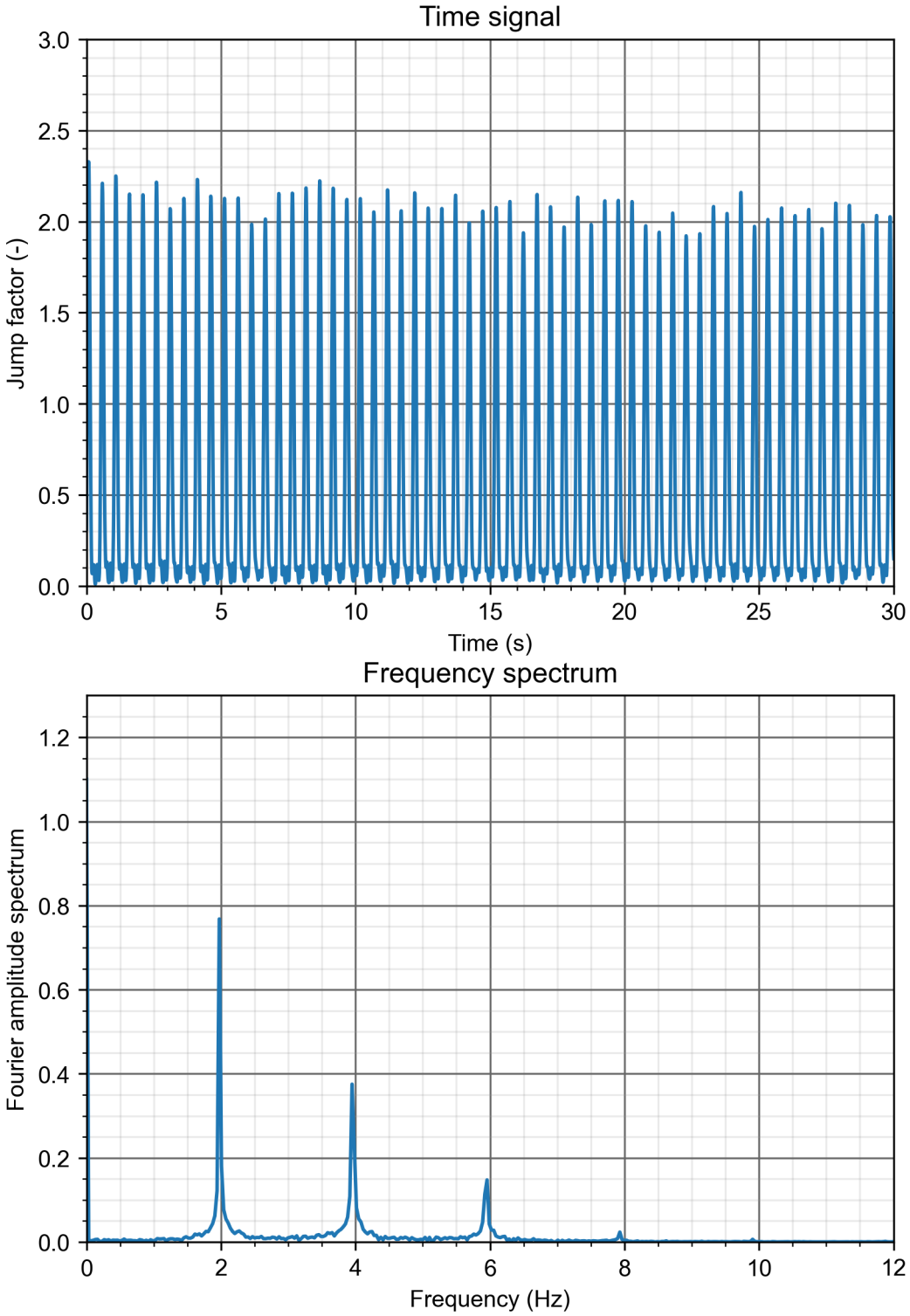

Figure B.17: $T_p = 0.02$, $\phi = 0.02$, $\alpha = 0.33$

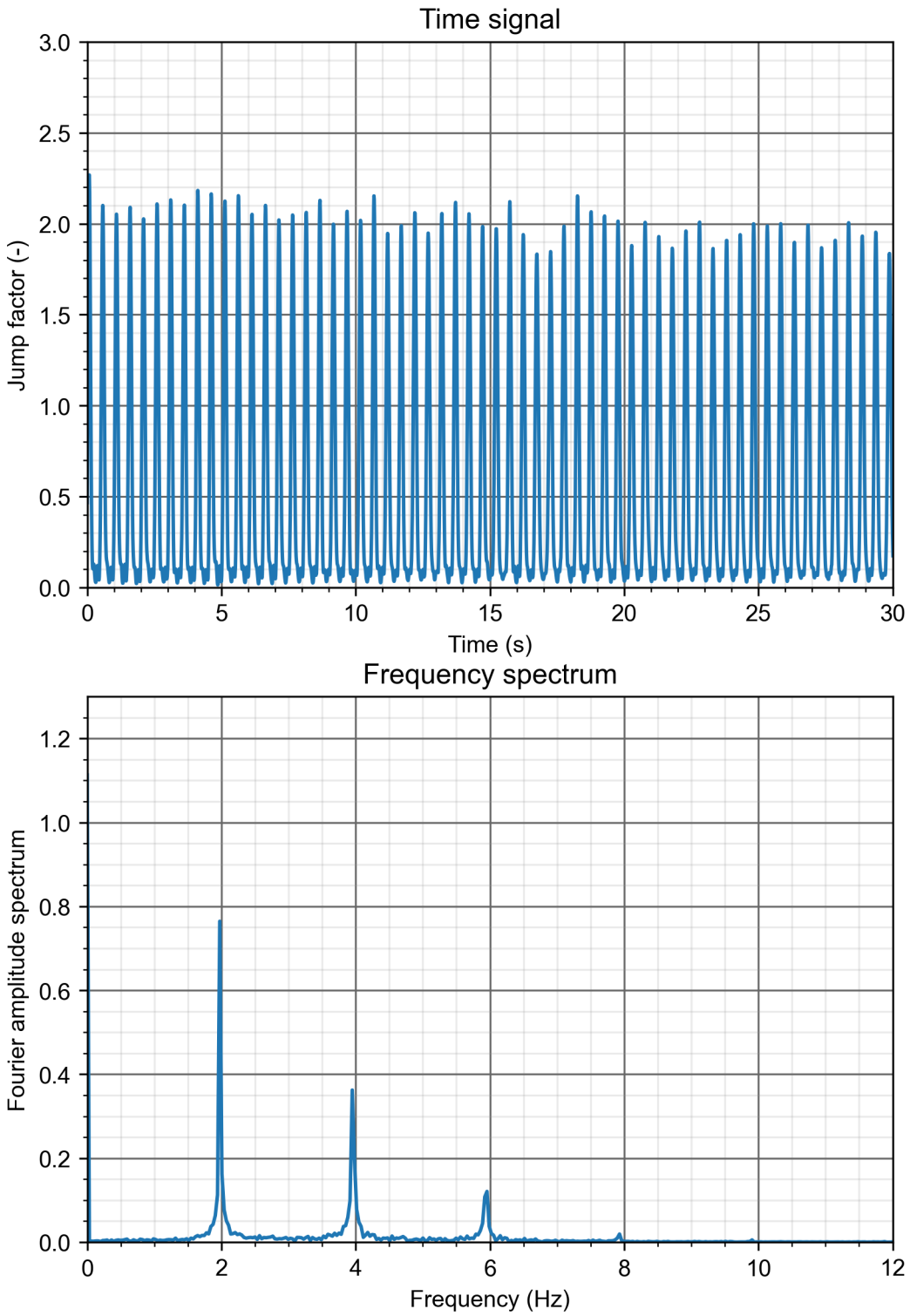

Figure B.18: $T_p = 0.02$, $\phi = 0.03$, $\alpha = 0.33$

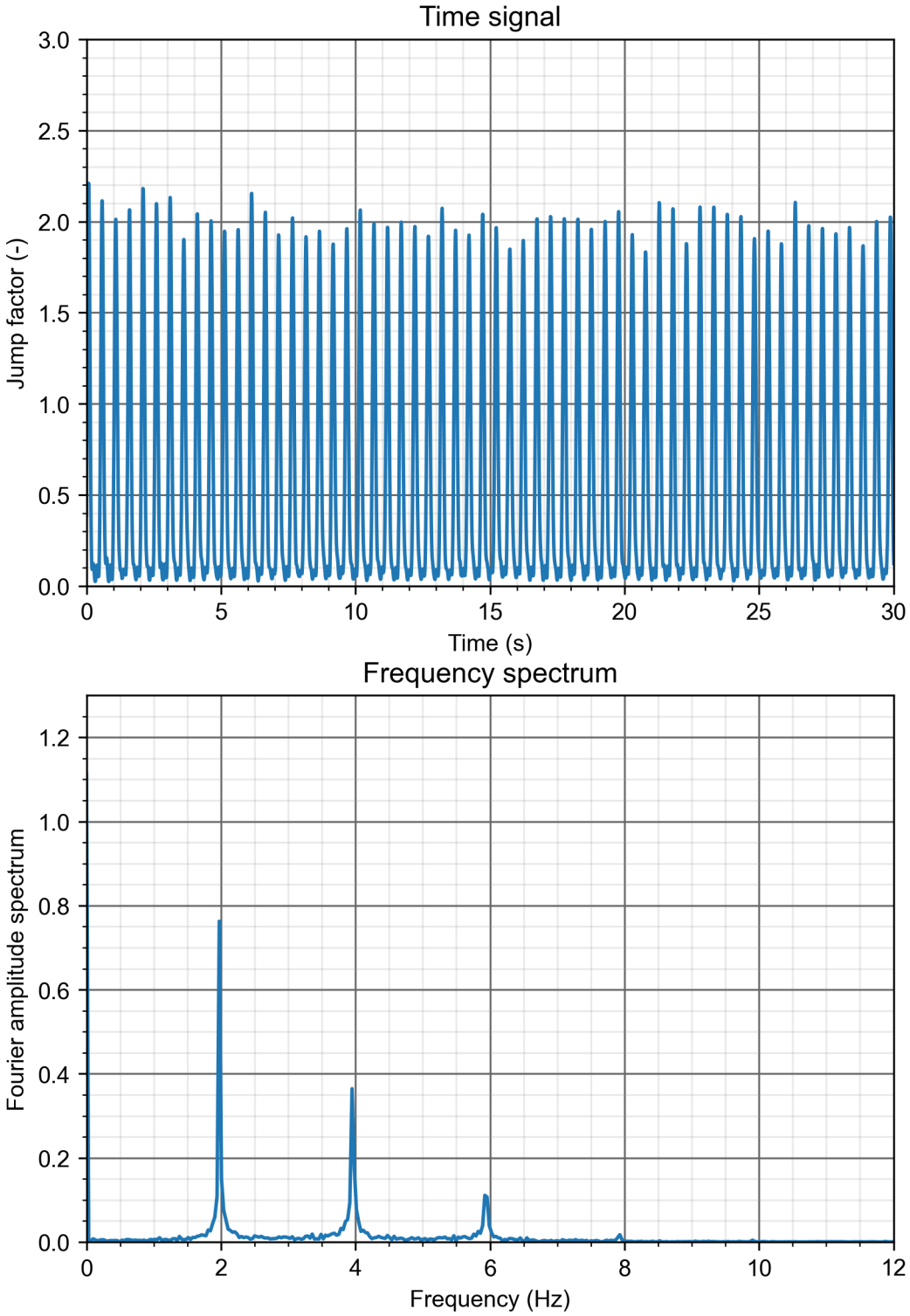

Figure B.19: $T_p = 0.02$, $\phi = 0.04$, $\alpha = 0.33$

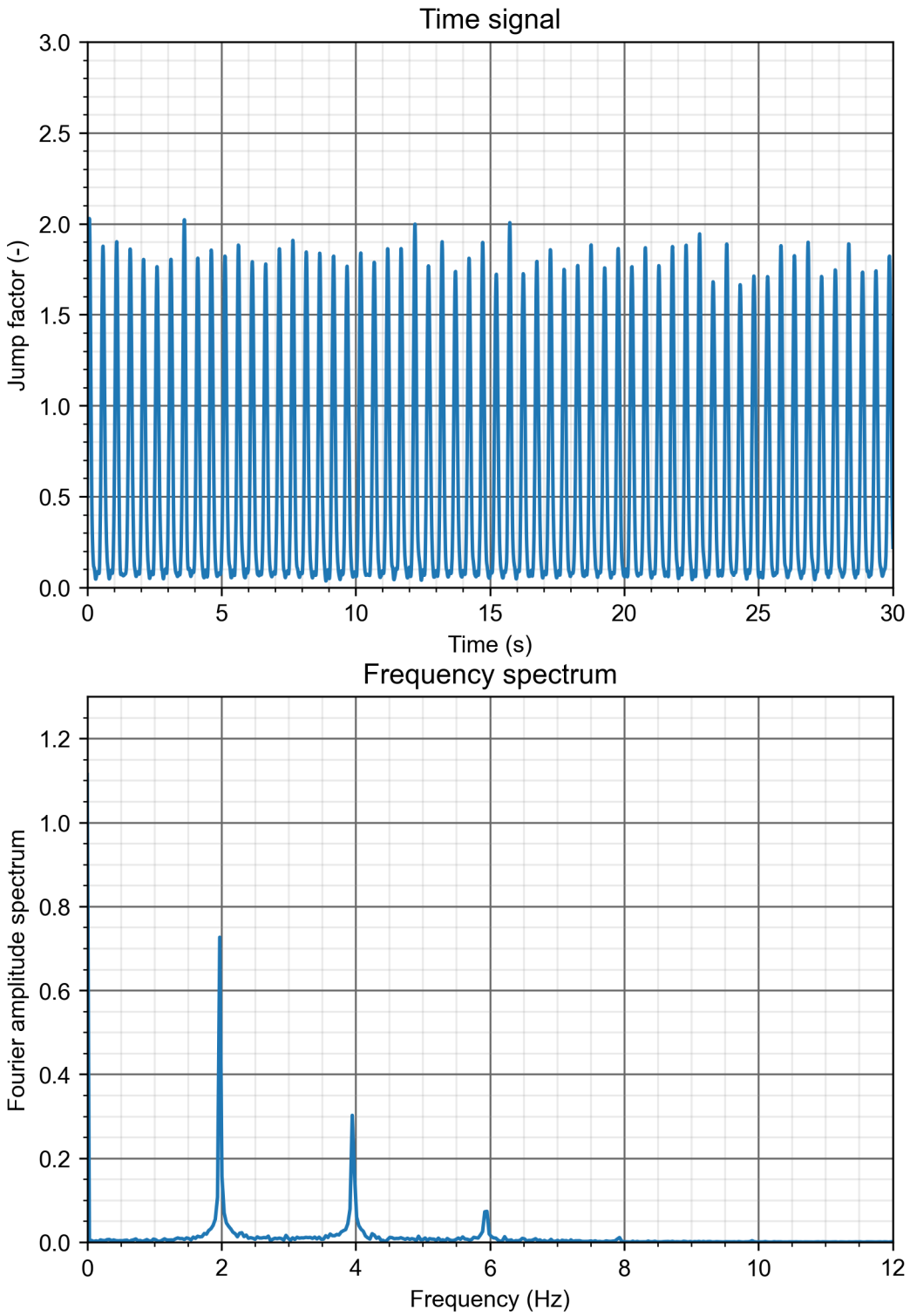

Figure B.20: $T_p = 0.02$, $\phi = 0.05$, $\alpha = 0.33$

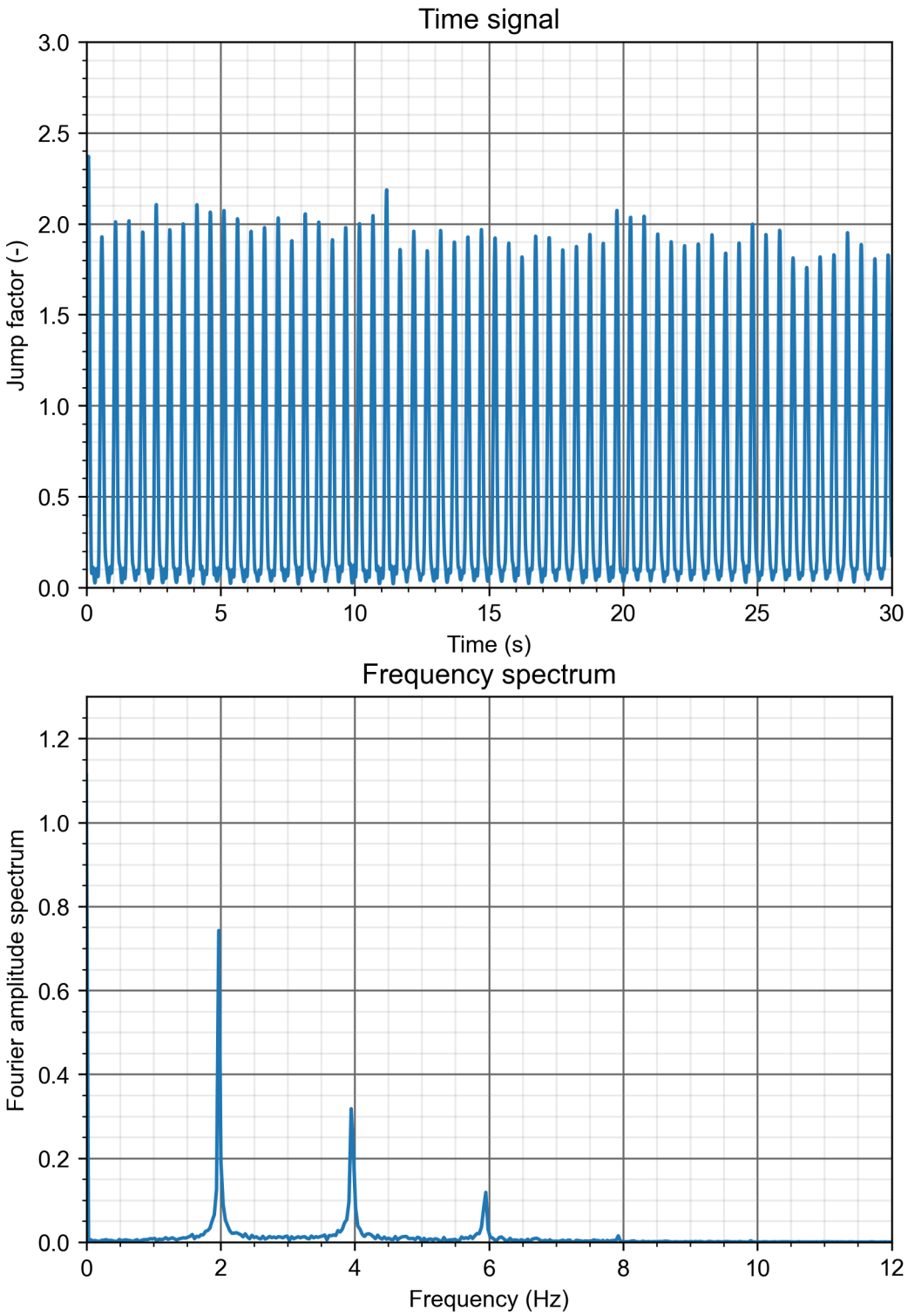

Figure B.21: $T_p = 0.03$, $\phi = 0.02$, $\alpha = 0.33$

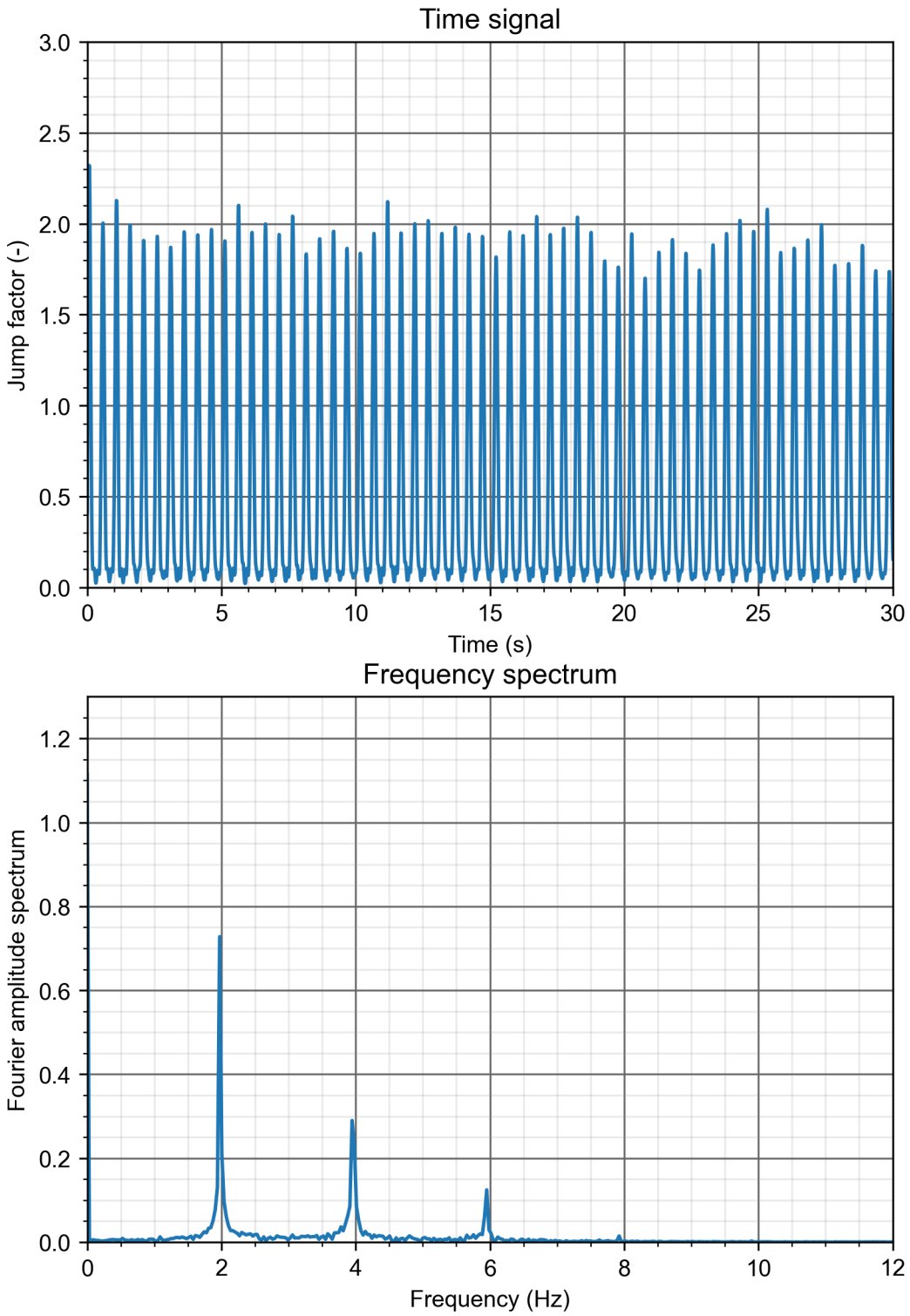

Figure B.22: $T_p = 0.03$, $\phi = 0.03$, $\alpha = 0.33$

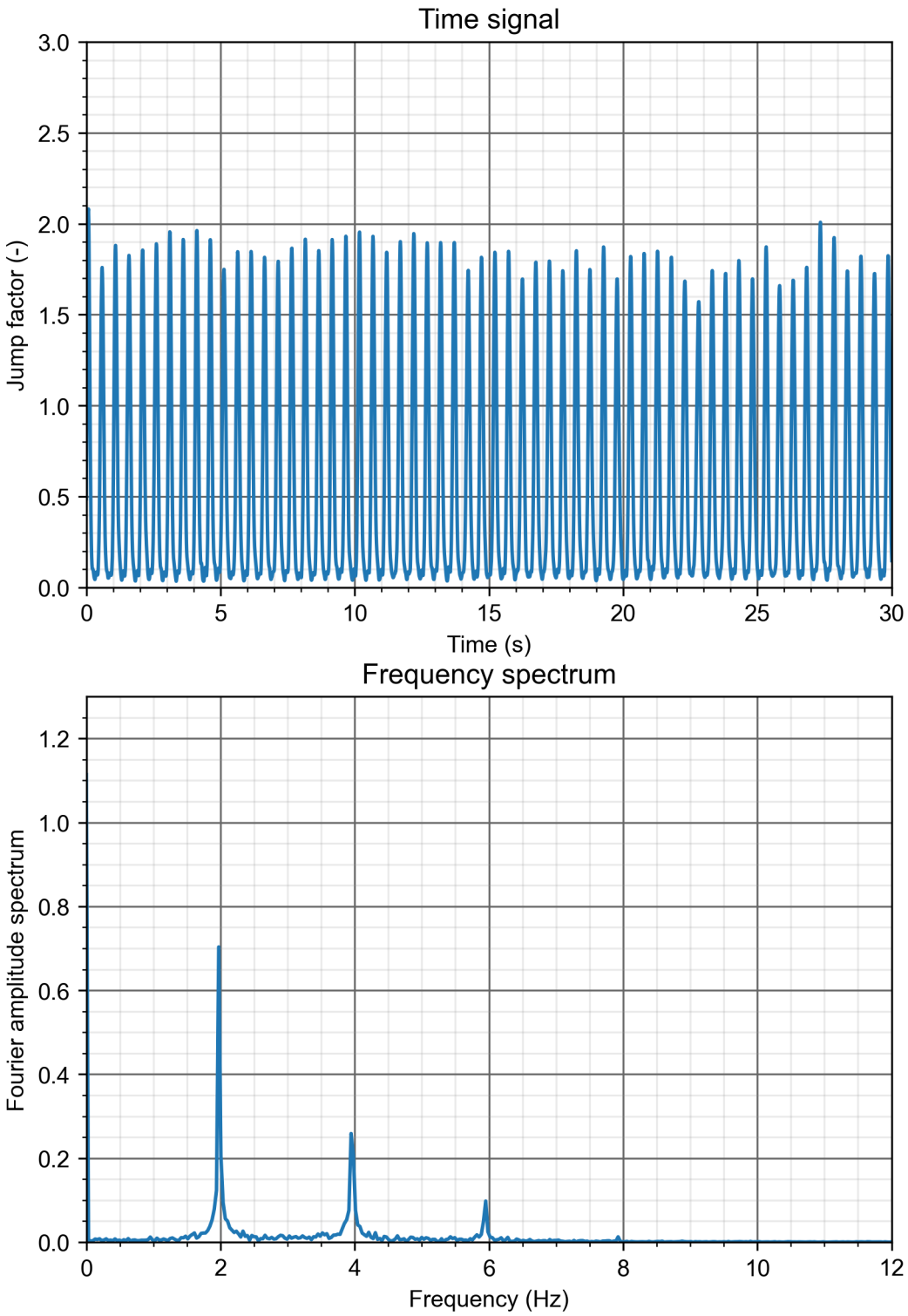

Figure B.23: $T_p = 0.03$, $\phi = 0.04$, $\alpha = 0.33$

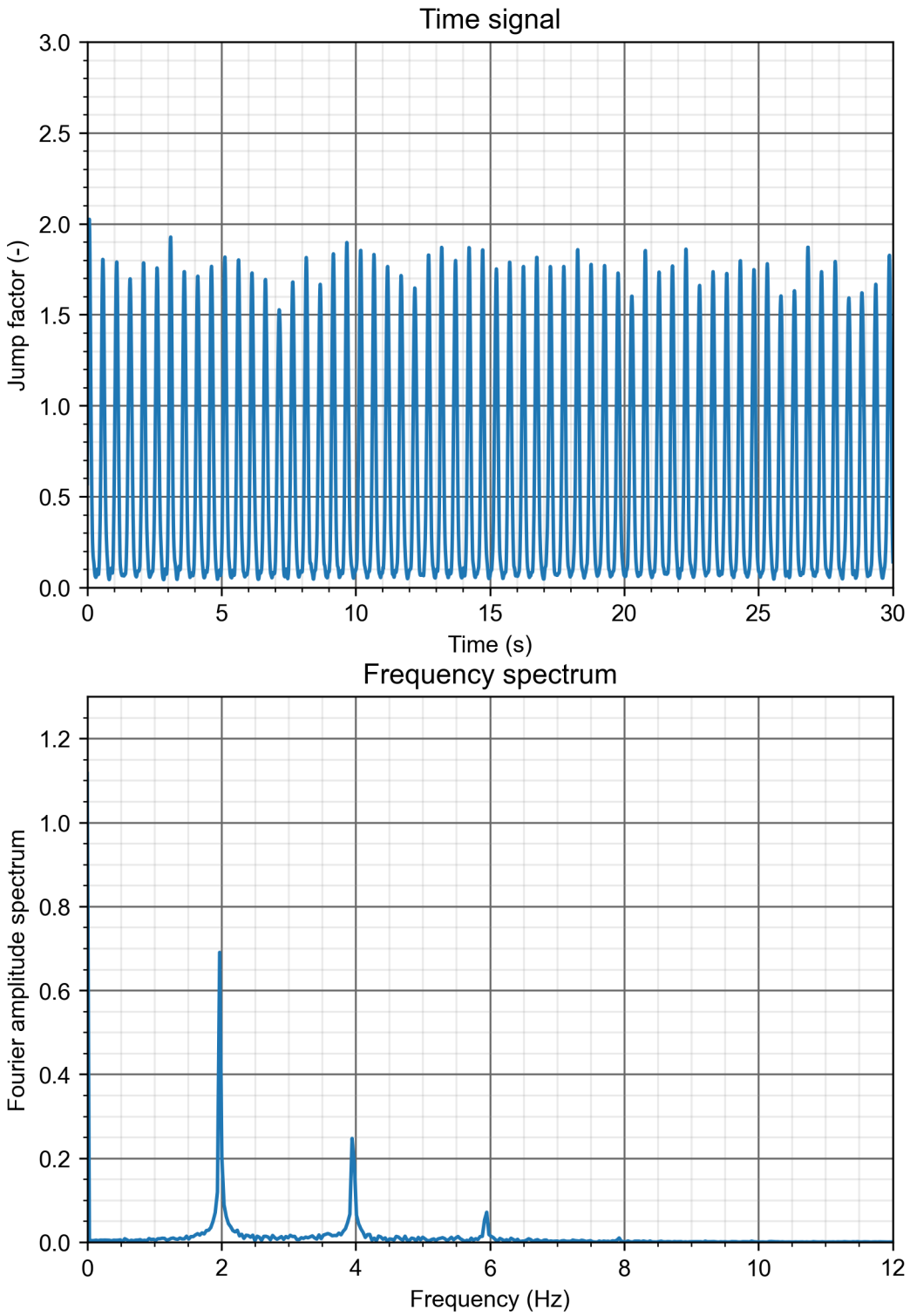

Figure B.24: $T_p = 0.03$, $\phi = 0.05$, $\alpha = 0.33$

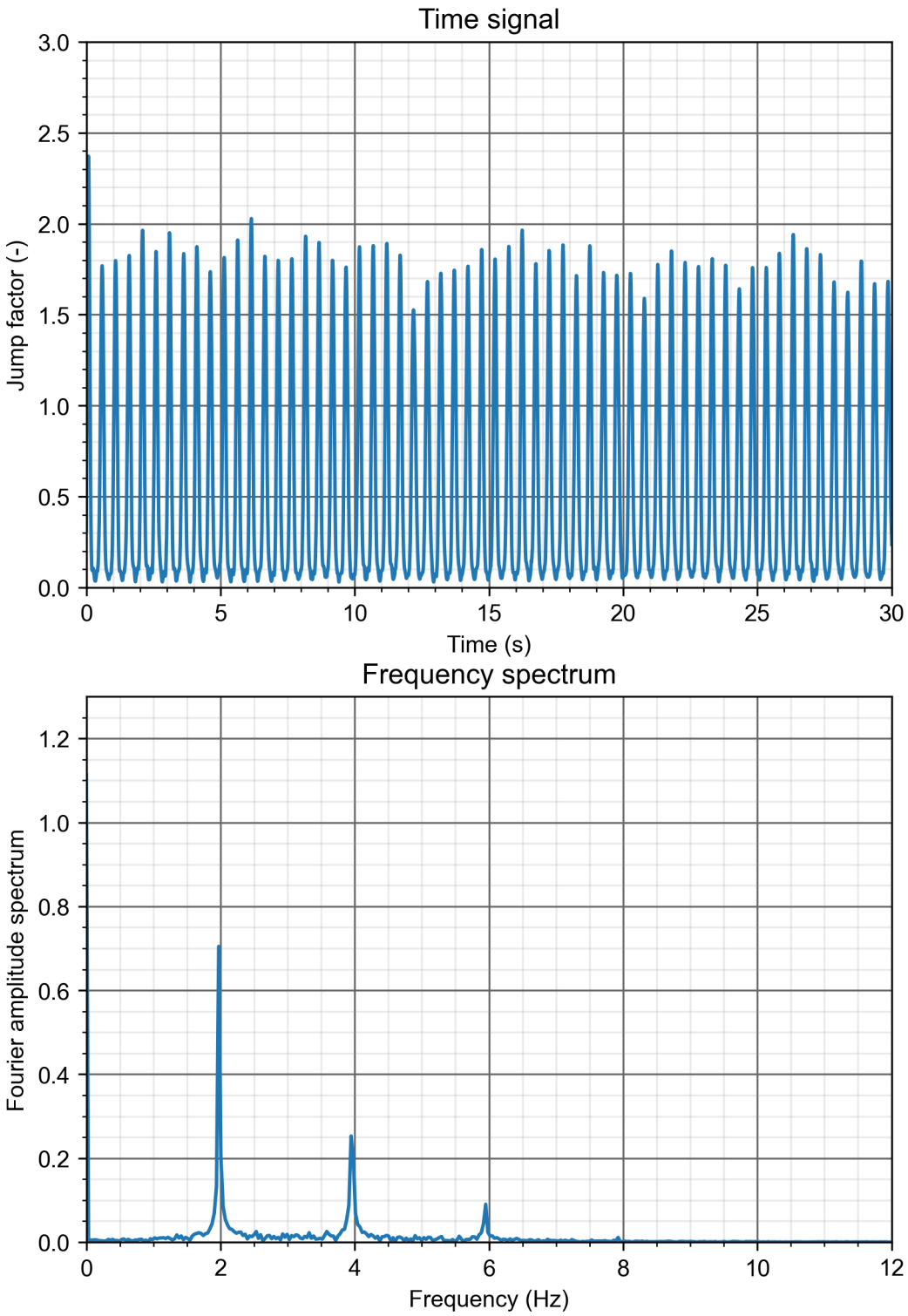

Figure B.25: $T_p = 0.04$, $\phi = 0.02$, $\alpha = 0.33$

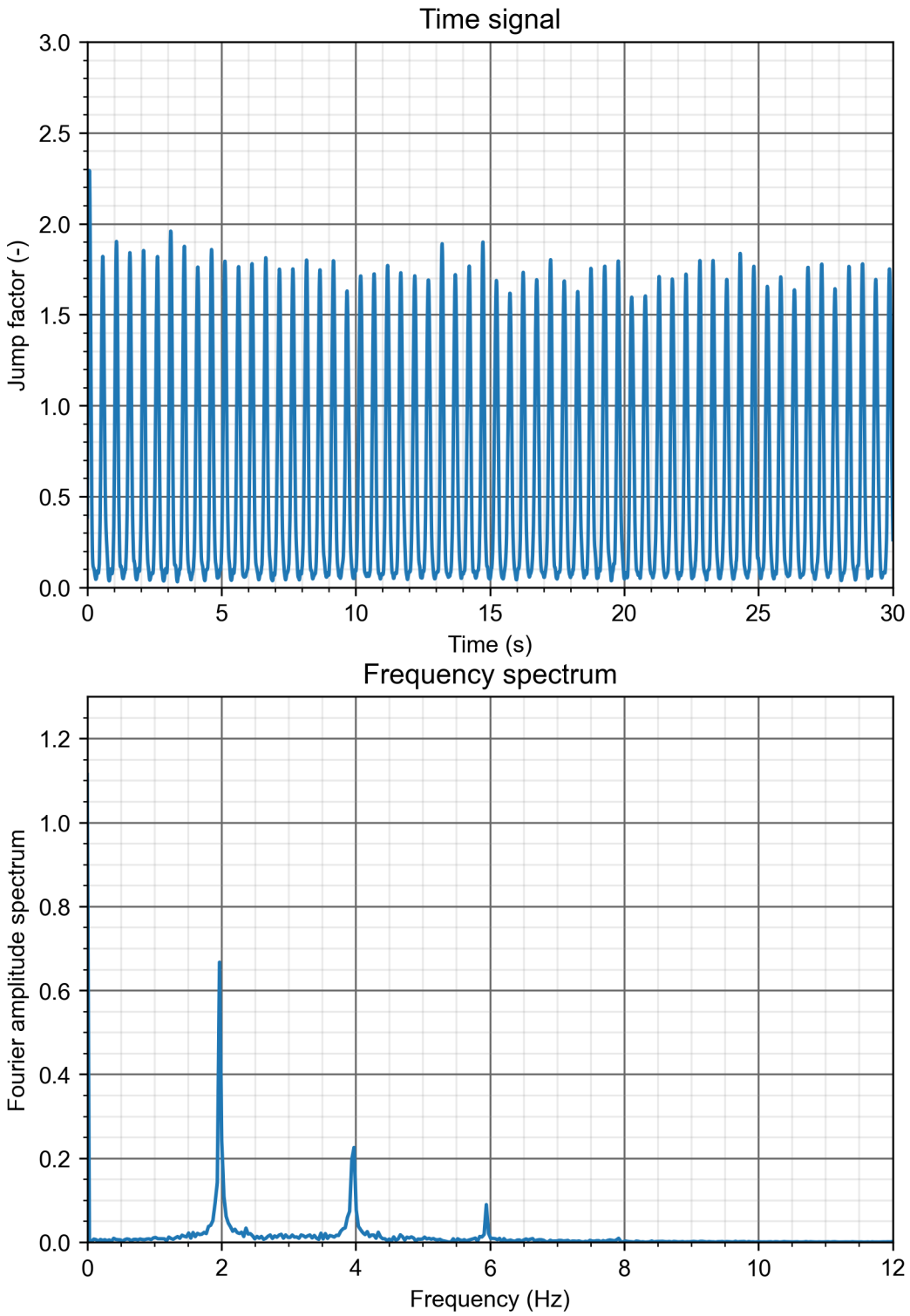

Figure B.26: $T_p = 0.04$, $\phi = 0.03$, $\alpha = 0.33$

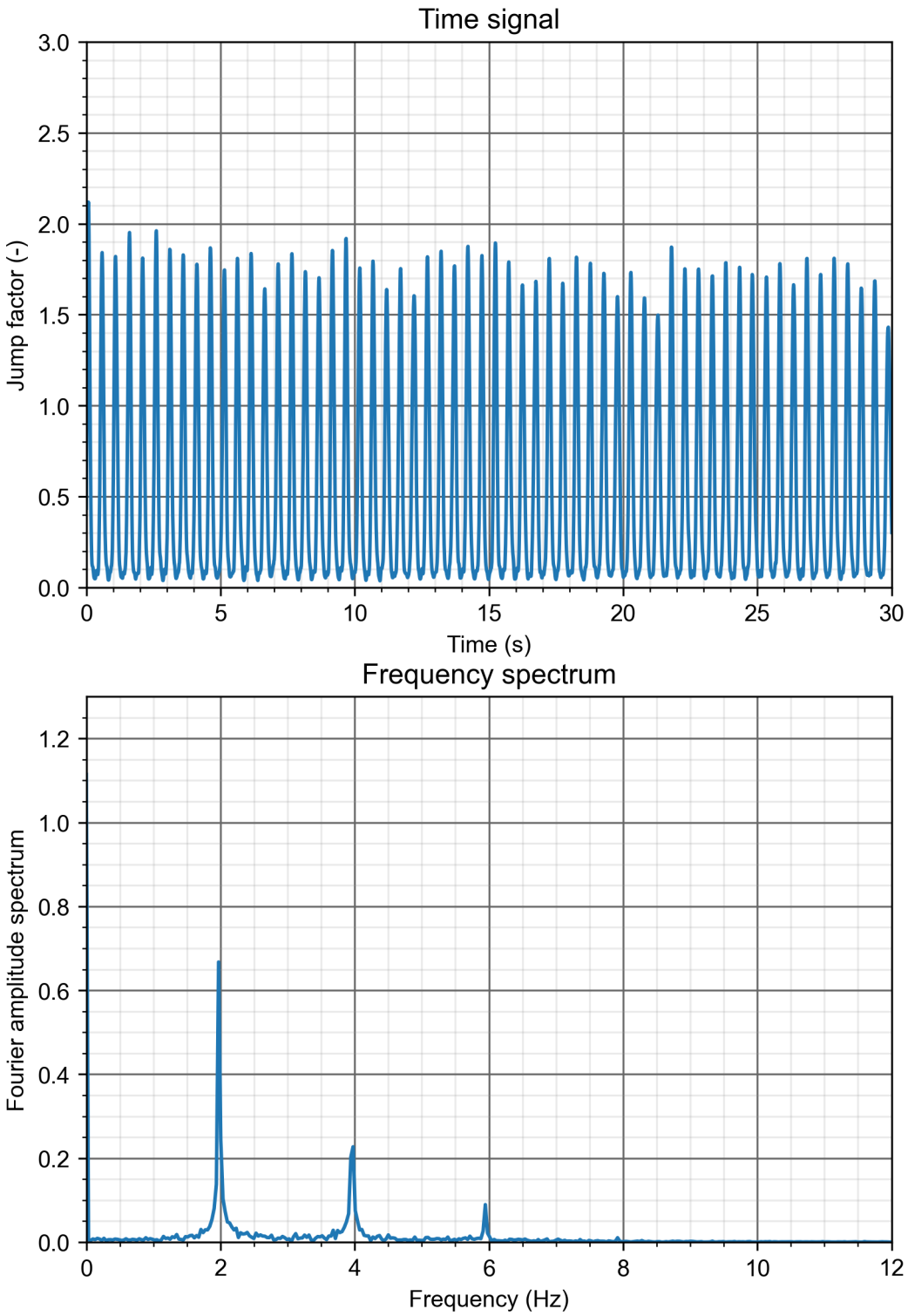

Figure B.27: $T_p = 0.04$, $\phi = 0.04$, $\alpha = 0.33$

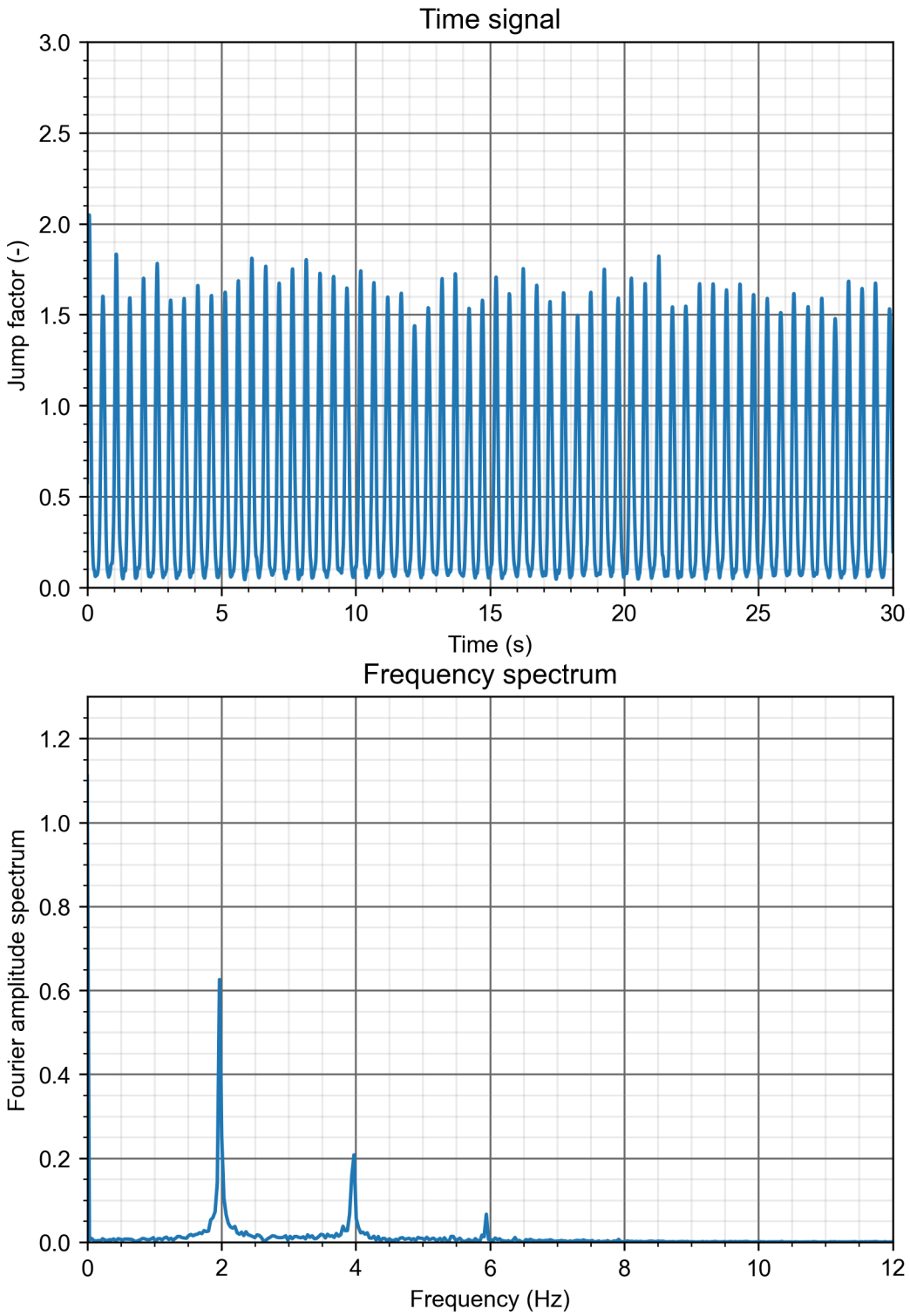

Figure B.28: $T_p = 0.04$, $\phi = 0.05$, $\alpha = 0.33$

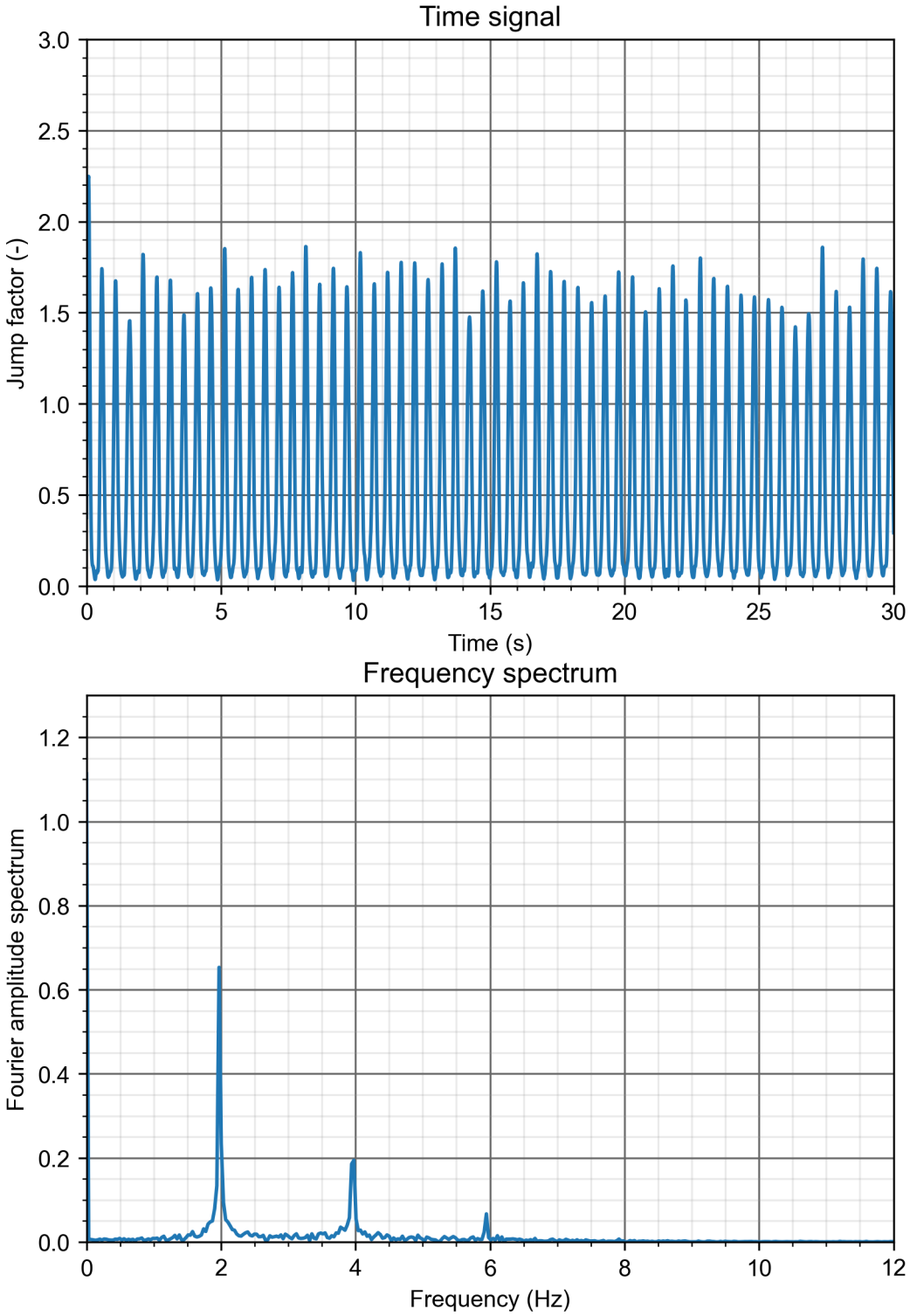

Figure B.29: $T_p = 0.05$, $\phi = 0.02$, $\alpha = 0.33$

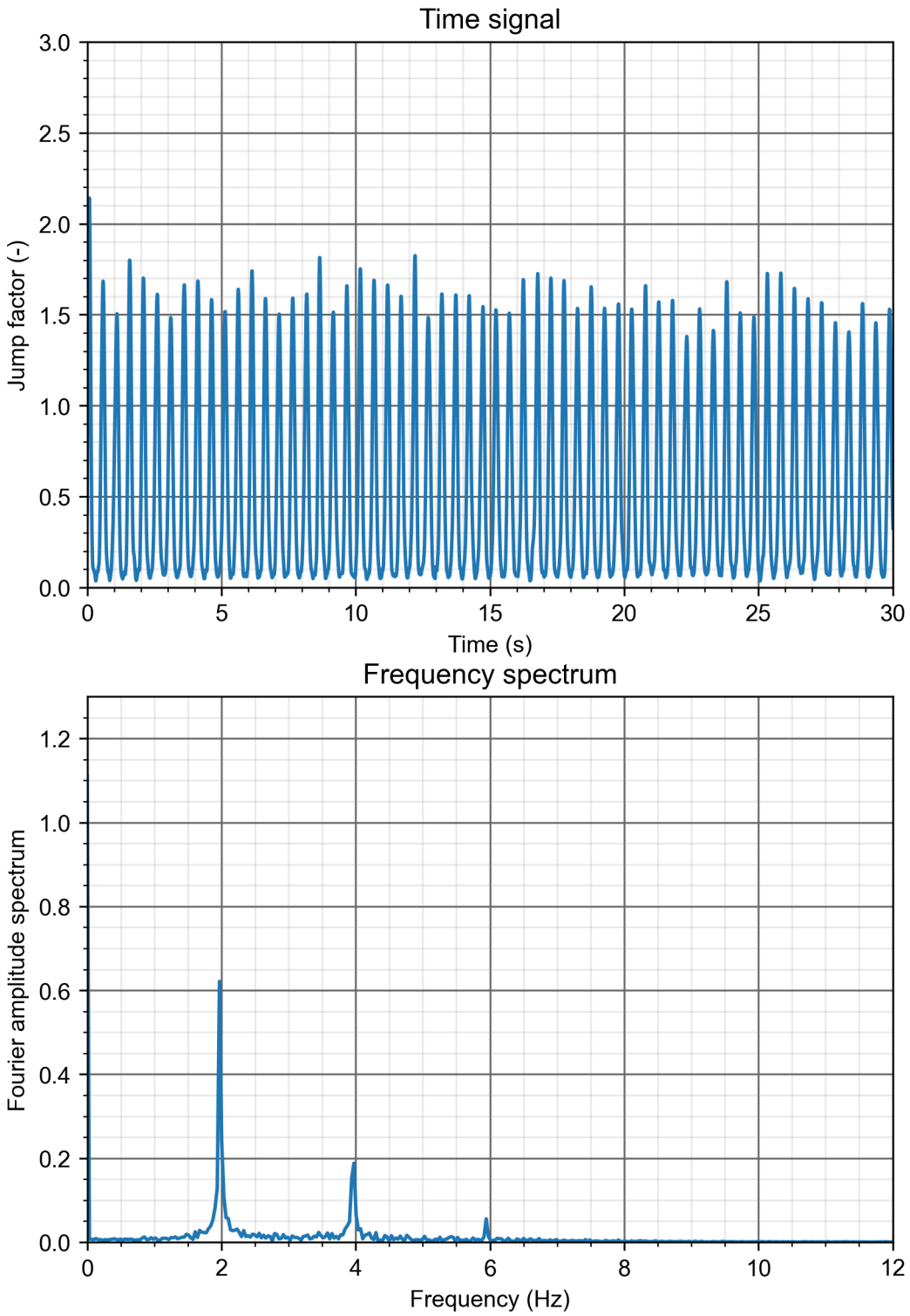

Figure B.30: $T_p = 0.05$, $\phi = 0.03$, $\alpha = 0.33$

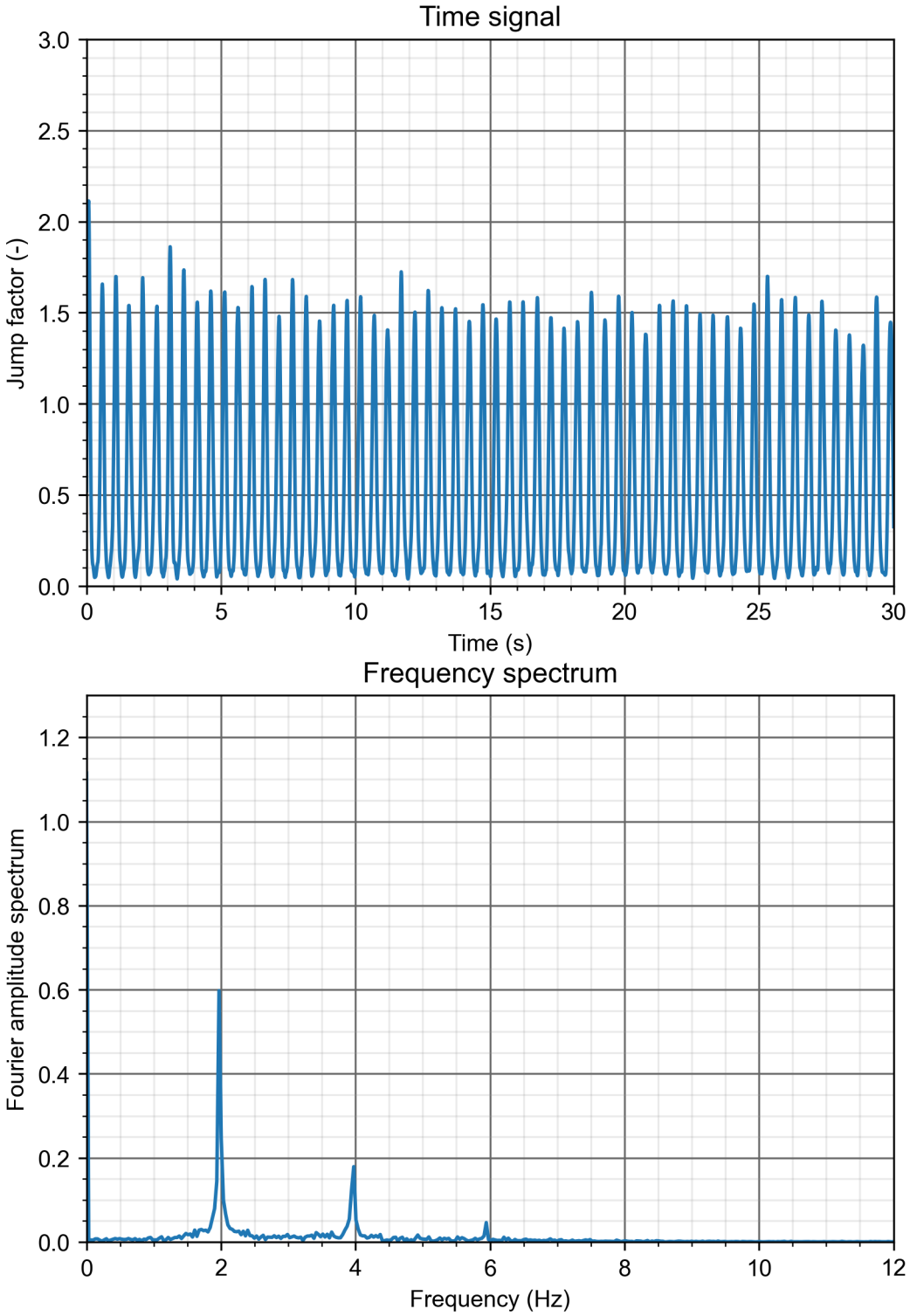

Figure B.31: $T_p = 0.05$, $\phi = 0.04$, $\alpha = 0.33$

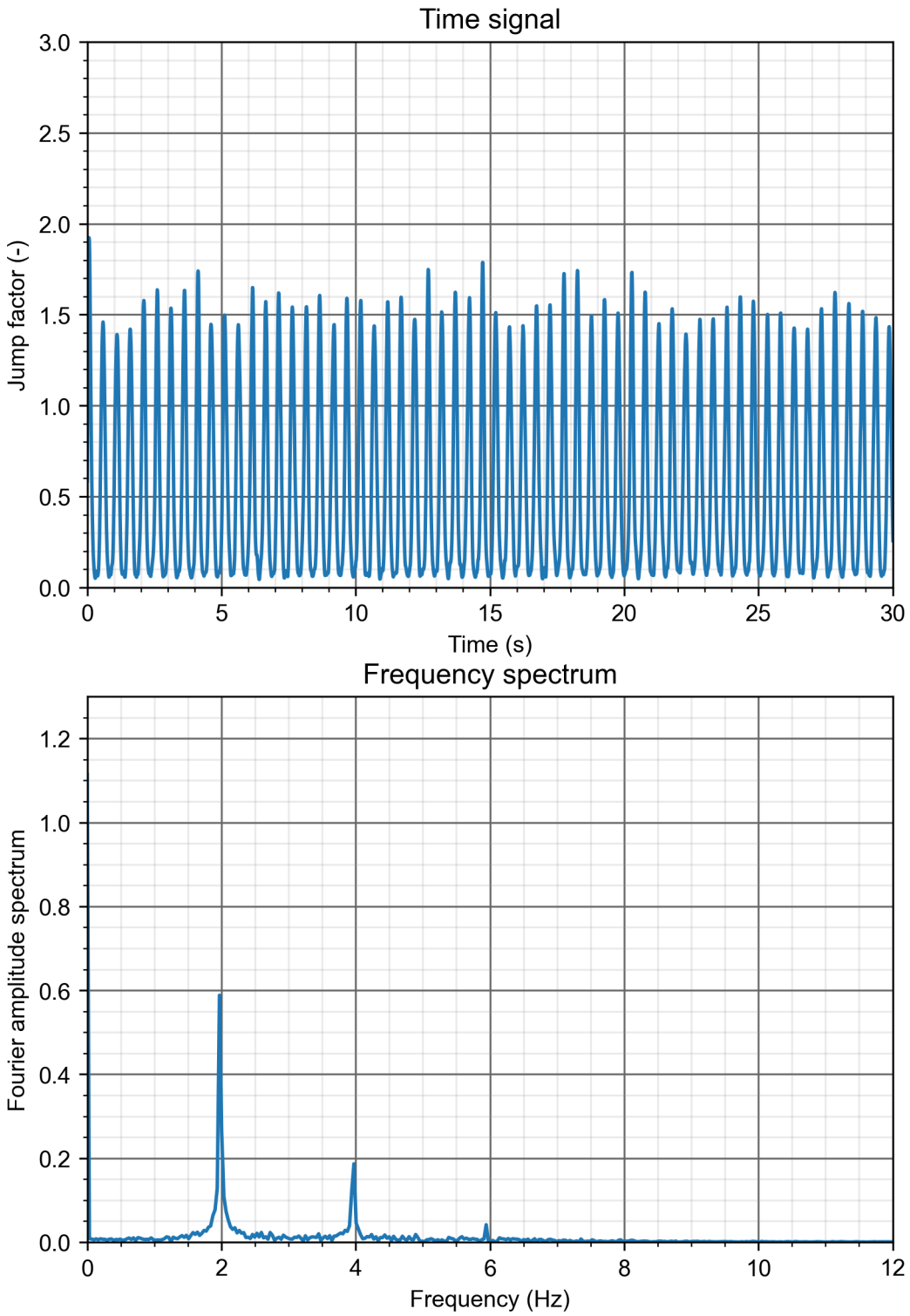

Figure B.32: $T_p = 0.05$, $\phi = 0.05$, $\alpha = 0.33$

C

Concrete cover measurements

Appendix C presents the measurements on the concrete cover. These measurements have been performed by a company that is specialized in inspections on behalf of the engineering consultancy firm, and can be read in detail in [7].

This company scanned 23 other grandstand elements in the Goffert stadium. In total, five scans were made: two in the longitudinal direction and three in the cross direction, one of which is at midspan. This thesis focuses on failure of a grandstand element due to exceedance of the bending moment capacity, which happens at midspan. Therefore, only the scanned concrete covers in midspan, in cross direction are included in this study.

In table C.1, the lowest, average, and highest value of the measured concrete covers are shared. Additionally, the highest, and lowest deviation are presented, expressed in both percentages and millimeters.

The highest deviations are, on average, 41% or 16 mm higher than the mean, with an extreme case of 103% or 35 mm. The lowest deviations are, on average, 24% or 10 mm lower than the mean, with an extreme case of 50% or 19 mm.

Table C.1 The minimum, average, and maximum measured concrete covers at midspan of other element types in the Goffert stadium.

Element type	Measured concrete cover (mm)				Deviation high		Deviation low	
	min	average	max		(%)	(mm)	(%)	(mm)
1	41	52	72		38	20	-21	-11
2	42	48	60		25	12	-13	-6
2a	33	43	65		51	22	-23	-10
3	41	46	52		13	6	-11	-5
4	44	57	72		26	15	-23	-13
5	38	58	83		43	25	-34	-20
6	33	41	69		68	28	-20	-8
8	25	41	59		44	18	-39	-16
9	27	34	48		41	14	-21	-7
10s	26	38	54		42	16	-32	-12
11s	21	37	56		51	19	-43	-16
13s	26	36	47		31	11	-28	-10
14s	21	34	62		82	28	-38	-13
15	34	39	58		49	19	-13	-5
16	32	41	55		34	14	-22	-9
17	27	34	39		15	5	-21	-7
18	24	34	69		103	35	-29	-10
19	19	38	54		42	16	-50	-19
20	29	38	51		34	13	-24	-9
21	24	34	49		44	15	-29	-10
22	25	28	34		21	6	-11	-3
23	33	36	49		36	13	-8	-3
24	38	41	45		10	5	-7	-3
				Average	41	16	-24	-10
				Extreme	103	35	-50	-19